AD-A154 049 THE MECHANICS OF INTERNAL STRESS AND MICROCRACK TOUGHENING MECHANISMS IN CERAMICS(U) ILLINOIS UNIV AT URBANA DEPT OF THEORETICAL AND APPLIED MECHA.. 1/2

UNCLASSIFIED R M MCMEEKING APR 85 N00014-81-K-0650 F/G 11/2 NL

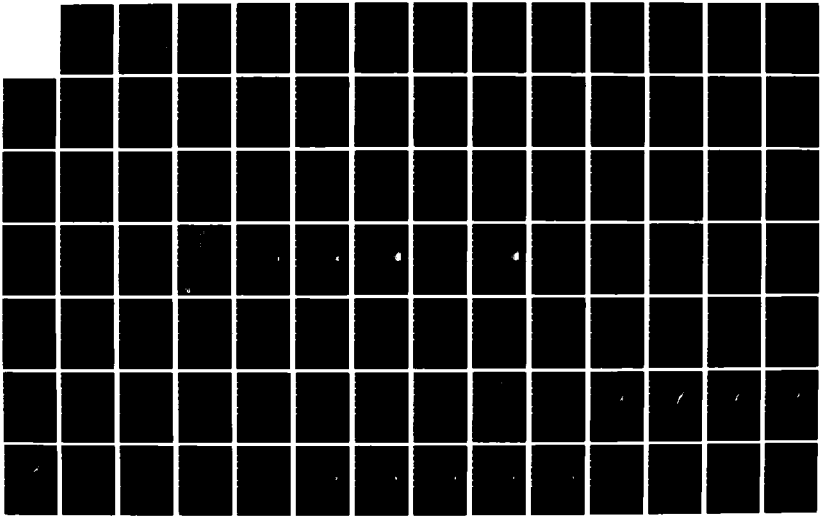

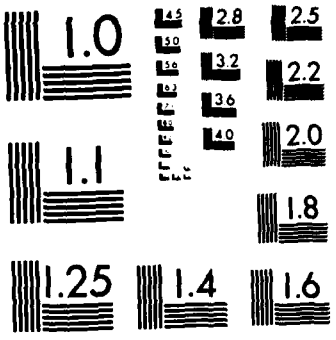

MICROCOPY RESOLUTION TEST CHART
NATIONAL BUREAU OF STANDARDS-1963-A

AD-A154 049

Final Report

Contract ONR N00014-81-K-0650

The Mechanics of Internal Stress and Microcrack Toughening Mechanisms in Ceramics

Robert M. McMeeking
Department of Theoretical and Applied Mechanics
University of Illinois
Urbana, IL 61801

April 1985

DTIC
ELECTE
MAY 2 2 1985
S D
B

DTIC FILE COPY

DISTRIBUTION STATEMENT A
Approved for public release;
Distribution Unlimited

85 04 22 024

Final Report Contract ONR N00014-81-K-0650

"The Mechanics of Internal Stress and Microcrack Toughening Mechanisms in Ceramics"

Contents

Unpublished manuscripts of research completed under the contract (all to be submitted for publication)

1. "The Shearing Contribution in Transformation Toughening of Brittle Materials," P. Sofronis and R. M. McMeeking.

2. "Mechanics of Near Tip Microcracking in Brittle Materials," P. Charalambides and R. M. McMeeking.

3. "Stress Intensity Factors for Slightly Kinked, Partially Closed Cracks in Compression," N. Aravas and R. M. McMeeking.

In addition the following paper was completed under the contract

4. "Estimates for the Constitutive Moduli of Ductile Materials Containing a Small Volume Fraction of Voids or Inclusions," R. M. McMeeking in Mechanics of Materials (D. C. Drucker Anniversary Volume) (eds. G. A. Dvorak and R. T. Shield) Elsevier, Amsterdam, 1984, pp. 275-288.

Accession For
PER LETTER
Dist
A-1

The Shearing Contribution in Transformation Toughening of Brittle Materials

P. Sofronis and R. M. McMeeking

Department of Theoretical and Applied Mechanics

University of Illinois at Urbana-Champaign

March 1985

SUMMARY

A simple constitutive law is proposed for the description of a ceramic composite which undergoes stress induced martensitic transformation. This law is used in finite element calculations to investigate the shear effect on the transformation zone near a crack tip. A formula describing the stress intensity factor change due to the shear contribution of the transformation is given. Significant loss of toughness is observed in the case of a stationary crack and is attributed entirely to the shear component of the transformation. On the contrary, the dilatant part brings about no change. As the crack grows, the wake of the transformed material left behind the crack constitutes a source of toughening. This toughening is due to both dilatancy and shear in the phase change and rises to a maximum level just after a propagation comparable with the zone height. Finally, it is shown that the shear component can be important when prediction of the fracture toughness of the transformation toughened ceramics are made.

1. INTRODUCTION

Transformation toughening is one of the mechanisms available to overcome the inherent brittleness of ceramics. It is a phenomenon applicable to ceramic matrices in which Zirconia (ZrO_2) and perhaps some other materials can be incorporated. To date it has been studied quite thoroughly [1-13].

An optimally-fabricated [13] partially stabilized zirconia (PSZ) is a two-phase ceramic. Its microstructure [5] at room temperature consists of: a cubic matrix which is a high solute content Zirconia 'alloy' containing one of the stabilizers MgO CaO, Y_2O_3 or any of the rare earth oxides: and fine coherent metastable tetragonal precipitates of low solute content Zirconia phase inside the cubic matrix. The stress induced martensitic transformation of those metastably retained tetragonal particles to monoclinic symmetry in the stress field of a crack tip is the mechanism responsible for the enhanced toughness observed experimentally in PSZ. The phenomenon of transformation toughening is also observed in the Al_2O_3 and ZrO_2 system. The pure tetrogonal ZrO_2 particles are retained metastably in the Al_2O_3 matrix by pressure.

There are two methods of analysis with regard to the phenomenon of toughening. The first incorporates the energy changes accompanying the transformation. The second concerns the stress intensity factor (SIF) changes that take place during transformation.

Quantitative analysis from a continuum mechanics viewpoint, based only on the dilatational component of the transformation with regard to the SIF reduction was done first by McMeeking and Evans [19] and Budiansky, Hutchinson and Lambropoulos [20]. The analysis of the latter workers is based on a constitutive relation between the mean stress and the dilatation for the composite ceramic. In both works mentioned, the predicted toughening is comparable with the experimental data, however, it underestimates them.

Recently, Lambropoulos [21] has suggested a promising constitutive law for the composite including both parts of the transformation, dilatant and shear. The treatment of the shear effect takes into consideration particle size and orientation. The results predicted for spherical particles are quite well in agreement with experimental observations but are based on a transformation zone size and shape estimated from the standard crack tip singular elastic field. That is, he assumes that the zone shape is the same as regions in the unperturbed elastic solution in which the transformation criterion is met or exceeded. Changes in stress due to the transformation are not addressed in detail.

In this paper, we shall study the shear effect's influence on the enhanced toughness through numerical calculations by means of a simple stress-strain relation for the composite. The model is based on a constitutive relation along the lines introduced by Budiansky et al. [20] and the condition for transformation is dominated by the dilatational component. When the hydrostatic stress reaches a critical level, the transformation takes place. This model is not entirely satisfactory as the shear effect is bound to influence the critical state for transformation. However, we regard this paper with the critical state determined solely by the hydrostatic stress as a first step towards a complete theory. The analysis is carried out around the crack tip of a long crack which is imbedded in a composite material rich in tetragonal particles whose presence in the matrix is defined by a volume concentration v_f. As such, the composite can be modelled as a continuum of transformable material.

In section 2 we discuss some aspects of the shear part of the transformation which are helpful in comprehending the nature of the shear strain that the transforming particles undergo. In section 3 we propose a

constitutive law for the composite. In section 4 we derive a formula for the SIF change due to the shear component of the transformation. Based on that formula, we make first estimates of the shearing contribution to SIF change by using the transformation zone derived from the unperturbed elastic solution [19]. In section 5 we formulate the boundary value problem for the stationary crack and solve it by means of the finite element method in section 6. As a result the transformation zone shape and size are estimated. In section 7 the estimated zone and the fracture toughness calculations for the stationary and for the propagating crack are presented. As it has already been proven in the past, the toughness increase is due to the transformed particles left in the wake of the crack tip. In sections 8 and 9 the discussion associated with the model results and the closure are presented respectively.

2. STRESS INDUCED TRANSFORMATION

The aim of this section is to introduce basic features of the stress induced transformation so that the shear component can be understood. The transformation is martensitic and has been discussed extensively elsewhere [1,16,17,18]. It involves a change from tetragonal to monoclinic symmetry in particles in the composite ceramic. In the situation of interest to us, the transformation is induced by critical conditions of stress. A component of the transformation is a dilatation and if the particles were unconstrained there would also be a substantial shear contribution. If we assume that the process is driven by the reduction of free energy [1,7,13] then we deduce that the shear strain component of the transformation would align itself to maximize the work done by the loads applied to the particle [7,13]. In addition, the critical state for transformation would arise just when the applied loads are capable of delivering sufficient energy to the system to

compensate for the increase in the internal energy [7,13]. This implies a transformation criterion involving some combination of hydrostatic and deviatoric stress. This issue has been addressed by Lambropoulos [21].

It has been observed that the situation is more complicated when the transforming particles are constrained in the composite matrix [12]. The particles are capable of twinning or undergoing some similar mode of deformation during transformation. The twins form in such a way that the average shear strain after transformation can be quite small compared with the potential unconstrained shear transformation strain. In addition, the final strain in the transformed particle differs because of the constraint of the surrounding matrix. There is not yet a comprehensive theory that accounts for transformation and twinning. However, it can be hypothesized that the orientation of the net shear strain that results from transformation and twinning will be aligned with the maximum shear stress applied by the matrix to the particle. This will tend to maximize the external energy absorption during transformation and suggests a critical state for the transformation based on strain energy. Lambropoulos [21] has developed a constitutive law for the constrained transformation along the above lines combining the effects of hydrostatic and deviatoric stress and accounting for dilatational and shear transformation.

In this paper we shall use a simpler law as a first step towards studying the interactions of shear transformation with the crack tip. The process will be considered to take place on a continuum scale and the description of the constitutive law applies to the composite ceramic. The criterion for transformation will be taken to be the achievement of a critical average hydrostatic stress in the composite. This neglects the contribution made by the shear component to the work absorbed during transformation. However, the

residual shear strains in constrained transformation particles are known to be small and the shear strain in an unconstrained composite element would be correspondingly small. The transformation will involve a deviatoric component as well as a dilatational contribution. The deviatoric part of the transformation strain for an unconstrained element of the composite ceramic will be taken to be proportional to the dilatational component of the unconstrained transformation. All calculations presented in this paper will be for plane strain situations. In that case there is a fixed ratio between the shear strain and the volumetric strain in the transformation. The orientation of the shear strain will be taken as that of the maximum shear stress when transformation commences (fig. 1). Once the transformation has taken place this orientation will be locked in so that changes of direction of the maximum shear stress will not cause rotation of the shear contribution of the transformation.

Finally, the transformation will be supercritical in the terminology of Budiansky et al. [20]. That is, at critical state, the material transforms completely without the existence of a partially transformed state. The details of the constitutive law are given in the next section.

3. THE CONSTITUTIVE LAW

The transformation of the composite occurs due to the martensitic transformation of the particles. It takes place when the macroscopic average stress in the composite is such that

$$\sigma_m = \sigma_m^{cr} \tag{1}$$

where $\sigma_m = \frac{\sigma_{kk}}{3}$ is the mean stress, σ_m^{cr} is a critical value and σ_{ij} is the macroscopic average stress tensor at a point in the composite.

The unconstrained transformation strain of the composite is ε_{ij}^T which is partly dilatational and partly deviatoric in general. It can be estimated to be the volume fraction v_f of particles in the composite times the unconstrained transformation strain of the transforming particles less the deviatoric strain nullified by twinning [20]. The supercriticality of the transformation implies that there is no transformation as long as $\sigma_m < \sigma_m^{cr}$ and complete transformation occurs if $\sigma_m > \sigma_m^{cr}$. The transformation will be assumed to be effectively irreversible in the conditions prevailing as observed in experiment [19]. The amount of the deviatoric strain arising during transformation is proportional to the amount of dilatation. We will carry out calculations for a variety of values of this ratio. The principal axes of the deviatoric strain will be taken to depend on the state of stress at transformation as discussed below.

The stress which arises [22] in a constrained element of the composite is

$$\sigma_{ij} = c_{ijk\ell} \, (\varepsilon_{k\ell} - \varepsilon_{k\ell}^T) \tag{2}$$

where ε_{ij} is the final strain and $c_{ijk\ell}$ is the tensor of linear elastic moduli of the composite material. For an isotropic composite

$$\sigma_{ij} = 2\mu \, (e_{ij} - e_{ij}^T) + B(\varepsilon_{kk} - \varepsilon_{kk}^T)\delta_{ij} \tag{3}$$

where μ is the shear modulus, B is the bulk modulus, $e_{ij} = \varepsilon_{ij} - \frac{1}{3}\varepsilon_{kk}\,\delta_{ij}$ is the deviatoric strain, δ_{ij} is the Kronecker delta and ε^T is the dilatational part of the unconstrained transformation of the composite ($\varepsilon^T = \varepsilon_{kk}^T$).

The calculations we have carried out are for plane strain. In this case $\varepsilon_{zz} = 0$ and we assume that $e_{zz}^T = 0$ as there are no macroscopic transverse shear strains. As a consequence

$$\sigma_{zz} = \nu(\sigma_{xx} + \sigma_{yy}) - \frac{2}{3}\mu(1 + \nu)\,\varepsilon^T \tag{4}$$

where ν is the poisson's ratio. The deviatoric transformation strain can be written as

$$e^T_{xx} = -\,e^T_{yy} = -\,\frac{\gamma^T}{2}\sin 2\Omega, \qquad e^T_{xy} = \frac{\gamma^T}{2}\cos 2\Omega$$

where Ω is the angle between the x-axis and a principal axis of the transformation shear. Thus, the transformation is determined by 3 parameters ε^T, γ^T and Ω. We will assume that Ω is coincident with the angle to the principal axes of shear stress in the macroscopic composite state of stress at the instant of transformation as shown in fig. 1. Calculations are carried out for a variety of ratios $\lambda = \gamma^T/\varepsilon^T$.

4. ESTIMATES OF THE SHEARING EFFECT AT THE CRACK TIP

Before proceeding to somewhat rigorous numerical calculations, we shall consider some approximate results for shearing transformation at the crack tip. The shape of the zone of transformed material at the crack tip is determined by the interaction of the stresses generated by the applied load and those generated by constraints on the transformed zone. If we neglect the latter, we can estimate the zone shape as the locus of points at critical state in the unperturbed linear elastic solution at the crack tip. This proves to be quite an accurate estimate of shape for the case of small scale dilatant transformation [20]. As we have approximated the critical state as one that depends only on hydrostatic stress, the zone shape will be given by the locus of points of equal hydrostatic stress. We will restrict ourselves to small scale transformation, so that the stresses of interest are given by the singular elastic stresses at the crack tip due to the applied load

$$\sigma_{ij} = \frac{K_A}{\sqrt{2\pi r}} f_{ij}(\theta) \tag{5}$$

where K_A is the stress intensity due to the applied loads causing tensile opening (Mode I) of the tip, (r,θ) are polar coordinates measured from the crack tip and f_{ij} is a given function which can be found for example in the article by Rice [24]. The shape that results for a stationary crack is shown in fig. 2.

Consider now, the material which transforms inside the zone. If it were not constrained by the material outside the zone, a certain change of shape would result. Tractions can be applied to the perimeter of this region of material to return it exactly to the shape of the zone prior to transformation. After the material is inserted into the crack tip location, the tractions can be removed to give the final state. However, the forces required to nullify the constraining tractions $\underline{T}^c$ will produce a change in the SIF at the crack tip. It is this change of stress intensity ΔK which is of interest.

As discussed by McMeeking and Evans [19] the change of stress intensity is given by

$$\Delta K = \int_{S_T} \underline{T}^c \cdot \underline{h}\, ds \tag{6}$$

where $\underline{h}$ is the weight function [25] whose form is stated in McMeeking and Evans [19] and used with the assumption that ε_{ij}^T is homogeneous in A_T, the transforming area which has perimeter S_T. We shall consider now transformations which are inhomogeneous $\varepsilon_{ij}^T(\underline{x})$. With the area A_T removed from constraint of the surrounding area, the displacements and strains [22] that result will be $\underline{u}^S$ and $\underset{\sim}{\varepsilon}^S$ respectively due to transformation and self-

sufficient in general to consider only the effect of very long wakes that produce an asymptotic value for ΔK.

For λ less than 1 the toughness enhancement is not as large as that given by equation (18). In table 5 we present the greatest toughness enhancements found for several λ values and the amount of crack advance for which they were obtained. This table shows that the toughness enhancement gets larger when λ gets larger. It should be mentioned that the values for ΔK tend to certain asymptotic values as $\Delta a/w \to \infty$ but these are less important than the maxima presented in table 5. Finally, we should mention the fact that the results of table 5 fit the curve for $\nu = 0.25$ of figure 4. This means that the results taken in section 4 and those after having solved the boundary value problem of the stationary crack are the same.

Applications

Next, we proceed to see how the maximum toughness enhancement results compare with the experimental data. We shall consider $\nu = 0.3$ even though our shearing contribution results have been taken by considering $\nu = 0.25$. Figure 4 indicates that no significant difference results. In the case of the Al_2O_3 toughened Zirconia whose material and transformation parameters are [21]: $E = 315$ GPa, $\varepsilon^T = 0.04$, $w = 10^{-6}$m, $v_f = 0.03$ one has

i) with purely dilatant transformation

$$\Delta K = -1.19 \quad \text{Mpa}\sqrt{m}$$

ii) with both parts of the transformation and $\lambda = 1$

$$\Delta K = -1.89 \quad \text{MPa}\sqrt{m}$$

iii) Lambropoulos' result (both part of the transformation, spherical particles and $K_{IC} = 5$ MPa $\sqrt{m}$)

based on equation (16). Such "R curves" are those shown in figures 12 and 13 for $\lambda = 0$ and $\lambda = 1$ respectively. Observing those curves and the tables 2 through 4 we deduce that the wake of the transformed material left behind the propagating crack is a source of fracture toughness enhancement. First, figure 12 shows that the toughness enhancement found for $\lambda = 0$ coincides with that found by McMeeking and Evans [19]. This coincidence becomes more pronounced for large values of crack advance.

The important result of this paper is the ΔK_S component that behaves as for examaple figure 13 shows for $\lambda = 1$. As mentioned previously, the crack will start to propagate sooner than in the absence of transformation because ΔK is initially positive due to ΔK_S. As the crack grows, ΔK diminishes and eventually becomes negative at about $\Delta a/w = 0.1$. This means that the applied loads must be increased to sustain crack growth and in a stiff loading system the crack will propagate stably under rising load. This will continue until $\Delta a/w$ is about 0.7 and the SIF change is then given by

$$\frac{(1-\nu)\ \Delta K}{E\ \varepsilon^T\ v_f\ \sqrt{w}} = -\ 0.35. \tag{23}$$

This expression represents the toughness enhancement and is larger than that given by equation (18). After this amount of crack growth, ΔK increases and so if the loads are kept constant or increased, the applied K will exceed K_{IC}. Thereafter the propagation will become unstable. Thus the maximum magnitude of ΔK represented by equation (23) is equivalent to the asymptotic value of ΔK due to dilatation alone observed by McMeeking and Evans [19]. It is interesting to note that the asymptotic value of ΔK due to dilatation plus shear is not the relevant quantity. The useful toughness enhancement is due to the minimum in the curve for ΔK at $\Delta a/w \simeq 0.7$. Thus it may not be

been extended to the cases when $\lambda \neq 0$.

In contrast with ΔK_D, ΔK_S is not zero and it does depend on the value of λ. In fact, ΔK_S increases as λ increases. Equation (16) indicates that the shearing effect results in fracture toughness reduction because ΔK_S is positive. This reduction for $\lambda = 1$ is comparable to the fracture toughness enhancement in the case of a purely dilatant transformation given by equation (18) when the crack has advanced $\Delta a \simeq 5w$. The ΔK_S results in table 1 can almost be reproduced by the equation (17) for the respective values of λ. This means that the transformed material and the shearing contribution do not affect the features of the transformation zone as it is found from the unperturbed elastic crack tip field. Therefore, the fact that ΔK_S is positive is a consequence of the nature of the equation (16). An attempt to justify this may be made by regarding the range of the positive contribution to the integral of equation (16). Since for the stationary crack $\Omega = \frac{3\theta}{4}$, the integral sign depends on the sign of the integrand $\sin(2\theta)$. Hence, it is positive when $\theta < \frac{\pi}{2}$ and negative when $\theta > \frac{\pi}{2}$. Therefore, it can be said that the positive contribution comes from a large sector and can very likely override the negative contribution.

The consequence of the computed ΔK_S values would be that crack propagation may take place sooner than when there is no transformation. This is because ΔK_S is positive for the stationary crack and K_A can become greater than K_{IC}^A earlier than otherwise. However, this growth is likely to be stable, a point which is elucidated in what follows.

Propagating crack

In order for the crack to advance quasi-statically it is required that the applied loads K_A be such that $K_A = K_{IC}^A$ where K_{IC}^A is given by equation (16). Therefore, by knowing ΔK , we can produce an "R curve" [15]

zones are developed inside a circle centered at the crack tip whose area is less than 0.15% of the mesh. Indeed, these numbers fall within the corresponding length range, set for small scale yielding condition in the elastic-plastic fracture analysis by Rice and Tracey [23]. In addition, the fact that the displacements of the elements near the perimeter of the domain (fig. 5) are the unperturbed elastic crack tip field displacements, ensures the small scale condition too. In figure 9, it can be seen that the zone taken numerically for $\lambda = 0$ is almost identical with that used by McMeeking and Evans [19] as predicted by Budiansky et al. [20]. This means that the transformed material does not affect the linear elastic crack tip field given by equation (5). The same argument applies to the case when $\lambda = 1$ (fig. 11). However, the shearing contribution affects the zone shape especially at small angles of θ. It is also worth mentioning that the zone height w is the same for all values of λ as shown in table 1.

Consider now the SIF change ΔK_D. It can be deduced from table 1 that $\Delta K_D = 0$ if we take into account the numerical error involved in the calculations. Therefore, for $\lambda > 0$ no ΔK_D is observed even though the zone boundaries differ from that with $\lambda = 0$. This independence of ΔK_D from λ can be justified by observing equation (13). The sign of the integral depends on the sign of the $\cos(\frac{3\theta}{2})$. The integral is positive for $\theta < \frac{\pi}{3}$ and negative for $\theta > \frac{\pi}{3}$. Thus, the positive contribution to the integral value comes from a much smaller section than the sector of the negative contribution. It is this wider ranging source of the negative effect which dominates the integral value. Therefore, the larger range of r for small θ when λ deviates from zero cannot be cause of a significant disturbance of the final result. This remark has already been made before [19], but only within the frame of a purely dilatant transformation. The argument now has

Propagating crack

The crack has been assumed to propagate quasi-statically under the conditions mentioned in section 4. The SIF change calculations ΔK_D and ΔK_S were carried out numerically for a given crack advance Δa. The formulae (13) and (14) were used again. The results are shown in tables 2 through 4. In figures 12 and 13 the changes ΔK_D and ΔK_S are plotted against the crack advance Δa for $\lambda = 0$ and $\lambda = 1$ respectively. In table 5 the symptotic, i.e. the maximum SIF change $\Delta K = \Delta K_D + \Delta K_S$ is shown.

8. DISCUSSION

In this discussion of the results quoted in the previous section, we shall focus mainly on how the shear component of the transformation influences the fracture toughness behavior of the material. It should be borne in mind that the shearing contribution is characterized by the parameter $\lambda = \gamma^T/\varepsilon^T$. Large values of λ denote large transformation shear strains for a given volume dilatation.

Stationary crack

It has been mentioned before that the dilatant part of the transformation does not affect the material fracture toughness, i.e. $\Delta K_D = 0$. Furthermore, Lambropoulos [21] based on a transformation zone derived from the unperturbed linear elastic crack tip field, concluded that $\Delta K_S = 0$ too. Our analysis' predictions are in accord with the above results only as far as ΔK_D is concerned. Table 1 shows that ΔK_S is not zero. However, we have used a different constitutive law from Lambropoulos.

Before discussing the nature of ΔK_D and ΔK_S we should emphasize that the small scale transformation condition is satisfied. This is because the

Stationary crack

The transformation zone for $\lambda = 0$ is shown in fig. 8. There is no shearing effect because $\gamma^T = 0$. The asterisks indicate the element integration stations where the condition for transformation was met. The transformed zone covers an area only 0.1% of the mesh. The nodal displacements of the elements near the external boundary of the domain (fig. 5) are identical within 3 significant figures to the linear elastic ones when transformation does not take place. The periphery of the transformation zone is shown in fig. 9. The curve denoted by the letter D is the periphery of the transformation zone used by McMeeking and Evans [19]. This last zone is given by $r = \frac{8}{3\sqrt{3}} w \cos^2 (\frac{\theta}{2})$ where the height w has been taken to agree with the height of the finite element zone.

The transformation zone for $\lambda = 1$ is shown in fig. 10. The boundary of the zone is shown in fig. 11 along with the zone used by McMeeking and Evans as described before. The zones have the same height as the zone for $\lambda = 0$. However, its leading front appears to be elongated along the x axis as $y \to 0$ compared to the other zone. As a result, an inflection point is observed. The zone boundary to the left of this point tends to be concave whereas the boundary to the right tends to be convex. It is worth noting that this tendency for elongation increases with increasing values of λ. This observation has been confirmed by the appearance of the zone boundaries that we generated for intermediate values of λ.

The SIF change calculations were carried out numerically by using the formulae (13) and (14) for the ΔK_D and ΔK_S changes respectively. These changes are shown in Table 1.

where [C] is the linear elastic stress-strain matrix for plane strain, for the composite, $\{T\}$ is the two-dimensional traction vector, $\{u_N\}$ is the nodal displacements and $\{E_T\}$ is the element transformation strain vector given by

$$\{E_T\} = \begin{matrix} \frac{2(1+\nu)}{3(1-2\nu)}\,\varepsilon^T - \gamma^T \sin 2\Omega \\ \frac{2(1+\nu)}{3(1-2\nu)}\,\varepsilon^T + \gamma^T \sin 2\Omega \\ \gamma^T \cos 2\Omega \end{matrix} \tag{22}$$

It is worth noting that the stiffness matrix [K] is independent of the transformation since it involves only the elasticity tensor [C] and the interpolation matrix [B]. The same is true for the vector $\{F_b\}$. However, the quantity $\{F_T\}$ depends on the transformation through $\{E_T\}$.

An iterative method was used to solve equations (21) as stated in section 5. All calculations were carried out for Poisson's ratio $\nu = 0.25$. Solutions were obtained for λ equal to 0, 0.25, 0.5, 0.75 and 1. Extremely rapid convergence was achieved with 3 iterations when the computed displacements were found to converge to within 3 significant figures.

7. RESULTS

In this section we shall discuss the results of the finite element analysis for the stationary crack problem. We shall also give the SIF changes for both stationary crack and quasi-statically advancing crack deduced through a model for that case. The shape and features of the transformation zone for the propagating crack are determined as discussed in section 4 starting from the stationary crack zone. However, the stationary crack zone is now the one deduced via the finite element calculations.

$$\int_A \varepsilon_{k\ell}\, C_{ijk\ell}\, \delta\varepsilon_{ij}\, dA = \int_S T_i\, \delta u_i\, ds + \int_A \varepsilon^T_{k\ell}\, C_{ijk\ell}\, \delta\varepsilon_{ij}\, dA \qquad (20)$$

Equation (20) illustrates the nonlinearity of the problem. That is, the second integral on the right hand side can only be determined after the solution is found. Thus, the solution procedure will involve iteration. Assuming a solution we determine the transformation zone. Next, we solve the resulting linear problem arising from equation (20) with the second integral on the right hand side evaluated and compare the solution with the assumed one. The process continues until convergence is achieved. The linear elastic solution can be used to initiate the process with $\varepsilon^T = 0$ i.e. with no transformed region. This method is addressed in detail in the next section.

6. FINITE ELEMENT CALCULATIONS

The finite element method was used to solve the boundary value problem as stated in the previous section. The domain (fig. 5) was discretized into 554 4-noded quadrilateral isoparametric elements with 4 integration stations. In figures 6 and 7 the 224 element near tip mesh and the 320 element far field mesh are shown respectively. The second mesh surrounds the first one. The fine near tip discretization was used in order to ensure that the transformation zone is determined fairly reliably. By using the standard element displacement and strain interpolation matrices [A] and [B] respectively, we rewrite the governing equation (20) as follows

$$[K]\,\{u_N\} = \{F_b\} + \{F_T\} \qquad (21a)$$

with

$$[K] = \int_A [B]^T\,[C]\,[B]\,dA \qquad \text{(stiffness matrix)} \qquad (21b)$$

$$\{F_b\} = \int_A [A]^T\,\{T\}\,ds \qquad \text{(applied load vector)} \qquad (21c)$$

$$\{F_T\} = \int_A [B]^T\,\{E_T\}\,ds \qquad \text{(transformation load vector)} \qquad (21d)$$

transformation zone appropriately. This is accomplished by taking into account the perturbation of the linear elastic crack field induced by the transformation. This subject is addressed in the next section.

5. THE BOUNDARY VALUE PROBLEM FOR THE STATIONARY CRACK

We are concerned with the stresses and deformations near the tip of a long crack in plain strain. The body is loaded so that only mode I (tensile opening mode) stresses arise at the tip. We are concerned with "small scale transformation" where the transformation zone is confined to a region very close to the crack tip. This can be achieved by imposing tractions on a circular boundary far from the tip in agreement with the standard singular linear elastic solution given by equation (5). Symmetry permits the analysis to be confined to a semi-circular domain as shown in fig. 5. The crack surface is traction free and the symmetry line is free of shear traction and displacements normal to the line.

The governing equations in the plane can be stated by the principle of virtual work in the absence of body forces.

$$\int_A \sigma_{ij}\, \delta\varepsilon_{ij}\, dA = \int_S T_i\, \delta u_i\, ds \tag{19}$$

where A is the area and S is the perimeter of the domain, T_i the tractions on S and u_i the displacements in A. The symbol δ indicates an arbitrary virtual variation of the quantity it precedes. In addition the stresses are related to the strains by the constitutive law given by equation (2). As a result, the governing equation (19) can be rewritten as follows

function of Δa , the amount of crack propagation. The slope versus Δa decreases continuously and the curve appears to approach an asymptote for large values of Δa. At that stage [19,20]

$$\frac{(1-\nu)\ \Delta K_D}{E\ \varepsilon^T\ v_f\ \sqrt{w}} = -\ 0.22 \tag{18}$$

To maintain the critical propagation value of $K = K_{IC}$ for the material at the crack tip the loads would have to be increased with Δa. This will mean an apparent higher value of $K = K_A$ computed from the applied loads. The material will appear to be toughened as a result.

Consider now the shearing contribution to ΔK. According to our hypothesis, particles enter the transformation zone ahead of the crack and the direction of shearing transformation will be determined by the state of stress there. We assume still that the stress field is unperturbed by the presence of a zone and so Ω equals to current value of $\frac{3\theta}{4}$ measured from the crack tip. As the crack propagates by, this value of Ω will remain unchanged for that particle. Thus all particles on a line parallel to the crack will have the same value of Ω , except those in the zone created before the crack propagated (fig. 3). The resulting contribution ΔK_S from such a wake zone is negative. The maximum of the absolute value of ΔK_S for all λ is achieved when the crack propagates 0.5w whereas the maximum of the absolute value of ΔK_D as found from equation (18), is achieved at $\Delta a = 5w$. In figure 4 the ratio $|\Delta K_S|_{max}/|\Delta K_D|_{max}$ is shown plotted against the ratio λ. As it is seen, the amount of the shearing contribution to the toughening can become the same as that of the dilatant contribution when λ approaches 1. In conclusion, the importance of the shearing contribution raises the need for a more rigorous estimation. Therefore, it is required that we compute the

Results for stationary crack

In this case, the transformed zone has a perimeter which is the locus of points of equal hydrostatic stress. McMeeking and Evans [19] and Budiansky et al. [20] have shown that $\Delta K_D = 0$ for this case.

As far as the shearing contribution is concerned, Ω is taken to be the angle to the principal shearing direction when the material transformed, i.e. at the edge of the zone then prevailing. The stress state is taken to be the unperturbed linear crack tip field and thus $\Omega = \frac{3\theta}{4}$. As a result

$$\frac{(1-\nu)\ \Delta K_S}{E\ \varepsilon^T\ v_f\ \sqrt{w}} = 0.15\lambda \tag{17}$$

where w is the height of the transformation zone as shown in fig. 2, λ is the ratio γ^T/ε^T and $\nu = 0.3$. The transformation strain has been rewritten as $v_f\ \gamma_p^T$ where γ_p^T is the unconstrained transformation strain after twinning for an individual particle.

Equations (16) and (17) indicate that the shearing effect causes fracture toughness reduction. This reduction becomes larger as λ increases i.e. the shear strain γ^T increases for a given ε^T. As a consequence, crack propagation may occur more readily than in the absence of transformation.

Results for propagating crack

If the crack propagates quasi-statically and there is no reverse transformation, a wake of transformed material is left along the newly created crack surfaces. This wake will be parallel to the crack surfaces if we assume that the tip propagates at a constant value of K (fig. 3). The dilatant contribution to ΔK due to such a transformed zone has been studied by McMeeking and Evans [19] and has been found to be a monotonically decreasing

McMeeking and Evans [19] have shown that

$$\Delta K_D = \frac{E\ \varepsilon^T}{6\ \sqrt{2\pi}\ (1-\nu)} \int_{A_T} r^{-\frac{3}{2}} \cos(\frac{3\theta}{2})\ dA \tag{13}$$

where E is the Young's modulus. From the form of the weight function $\underline{h}$ and $\underset{\sim}{e}^T$ it can be deduced that

$$\Delta K_S = \frac{3E\ \gamma^T}{8\ \sqrt{2\pi}\ (1-\nu^2)} \int_{A_T} r^{-\frac{3}{2}} \cos(2\Omega - \frac{3\theta}{2}) \sin\theta\ dA \tag{14}$$

The fact that $\cos(\frac{3\theta}{2})$ is an even function of θ allows the integral in equation (13) to be computed in the region $0 < \theta < \pi$ (figures 2,3). The same argument applies to equation (14) because $\gamma^T \sin\theta$ is an even function of θ. That is because both γ^T and $\sin\theta$ are odd functions of θ.

The SIF change ΔK is related to the applied field K_A as follows

$$K_t = K_A + \Delta K \tag{15}$$

where K_t is the S.I.F. that actually describes the crack tip field when the transformation has taken place. If ΔK is negative equation (15) implies that the stress intensity at the crack tip is lower than that associated with the applied loads. In particular, since the crack propagates when K_t becomes equal to the fracture toughness K_{IC} of the pretransformed material [14] the apparent fracture toughness K_{IC}^A is given by

$$K_{IC}^A = K_{IC} - \Delta K \tag{16}$$

If ΔK is negative the material appears to be tougher than the pretransformed one.

principle of virtual work

$$\Delta K = -\int_{A_T} \sigma^R_{ij}\, h_{j,i}\, ds \tag{9}$$

Substitution of (8a) into (9) furnishes

$$\Delta K = \int_{A_T} (\varepsilon^T_{ij} - \varepsilon^R_{ij} - \varepsilon^S_{ij})\, C_{ijk\ell}\, h_{\ell,k}\, dA \tag{10}$$

As further noted by Rice [25] $C_{ijk\ell}\, h_{\ell,k}$ is a stress field in equilibrium in A_T because $\underline{h}$ is related to the difference between two displacement fields each possessing equilibrium stress fields. This means that the virtual work principle can be used to show

$$\int_{A_T} (\varepsilon^R_{ij} + \varepsilon^S_{ij})\, C_{ijk\ell}\, h_{\ell,k}\, dA_T = \int_{S_T} n_i\, C_{ijk\ell}\, h_{\ell,k} (u^R_j + u^S_j)\, dS$$

$$= 0 \quad \text{due to (8c)}$$

This means that equation (10) is written as

$$\Delta K = \int_{A_T} \varepsilon^T_{ij}\, C_{ijk\ell}\, h_{\ell,k}\, dA_T \tag{11}$$

For isotropic material, equation (11) becomes

$$\Delta K = \Delta K_D + \Delta K_S \tag{12a}$$

where $\Delta K_D = B \int_{A_T} \varepsilon^T\, h_{k,k}\, dA$ (dilatational contribution) (12b)

$\Delta K_S = 2\mu \int_{A_T} e^T_{ij}\, h_{i,j}\, dA$ (shearing contribution) (12c)

constraint within A_T. This will give rise to an elastic stress such that

$$\sigma^S_{ij} = C_{ijk\ell}\,(\varepsilon^S_{k\ell} - \varepsilon^T_{k\ell})$$

$$\sigma^S_{ij,i} = 0 \qquad \text{in } A_T \tag{7}$$

$$n_i\,\sigma^S_{ij} = 0 \qquad \text{on } S_T$$

where $\underline{n}$ is the unit outward normal to S_T and $\sigma^S_{ij,i} = \dfrac{\partial\sigma^S_{ij}}{\partial x_i}$ with x_i denoting position in a fixed cartesian coordinate system. Tractions are now applied around A_T producing further displacements $\underline{u}^R$ and strains $\underset{\sim}{\varepsilon}^R$ so that A_T has its original shape prior to transformation. As a result

$$\sigma^R_{ij} = C_{ijk\ell}\,(\varepsilon^R_{k\ell} + \varepsilon^S_{k\ell} - \varepsilon^T_{k\ell}) \tag{8a}$$

$$\sigma^R_{ij,i} = 0 \qquad \text{in } A_T \tag{8b}$$

$$u^R_i + u^S_i = 0 \qquad \text{on } S_T. \tag{8c}$$

Using σ^R_{ij} we can express $\underline{T}^c$ as follows

$$T^c_j = -\,n_i\,\sigma^R_{ij}$$

Thus, equation (6) becomes

$$\Delta K = -\int_{S_T} n_i\,\sigma^R_{ij}\,h_j\,ds$$

As noted by Rice [25], $\underline{h}$ can be treated as a displacement and so by the

$$\Delta K = -1.70 \quad \text{MPa}\sqrt{m}$$

iv) experimentally measured value

$$\Delta K = -2.4 \quad \text{MPa}\sqrt{m} \text{ (implies } \lambda \simeq 1.7)$$

For another system whose the parameters are [21]: $E = 470$ GPa, $\varepsilon^T = 0.04$ $w = 5.10^{-6}$m, $v_f = 0.3$ one has

i) with purely dilatant transformation

$$\Delta K = -3.96 \quad \text{MPa}\sqrt{m}$$

ii) with both parts of the transformation and $\lambda = 1$

$$\Delta K = -6.30 \quad \text{MPa}\sqrt{m}$$

iii) Lambropoulos' result (both parts of the transformation, spherical particles and $K_{IC} = 6$ MPa $\sqrt{m}$)

$$\Delta K = -4.5 \quad \text{MPa}\sqrt{m}$$

iv) experimentally measured value

$$\Delta K = -6 \quad \text{MPa}\sqrt{m} \text{ (implies } \lambda \simeq 0.9)$$

In the case of the <u>MgO partially stabilized Zirconia</u> whose parameters are [19]: $E = 200$ GPa, $\varepsilon^T = 0.058$, $w = 6.10^{-6}$m, $v_f = 0.3$ one has:

i) with purely dilatant transformation

$$\Delta K = -0.85 \quad \text{MPa}\sqrt{m}$$

ii) with both parts of the transformation and $\lambda = 1$

$$\Delta K = -1.35 \quad \text{MPa}\sqrt{m}$$

iii) Lambropoulos' result (both parts of the tranformation, spherical particles and $K_{IC} = 1.97$ MPa $\sqrt{m}$)

$$\Delta K = -1.04 \quad \text{MPa}\sqrt{m}$$

iv) experimentally measured value

$$\Delta K = -2.3 \quad \text{MPa}\sqrt{m} \quad (\text{implies } \lambda \simeq 3)$$

The preceding toughness enhancement calculations should be regarded tentative because of the uncertainties involved in the material parameters. Nevertheless, it is clear that the predicted toughness increase may be in agreement with the experimental data when the shearing contribution is considered in the transformation mechanism analysis. An important role is played by the parameter λ which determines the amount of the shearing contribution. We have arbitrarily used 1 because we have no information on what values may be realistic. Alternately, we can compute a value of λ necesssary to bring our estimates into agreement with the experimental values. These are the implied values of λ listed. Some of these values are rather large. However, the amount of shear strain during transformation is typically quite large compared to the dilatation. Even if substantial amounts of this are nullified by twinning, this could still leave values of λ of the order implied.

9. CLOSURE

For further and more elaborate treatment of the shear effect one may need to incorporate size and particle orientation effects via a more realistic constitutive law for the composite. This must include a consideration of the effect of twinning during the transformation. However, our simple calculations have indicated that shear strain effects may be significant and that further work on the mechanics of the phenomenon may be profitable.

ACKNOWLEDGEMENT

This research was supported by the Office of Naval Research through Contract NR 064-N00014-81-K-0650 with the University of Illinois.

REFERENCES

1. A. G. Evans and A. H. Heuer: J. Am. Ceram. Soc., 63, 241 (1980).

2. R. C. Garvie, R. H. Hannink and R. T. Pascoe: Nature, 258, 703 (1975).

3. N. Claussen: J. Am. Ceram. Soc., 59, 49 (1976).

4. T. G. Gupta, F. F. Lange and J. H. Bechtold: J. Mater. Sci., 13, 1464 (1978).

5. D. L. Porter, A. G. Evans and A. H. Heuer: Acta Metall., 27, 1649 (1979).

6. D. L. Porter and A. H. Heuer: J. Am. Ceram. Soc., 60, 183 (1977).

7. L. H. Schoenlein and A. H. Heuer: Fracture Mechanics of Ceramics, R. C. Bradt et al., Eds., Plenum Press, Vol. 6, 309 (1983).

8. P. F. Becher and V. J. Tennery: Fracture Mechanics of Ceramics, R. C. Bradt et al., Eds., Plenum Press, Vol. 6, 383 (1983).

9. H. Ruf and A. G. Evans: J. Am. Ceram. Soc., 66, 328 (1983).

10. F. F. Lange: J. Mater. Sci., 17, 225 (1982).

11. M. V. Swain, R. H. Hannink and R. C. Garvie: Fracture Mechanics of Ceramics, R. C. Bradt et al., Eds., Plenum Press, Vol. 6, 339 (1983).

12. A. G. Evans, N. Burlingame, M. Drory and W. M. Kriven: Acta Metall., 29, 447 (1981).

13. A. H. Heuer: Advances in Ceramics, American Ceramics Society, A. H. Heuer and L. W. Hobbs, Eds., Vol. 3, 98 (1981).

14. A. G. Evans: Advances in Ceramics, American Ceramics Society, N. Claussen, M. Ruhle and A. H. Heuer, Eds., Vol. 12, 193 (1984).

15. M. V. Swain and R.H.J. Hannink: Advances in Ceramics, American Ceramics Society, N. Claussen, M. Ruhle and A. H. Heuer, Eds., Vol. 12, 225 (1984).

16. G. K. Bansal and A. H. Heuer: Acta Metall. 20, 1281 (1972).

17. G. K. Bansal and A. H. Heuer: Acta Metall. 22, 409 (1974).

18. G. M. Wolten: J. Am. Ceram. Soc., 46, 418 (1963).

19. R. M. McMeeking and A. G. Evans: J. Am. Ceram. Soc., 65, 242 (1982).

20. B. Budiansky, J. W. Hutchinson and J. C. Lambropoulos: Int. J. Solids Structures, 19, 337 (1983).

21. J. C. Lambropoulos: "Shear, Shape and Orientation Effects in Transformation Toughening". Harvard University Report, Division of Applied Sciences, MECH-55 (July 1984).

22. J. D. Eshelby: Proc. Roy. Soc., A 241, 376 (1957).

23. J. R. Rice and D. M. Tracey: Numerical and Computer methods in structural mechanics, S. J. Fenves et al., Eds. (Academic Press, New York, 1973) 585-623.

24. J. R. Rice: Fracture: an advanced treatice 2, H. Liebowitz, Ed. (Academic Press, New York, 1968) 191-311.

25. J. R. Rice: Int. J. Solids Structures, 8, 751 (1972).

TABLE CAPTIONS

Table 1. Stress intensity factor changes for the stationary crack calculated by the finite element method.

Table 2. Stress intensity factor changes for the propagating crack when $\lambda = \gamma^T/\varepsilon^T = 0$ deduced from the finite element calculations.

Table 3. Stress intensity factor changes for the propagating crack when $\lambda = \gamma^T/\varepsilon^T = 0.5$ deduced from the finite element calculations.

Table 4. Stress intensity factor changes for the propagating crack when $\lambda = \gamma^T/\varepsilon^T = 1$ deduced from the finite element calculations.

Table 5. Maximum fracture toughness changes achieved after the crack has advanced quasi-statically.

Table 1

Stress Intensity Factor Changes for the Stationary Crack

λ	w (zone height)	$\frac{(1-\nu)\ \Delta K_D}{E\ e^T\ v_f\ \sqrt{w}}$	$\frac{(1-\nu)\ \Delta K_S}{E\ e^T\ v_f\ \sqrt{w}}$
0.00	2.14	-0.0085	0.0000
0.25	2.14	-0.0066	0.0381
0.50	2.14	-0.0066	0.0762
0.75	2.14	-0.0049	0.1145
1.00	2.14	-0.0049	0.1527

ΔK_D = Dilatational SIF change

ΔK_S = Shearing SIF change

Table 2

Stress Intensity Factor Changes for the Advancing Crack When $\lambda = 0$

$\frac{\Delta a}{w}$	$\frac{(1-\nu)\,\Delta K_D}{E\,e^T\,v_f\,\sqrt{w}}$	$\frac{(1-\nu)\,\Delta K_S}{E\,e^T\,v_f\,\sqrt{w}}$	$\frac{(1-\nu)\,\Delta K}{E\,e^T\,v_f\,\sqrt{w}}$
0.0	-0.0085	0	-0.0085
0.2	-0.0780	0	-0.0780
0.5	-0.1270	0	-0.1270
0.8	-0.1550	0	-0.1550
1.1	-0.1723	0	-0.1723
2.0	-0.1961	0	-0.1961
3.0	-0.2055	0	-0.2055
4.0	-0.2097	0	-0.2097
5.0	-0.2119	0	-0.2119
7.0	-0.2142	0	-0.2142
10.0	-0.2157	0	-0.2157
15.0	-0.2167	0	-0.2167
20.0	-0.2171	0	-0.2171
30.0	-0.2174	0	-0.2174

$\frac{\Delta a}{w}$ = Dimensionless crack advance

ΔK_D = Dilatational SIF change

ΔK_S = Shearing SIF change

ΔK = Total SIF change

Table 3

Stress Intensity Factor Changes for the Advancing Crack When $\lambda = 0.5$

$\frac{\Delta a}{w}$	$\frac{(1-\nu)\ \Delta K_D}{E\ e^T\ v_f\ \sqrt{w}}$	$\frac{(1-\nu)\ \Delta K_S}{E\ e^T\ v_f\ \sqrt{w}}$	$\frac{(1-\nu)\ \Delta K}{E\ e^T\ v_f\ \sqrt{w}}$
0.0	-0.0066	0.0762	0.0695
0.3	-0.0961	-0.0954	-0.1915
0.6	-0.1362	-0.1057	-0.2419
1.0	-0.1656	-0.0860	-0.2516
2.0	-0.1943	-0.0376	-0.2319
3.0	-0.2037	-0.0312	-0.2348
4.0	-0.2079	-0.0298	-0.2377
5.0	-0.2101	-0.0287	-0.2388
10.0	-0.2139	-0.0268	-0.2407
15.0	-0.2149	-0.0258	-0.2406
20.0	-0.2153	-0.0247	-0.2400
30.0	-0.2156	-0.0230	-0.2386

$\frac{\Delta a}{w}$ = Dimensionless crack advance

ΔK_D = Dilatational SIF change

ΔK_S = Shearing SIF change

(ΔK) = Total SIF change

Table 4

Stress Intensity Factor Changes for the Advancing Crack When $\lambda = 1$

$\frac{\Delta a}{w}$	$\frac{(1-\nu)\,\Delta K_D}{E\,e^T\,v_f\,\sqrt{w}}$	$\frac{(1-\nu)\,\Delta K_S}{E\,e^T\,v_f\,\sqrt{w}}$	$\frac{(1-\nu)\,\Delta K}{E\,e^T\,v_f\,\sqrt{w}}$
0.0	-0.0049	0.1527	0.1479
0.3	-0.0944	-0.1904	-0.2848
0.6	-0.1344	-0.2110	-0.3454
1.0	-0.1638	-0.1718	-0.3356
2.0	-0.1925	-0.0744	-0.2669
3.0	-0.2019	-0.0620	-0.2638
4.0	-0.2061	-0.0592	-0.2653
5.0	-0.2084	-0.0570	-0.2653
10.0	-0.2121	-0.0532	-0.2653
15.0	-0.2131	-0.0512	-0.2643
20.0	-0.2135	-0.0492	-0.2626
30.0	-0.2138	-0.0455	-0.2594

$\frac{\Delta a}{w}$ = Dimensionless crack advance

ΔK_D = Dilatational SIF change

ΔK_S = Shearing SIF change

ΔK = Total SIF change

Table 5

"Asymptotic" Fracture Toughness Changes for the Quasi-Statically Advancing Crack

λ	$\frac{\Delta a}{w}$	$\frac{(1-\nu)\ \Delta K}{E\ e^T\ v_f\ \sqrt{w}}$
0.00	5.0	-0.2119
0.25	3.2	-0.2202
0.50	0.9	-0.2527
0.75	0.8	-0.2991
1.00	0.7	-0.3494

$\lambda = \gamma^T/\varepsilon^T$

$\frac{\Delta a}{w}$ = Dimensionless crack advance

ΔK = SIF change

Figure Captions

Fig. 1 a. Direction Ω of the maximum shear stress τ

b. Shape change of an unconstrained transforming element. The shearing direction is along the maximum shear stress direction.

Fig. 2. Transformation zone shape based on critical hydrostatic stress transformation and the unperturbed elastic solution for the stationary crack. The maximum height w of the zone appears at $\phi = 60°$. The shearing direction Ω at transformation is also indicated at an arbitrary point (r,θ).

Fig. 3. Transformation zone shape for the quasi-statically advancing crack. The flank of the zone is parallel to the crack surface and tangent to the leading front of the zone at $\theta = 60°$. The shearing direction of the newly transforming elements is determined by the angle Ω at the leading front of the zone. The initially transformed elements retain their own shearing directions.

Fig. 4. Comparison of the maximum shearing contribution to the toughness enhancement with the maximum dilatant contribution. Those contributions are derived from a zone shape shown in fig. 3 when the crack propagated. The zone for the stationary crack is shown in fig. 1. The ΔK_S is achieved after $\Delta a = 0.5w$ whereas the ΔK_D is achieved after $\Delta a = 5w$.

Fig. 5. Domain and boundary conditions for the boundary value problem for the stationary crack.

Fig. 6. Near tip finite element mesh.

Fig. 7. Far field finite element mesh which surrounds the mesh shown in fig. 6.

Fig. 8. Transformation zone for the stationary crack in the case of purely dilatant transformation ($\gamma^T = 0$) derived by solving the boundary value problem by the finite element method.

Fig. 9. Comparison of the zone boundary of fig. 8 with the zone boundary derived by McMeeking and Evans [19] for the purely dilatational transformation and marked D. (fig. 2).

Fig. 10. Transformation zone for the stationary crack when the unconstrained shear transformation strain is equal to the unconstrained volume dilatation. The zone has been derived by solving the boundary value problem by the finite element method.

Fig. 11. Comparison of the zone boundary of fig. 10 with the zone boundary derived by McMeeking and Evans [19] for the purely dilatational transformation (fig. 2) (D).

Fig. 12. The R-curve predicted from the stress intensity factor analysis in the case of purely dilatational transformation.

Fig. 13. The R-curve predicted from the stress intensity factor analysis in the case when the unconstrained shear transformation strain is equal to the unconstrained volume dilatation.

a.

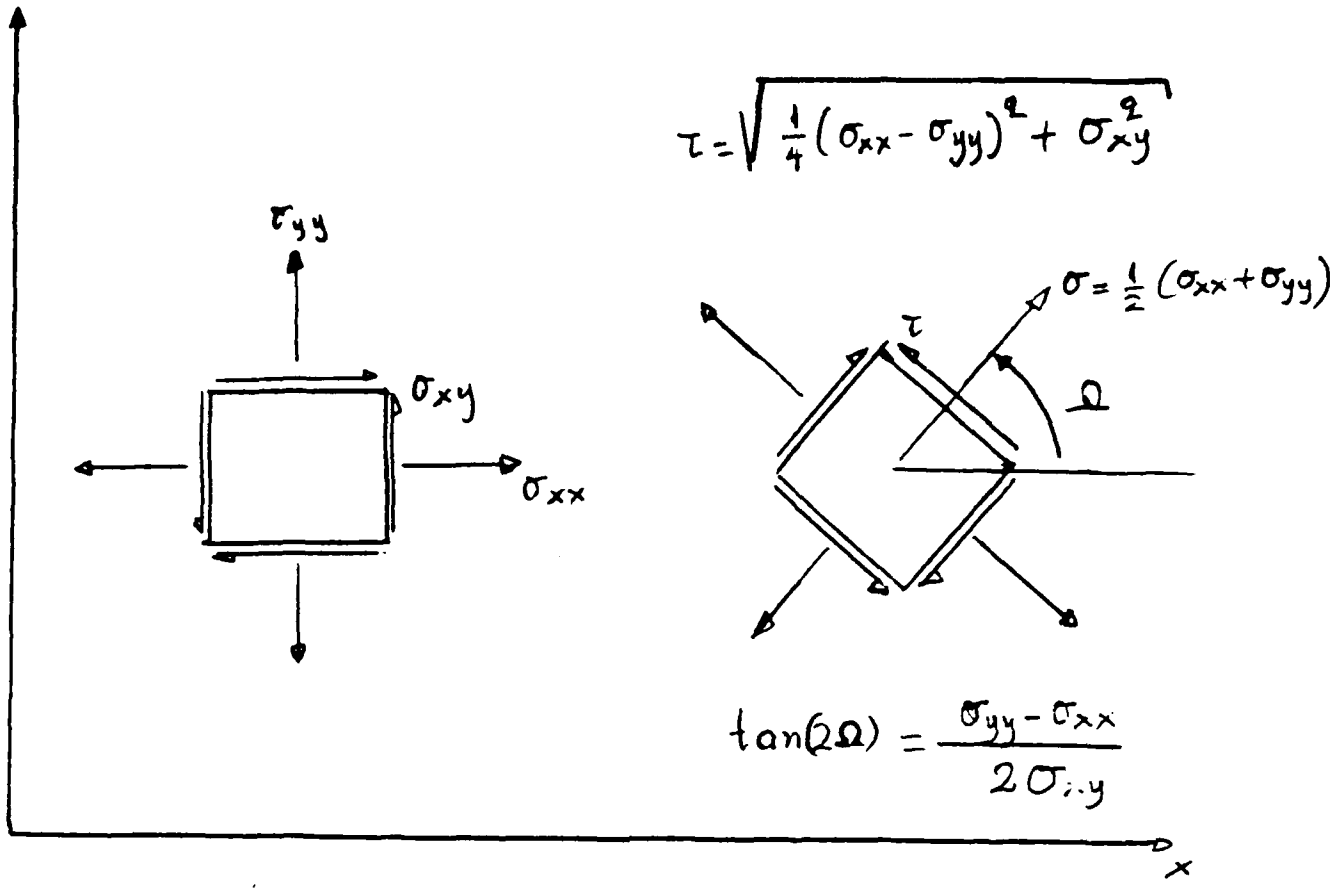
y
x
σ_{yy}
σ_{xy}
σ_{xx}
$\tau = \sqrt{\frac{1}{4}(\sigma_{xx} - \sigma_{yy})^2 + \sigma_{xy}^2}$
$\sigma = \frac{1}{2}(\sigma_{xx} + \sigma_{yy})$
τ
Ω
$\tan(2\Omega) = \frac{\sigma_{yy} - \sigma_{xx}}{2\sigma_{xy}}$

b.

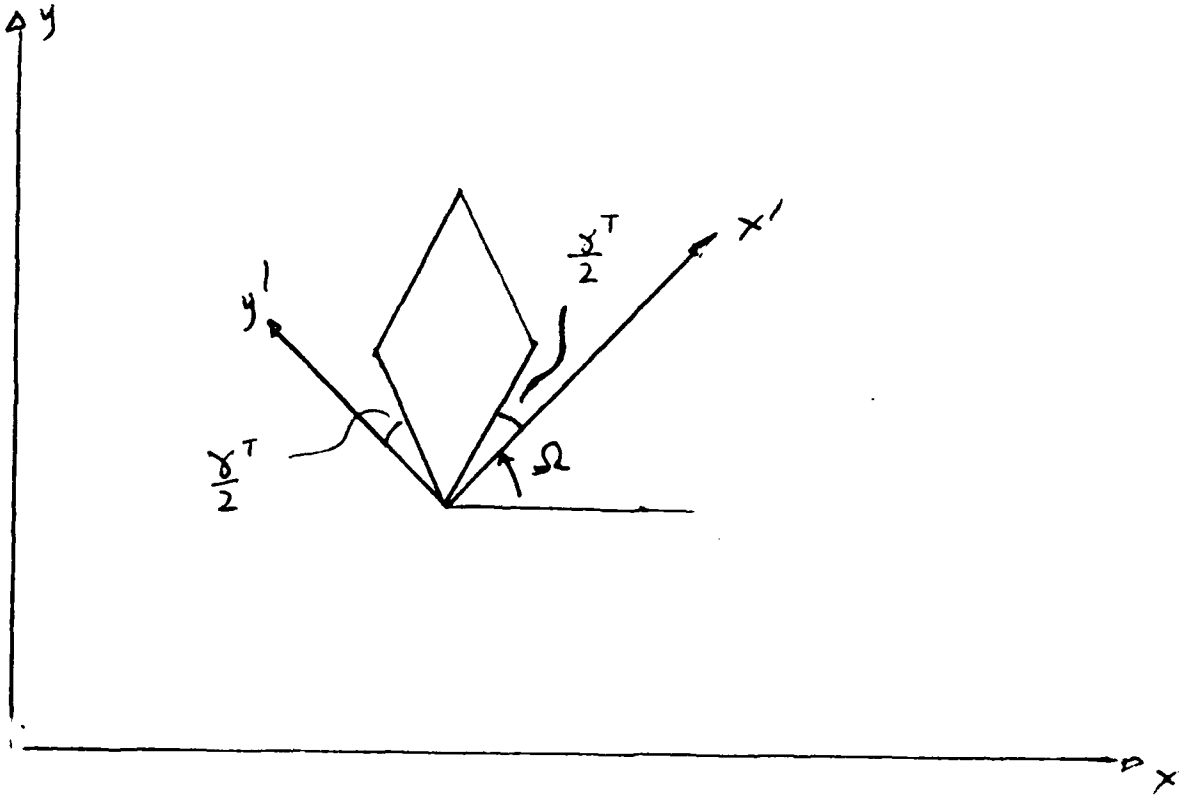
y
x
x'
y'
$\frac{\gamma^T}{2}$
$\frac{\gamma^T}{2}$
Ω

fig 1

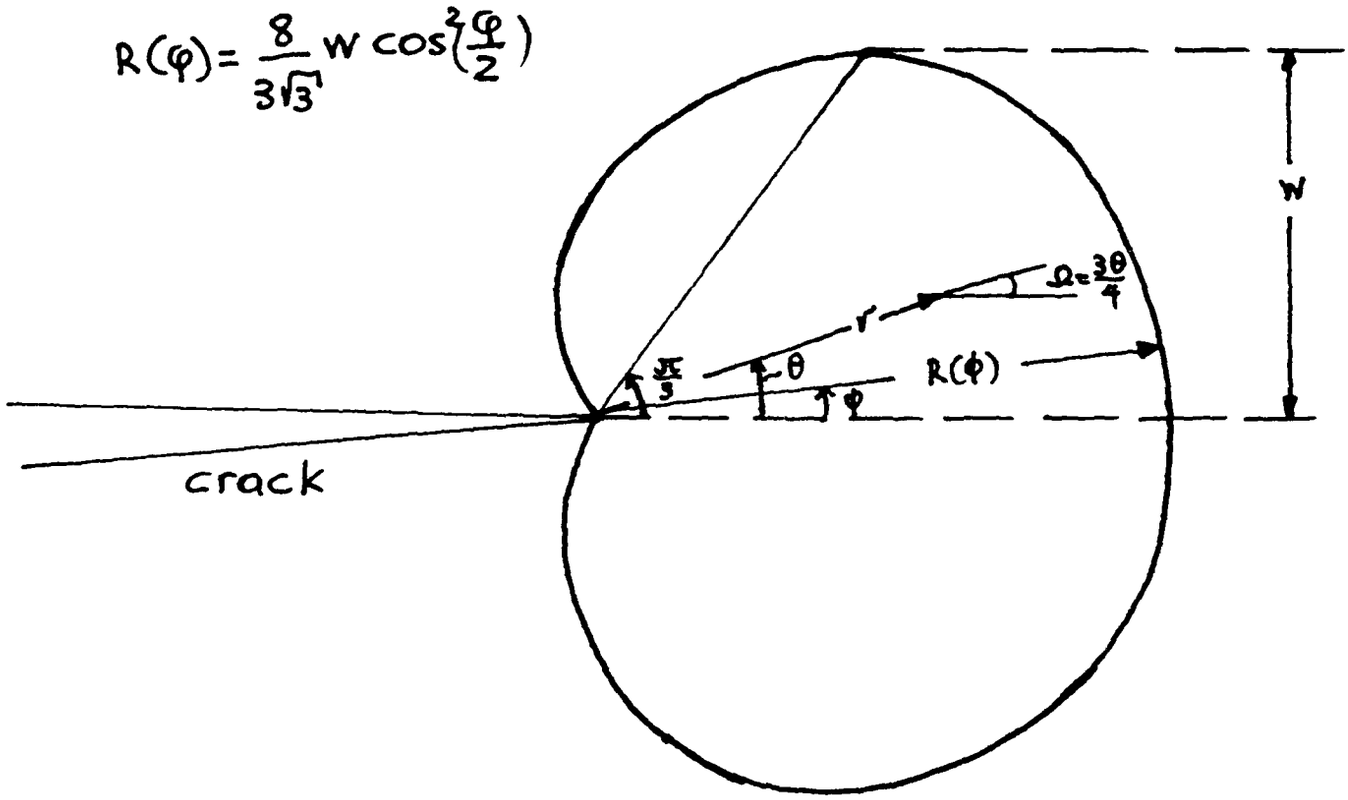
$R(\varphi) = \frac{8}{3\sqrt{3}} W \cos^2\left(\frac{\varphi}{2}\right)$
W
$\Omega = \frac{3\theta}{4}$
r
$\frac{\pi}{3}$
θ
$R(\phi)$
ϕ
crack

fig 2.

SUMMARY

A continuum mechanics description, of the phenomenon of stress induced microcracking has been used to study the near tip stress and strain fields and the size and shape of a small scale damaged zone for a stationary mode I crack in an elastic body. The material model is characterized by a microcracking criterion, which is an extension and simplification of the generalized microcracking criterion proposed by Fu and Evans [10] for the case of thermal stress-induced microcracking. That together with approximate expressions relating the effective composite moduli to the elastic properties of the brittle material, via the microcrack density ε first introduced by Budiansky and O'Connell [1], yield a self consistent approach to the stress induced microcracking phenomenon.

The microcrack density was found to characterize three regions of interest. In the outer region the microcrack density is zero and the stress and strain fields are purely those for linear elastic deformation. This elastic field constrains the microcracking deformation which in combination with material weakening due to microcracking causes stress relaxation in a region of intermediate microcracking. Very close to the crack tip the microcrack density is saturated and the stress field becomes again singular but with a lower stress intensity than would prevail in the absence of microcracking. In the case where very rapid microcracking occurs as the strain is increased, the intermediate microcracking zone is still present providing continuity of the strain field and a smooth transition of the stress field from the purely elastic region to the region with saturated microcrack density. It appears that the existance of the region of intermediate microcrack density is essential to preserving the assumption of a continuum composite because it helps to avoid any strain and stress discontinuity.

MECHANICS OF NEAR TIP MICROCRACKING IN BRITTLE MATERIAL

P. Charalambides and R. M. McMeeking
Department of Theoretical and Applied Mechanics
University of Illinois at Urbana-Champaign

March 1985

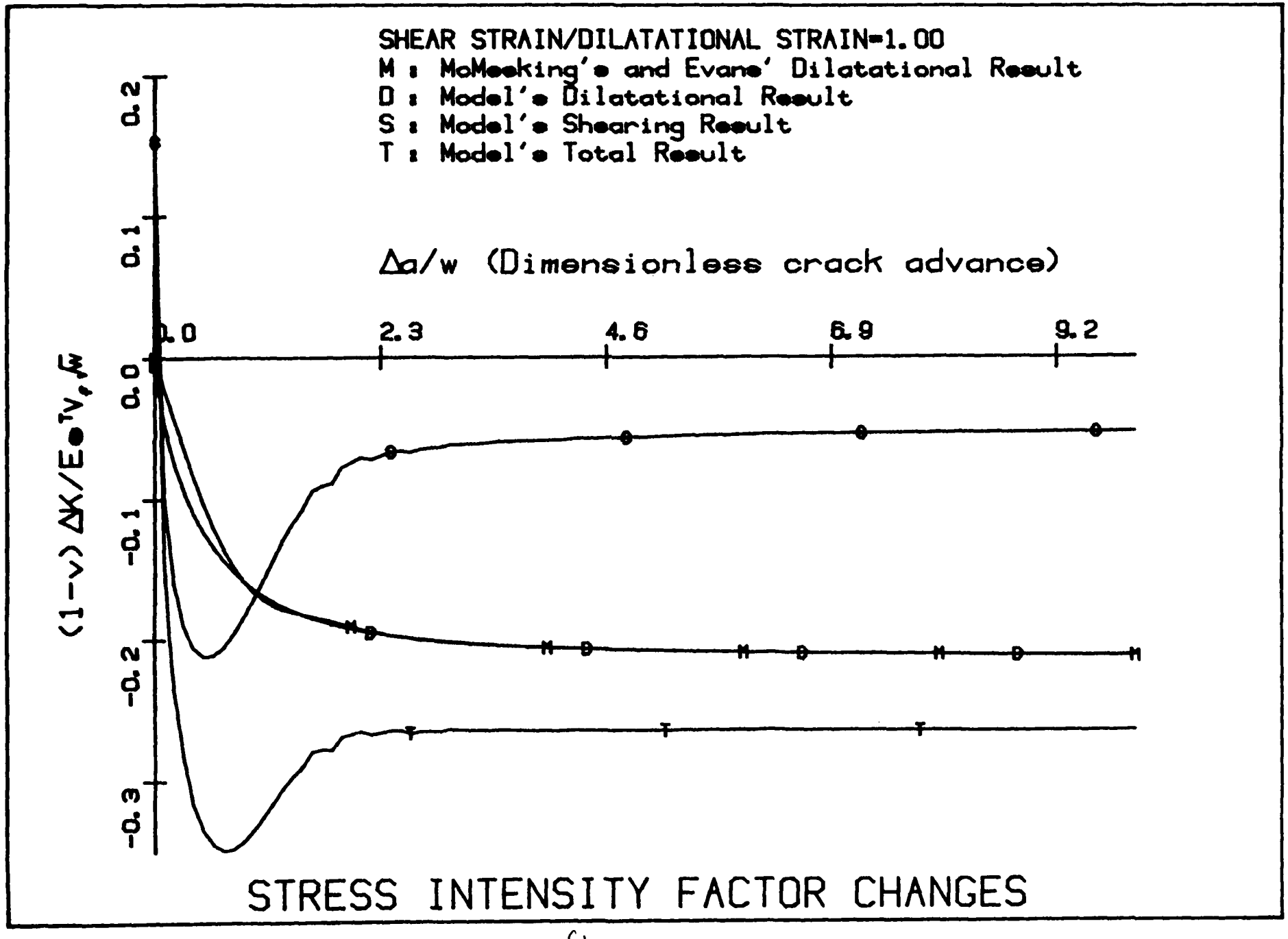
SHEAR STRAIN/DILATATIONAL STRAIN=1.00
M : McMeeking's and Evans' Dilatational Result
D : Model's Dilatational Result
S : Model's Shearing Result
T : Model's Total Result
Δa/w (Dimensionless crack advance)
0.0
2.3
4.6
6.9
9.2
0.2
0.1
0.0
-0.1
-0.2
-0.3
(1-ν) ΔK/E•τV_p√W
STRESS INTENSITY FACTOR CHANGES

fig 13

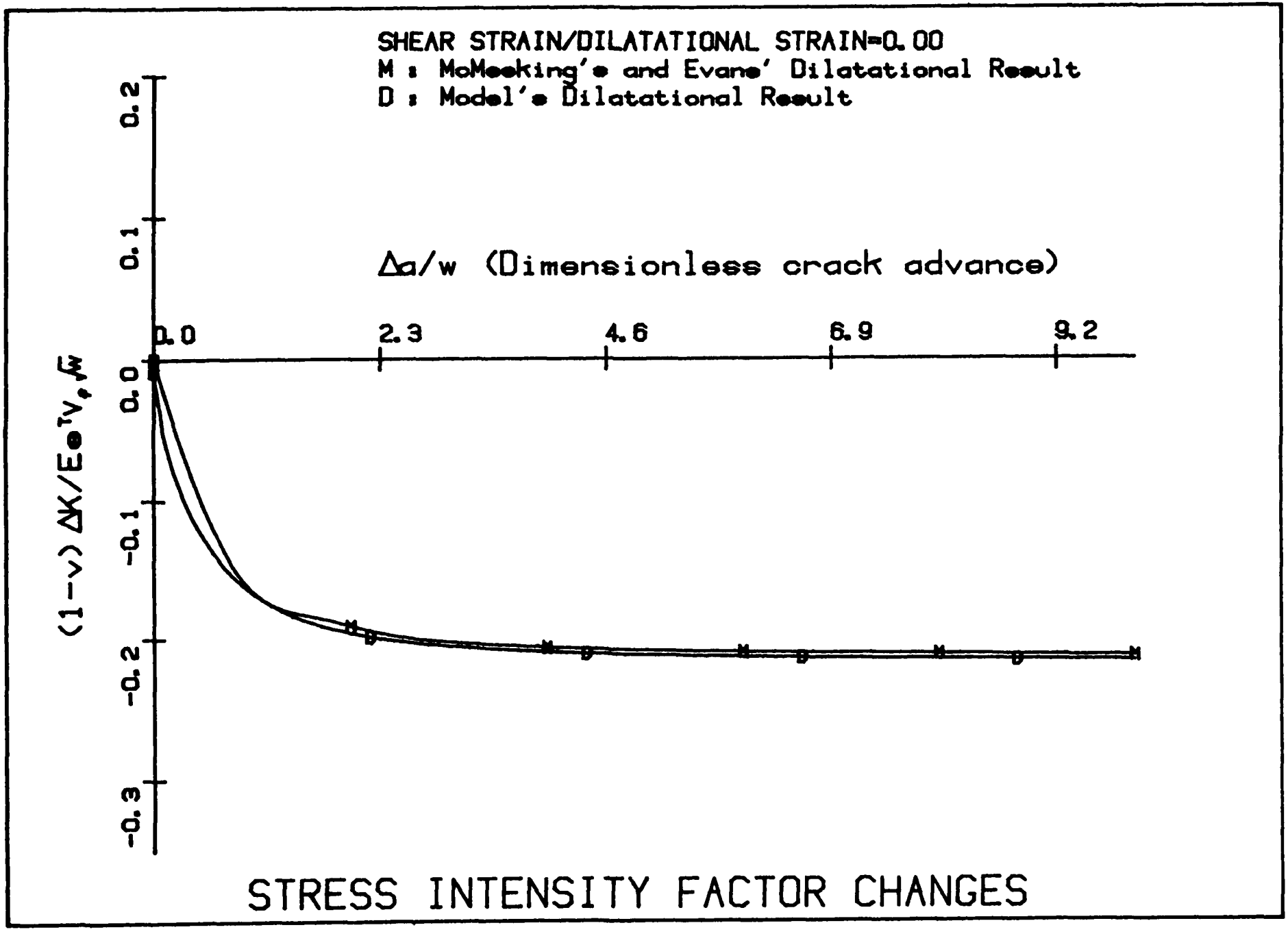
SHEAR STRAIN/DILATATIONAL STRAIN=0.00
M : McMeeking's and Evans' Dilatational Result
D : Model's Dilatational Result
Δa/w (Dimensionless crack advance)
0.0
2.3
4.6
6.9
9.2
0.2
0.1
0.0
-0.1
-0.2
-0.3
(1-ν) ΔK/Eε^T V_p √w
STRESS INTENSITY FACTOR CHANGES

fig. 12

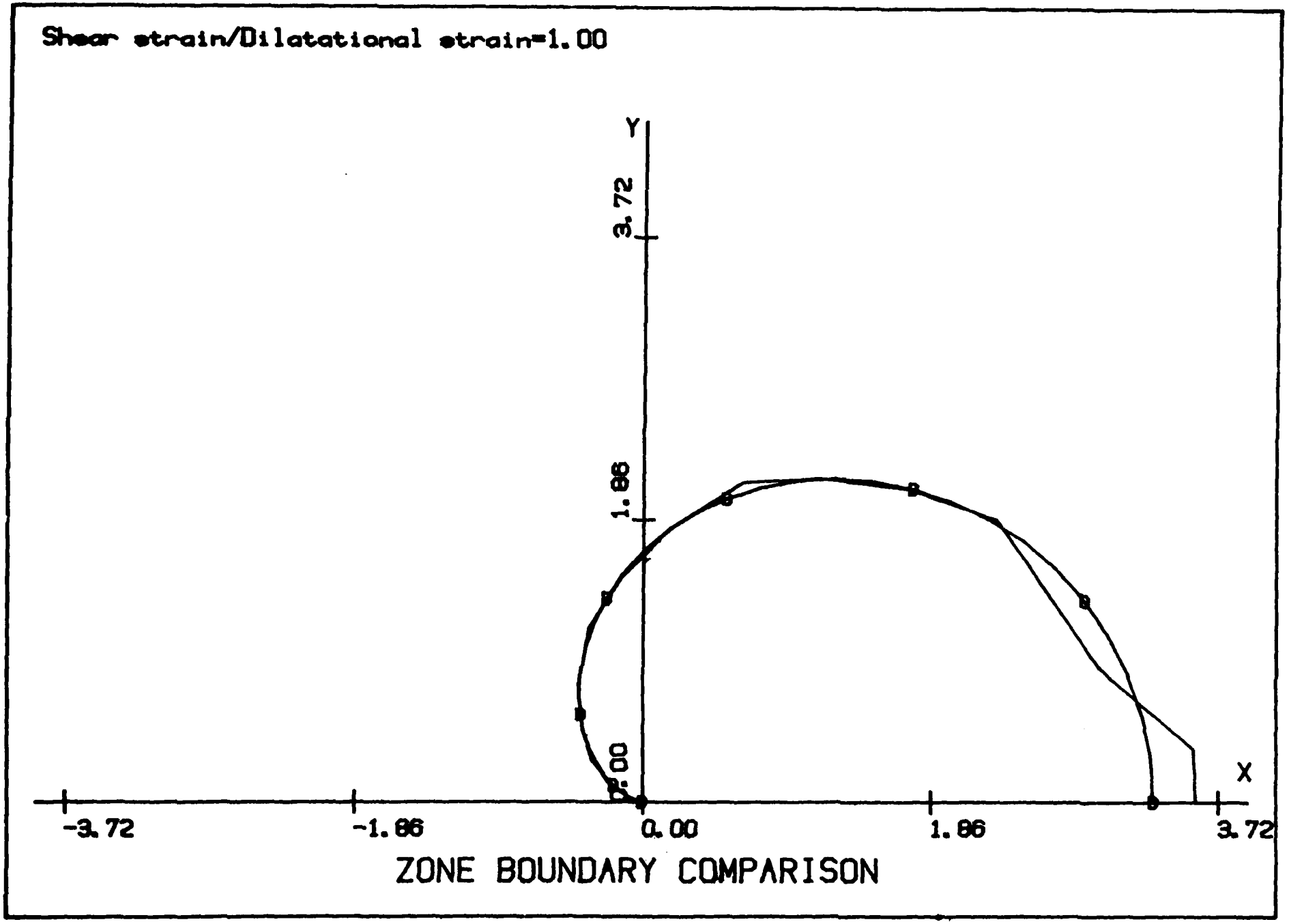
Shear strain/Dilatational strain=1.00
Y
3.72
1.86
0.00
X
-3.72
-1.86
0.00
1.86
3.72
ZONE BOUNDARY COMPARISON

fig 11

Radial distance of the furthest transformed point= 3.38

Shear strain/Dilatational strain=1.00

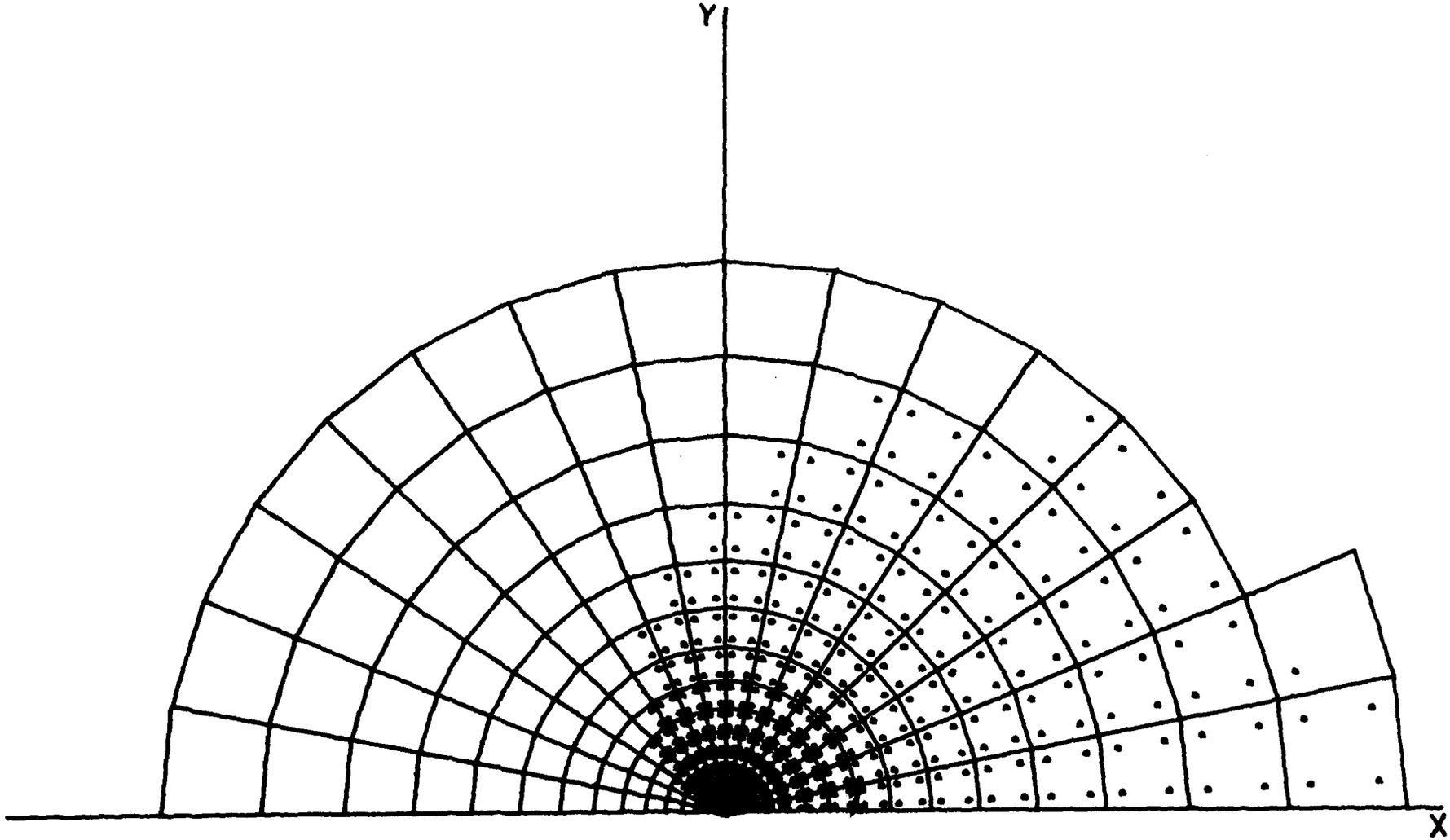

TRANSFORMATION ZONE

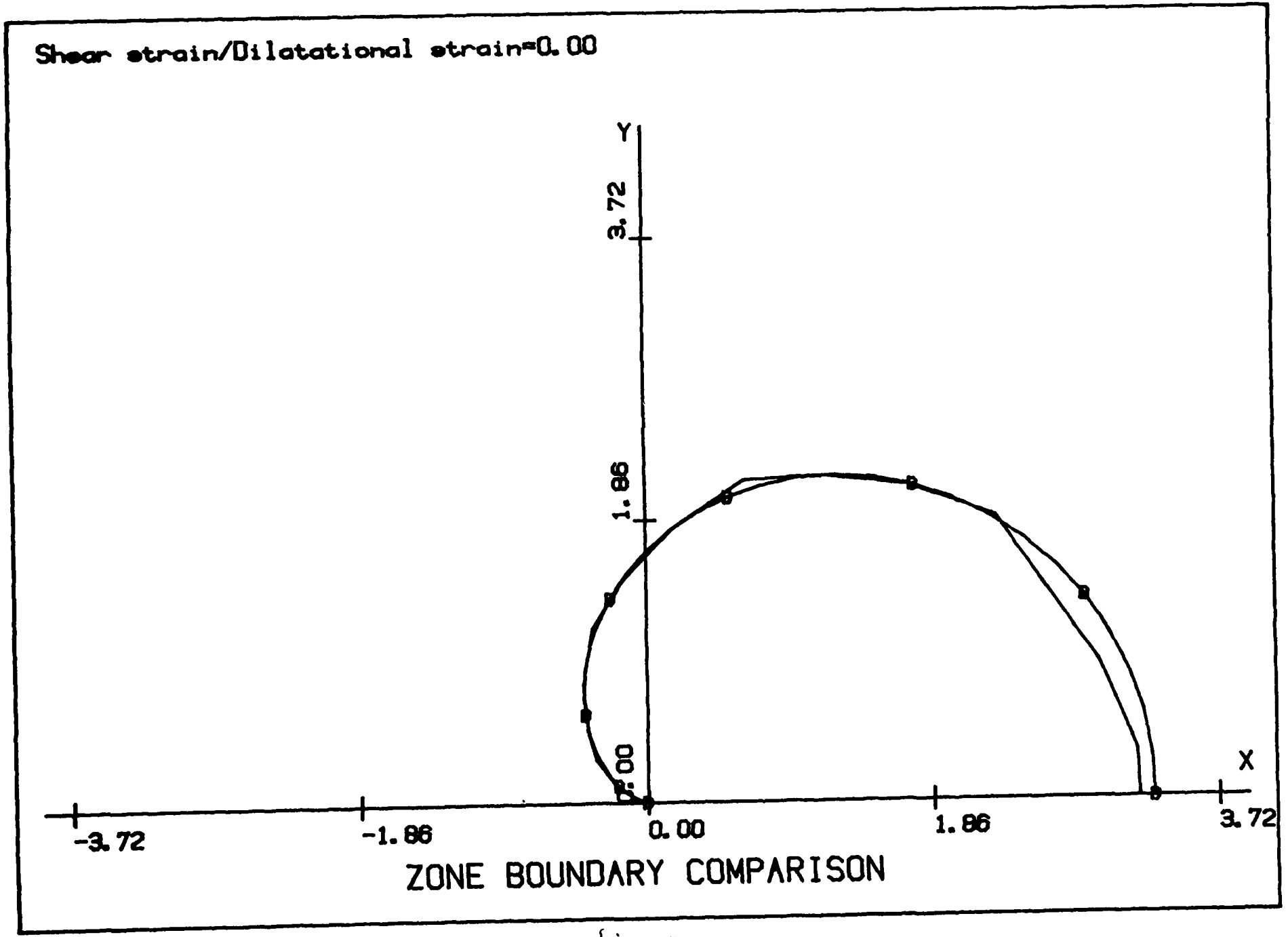
Shear strain/Dilatational strain=0.00
Y
3.72
1.86
0.00
X
-3.72
-1.86
0.00
1.86
3.72
ZONE BOUNDARY COMPARISON

fig 9

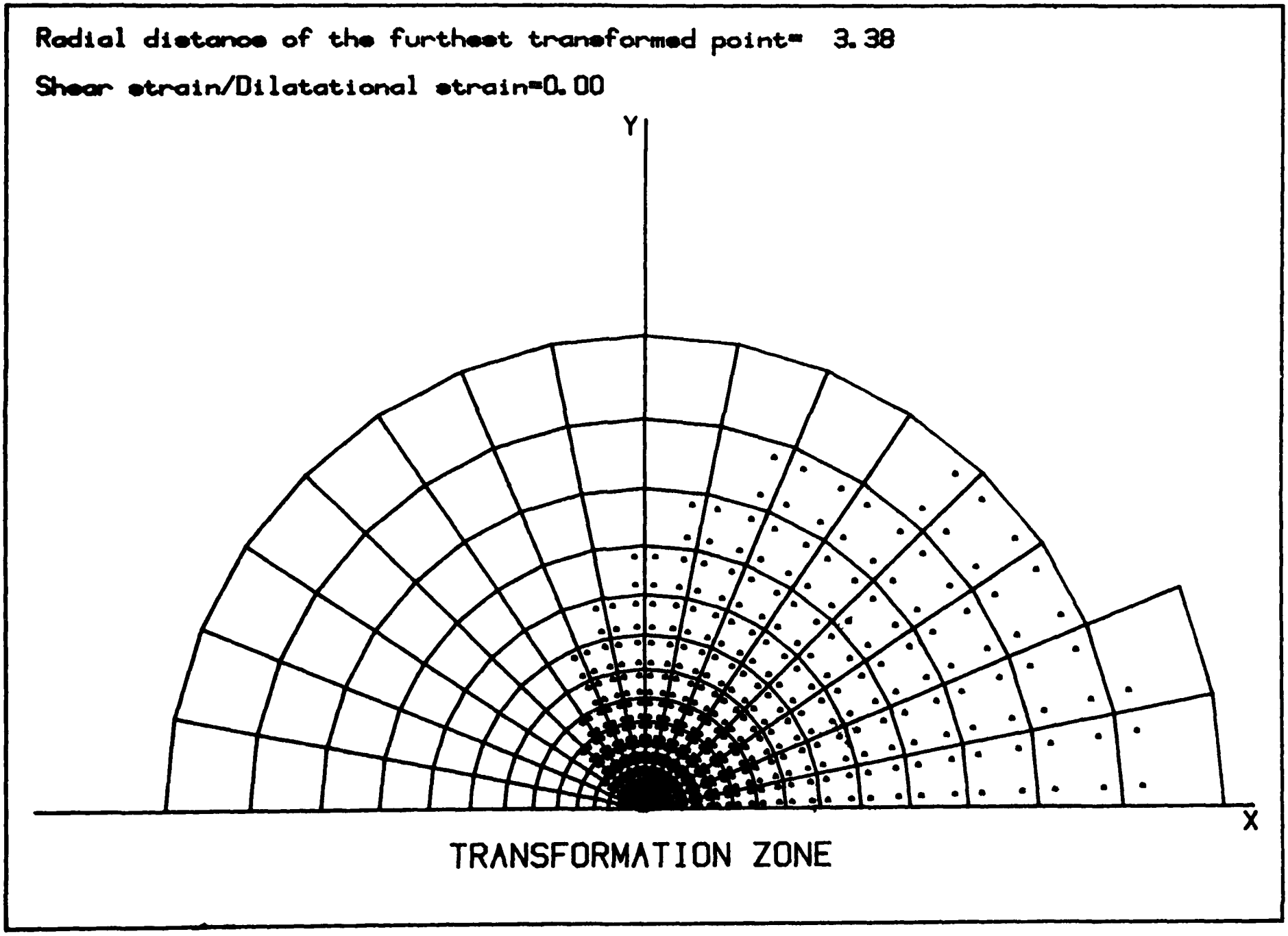
Radial distance of the furthest transformed point= 3.38
Shear strain/Dilatational strain=0.00
Y
X
TRANSFORMATION ZONE

fig 8

INNER RADIUS= 2.53
OUTER RADIUS=100.00

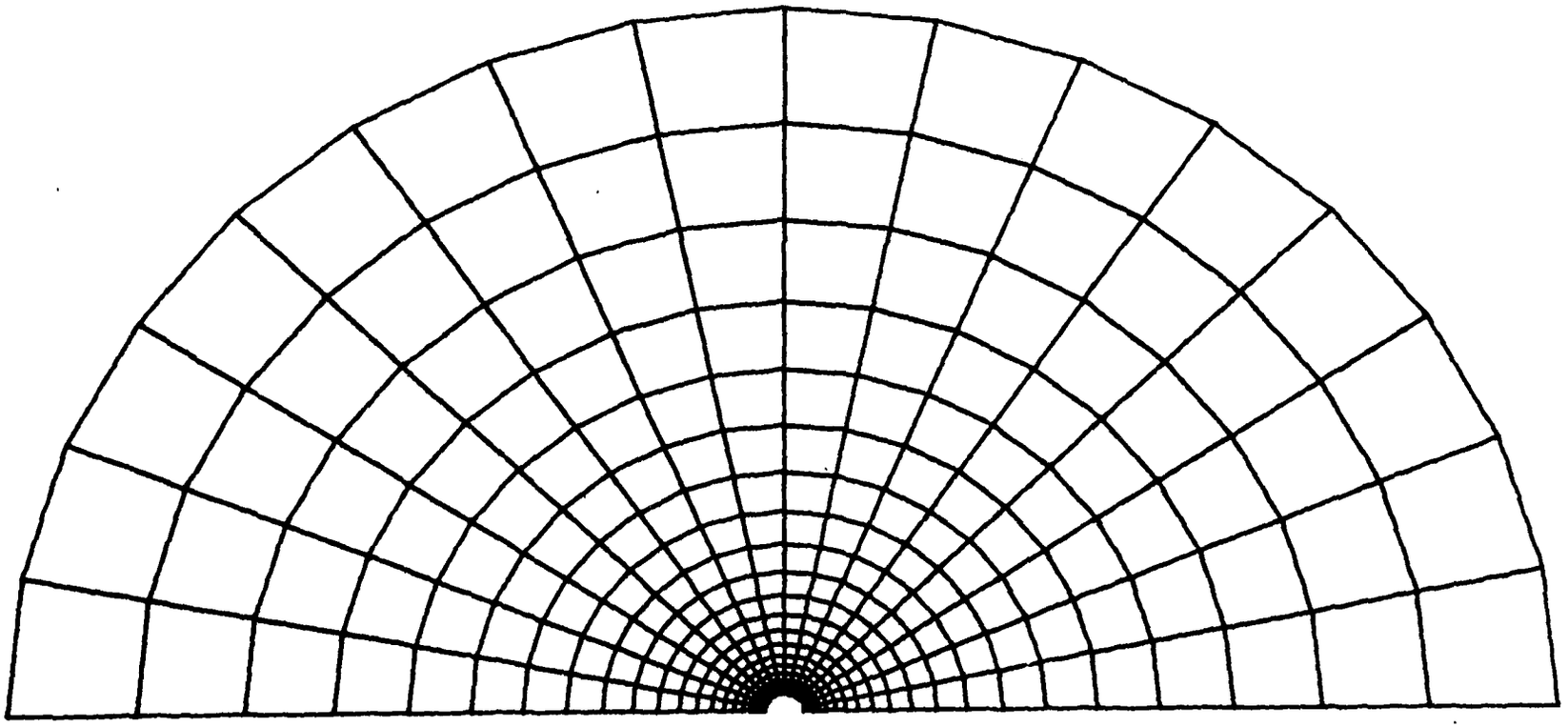

fig 7

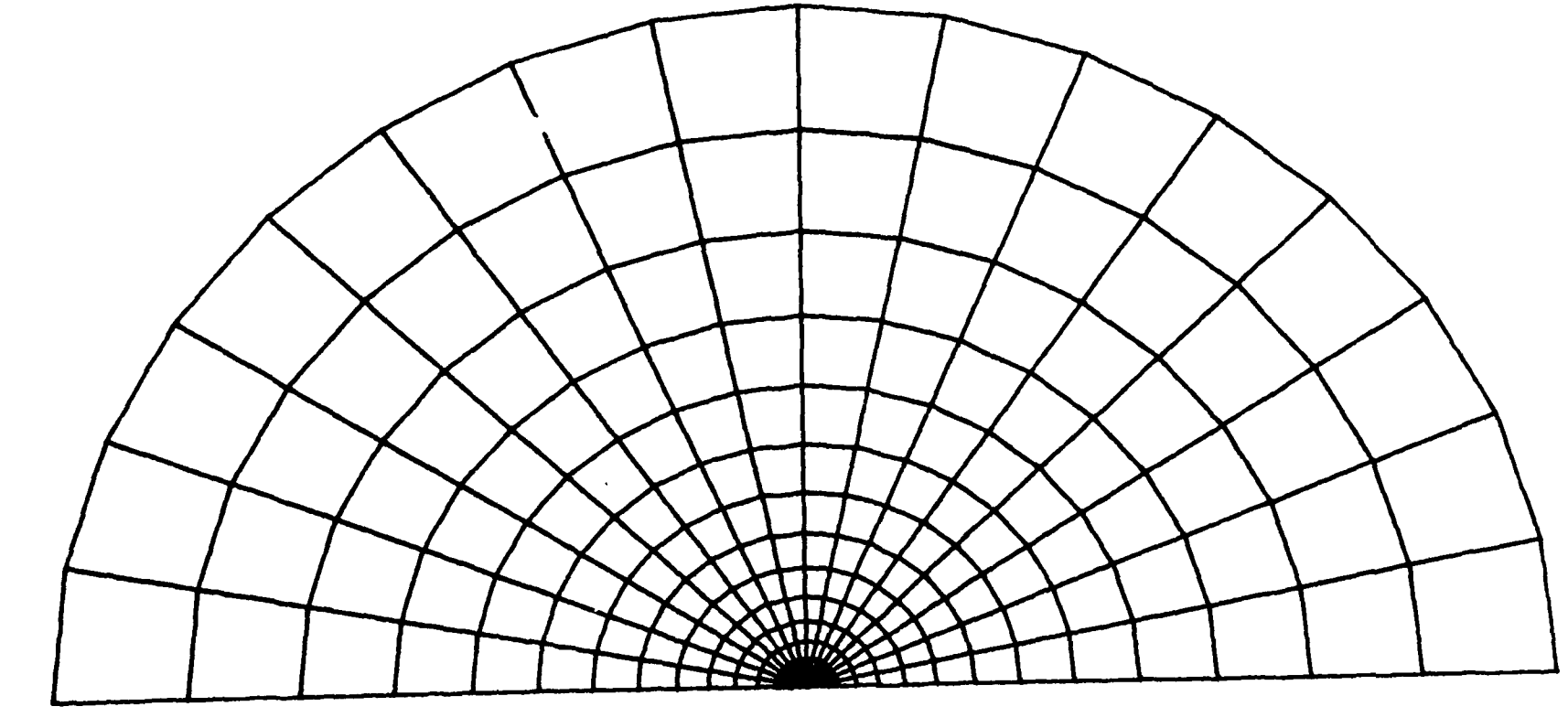

fig 6

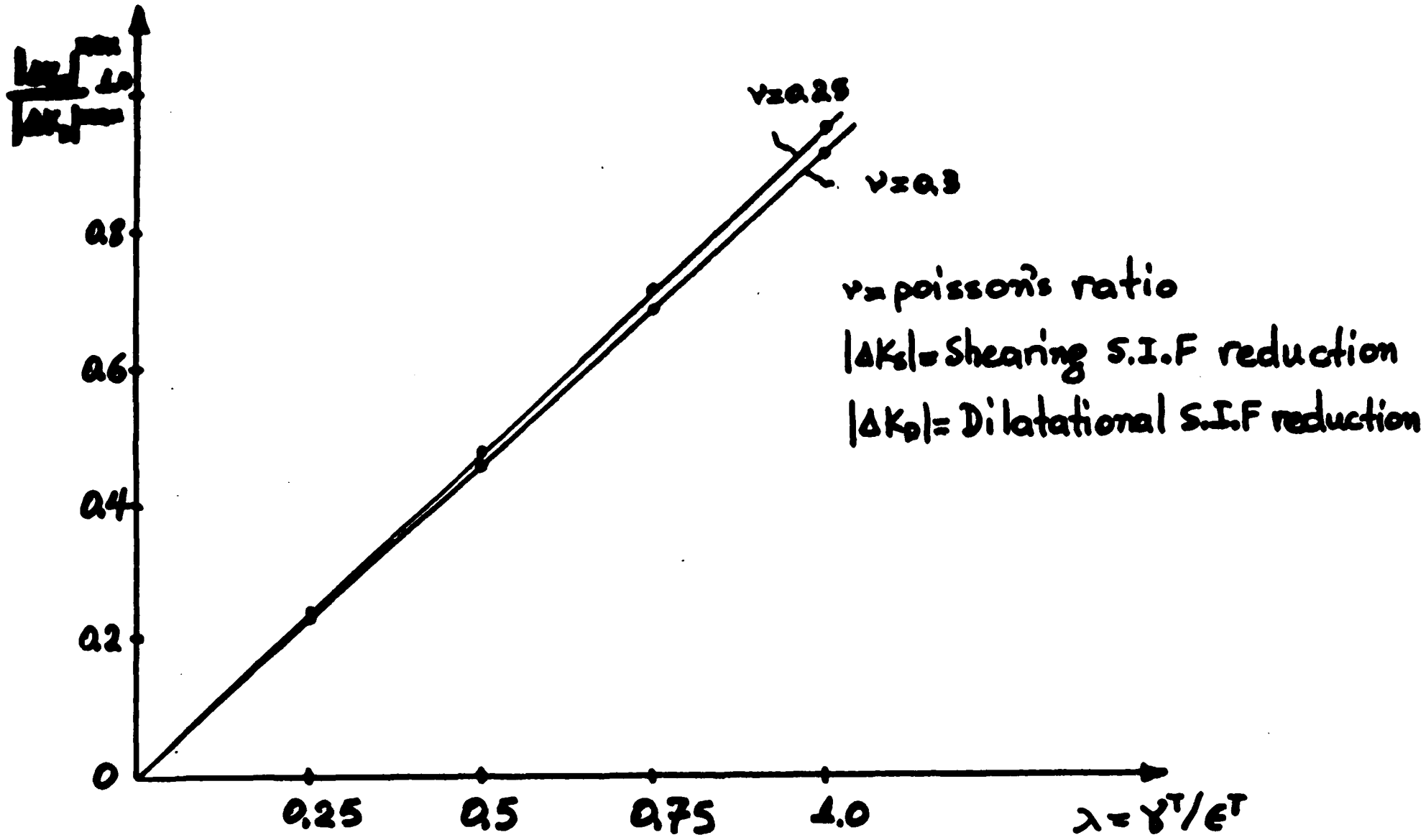
$\frac{|\Delta K_s|}{|\Delta K_d|}$
1.0
0.8
0.6
0.4
0.2
0
0.25
0.5
0.75
1.0
$\lambda = \gamma^T/\epsilon^T$
ν=0.25
ν=0.3
ν= poisson's ratio
|ΔKs|= Shearing S.I.F reduction
|ΔKd|= Dilatational S.I.F reduction

fig 4

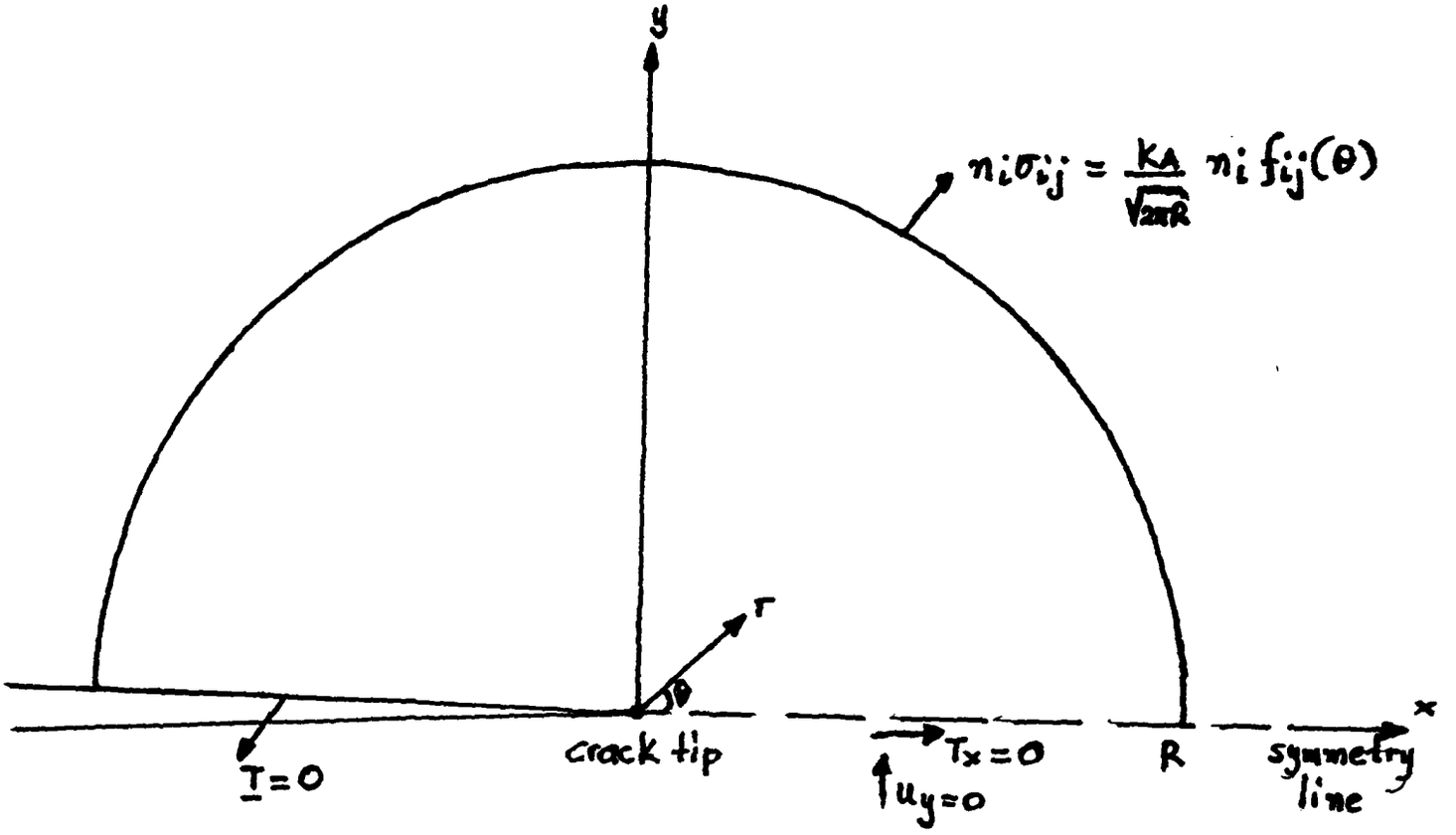
y
$n_i\sigma_{ij} = \frac{K_A}{\sqrt{2\pi R}} n_i f_{ij}(\theta)$
r
θ
x
crack tip
$T_x = 0$
$u_y = 0$
R
symmetry line
$\underline{T} = 0$

fig 5:

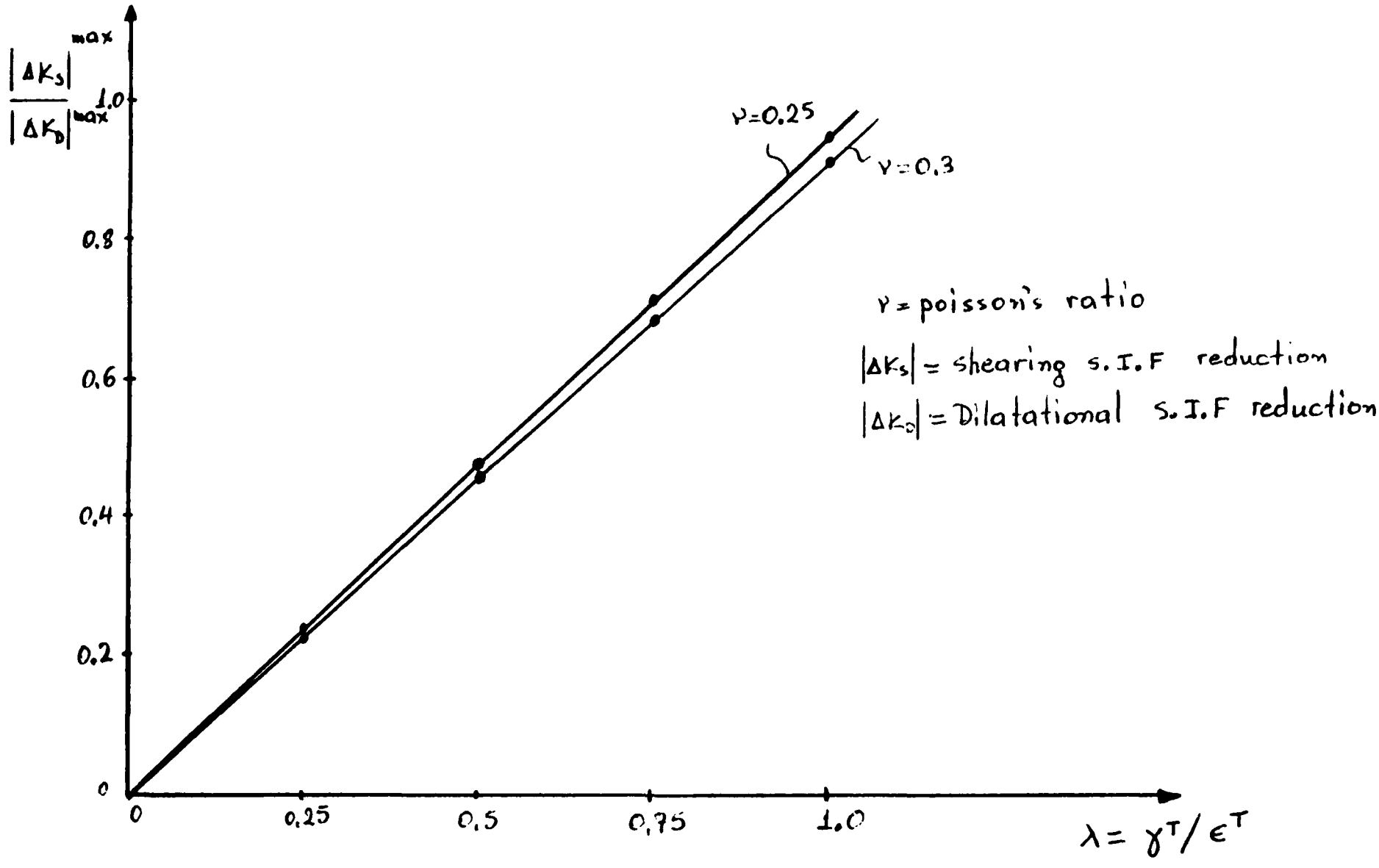
$\frac{|\Delta K_s|^{max}}{|\Delta K_D|^{max}}$
1.0
0.8
0.6
0.4
0.2
0
0
0.25
0.5
0.75
1.0
$\lambda = \gamma^T / \epsilon^T$
$\nu = 0.25$
$\nu = 0.3$
ν = poisson's ratio
$|\Delta K_s|$ = shearing s.I.F reduction
$|\Delta K_D|$ = Dilatational s.I.F reduction

fig 4

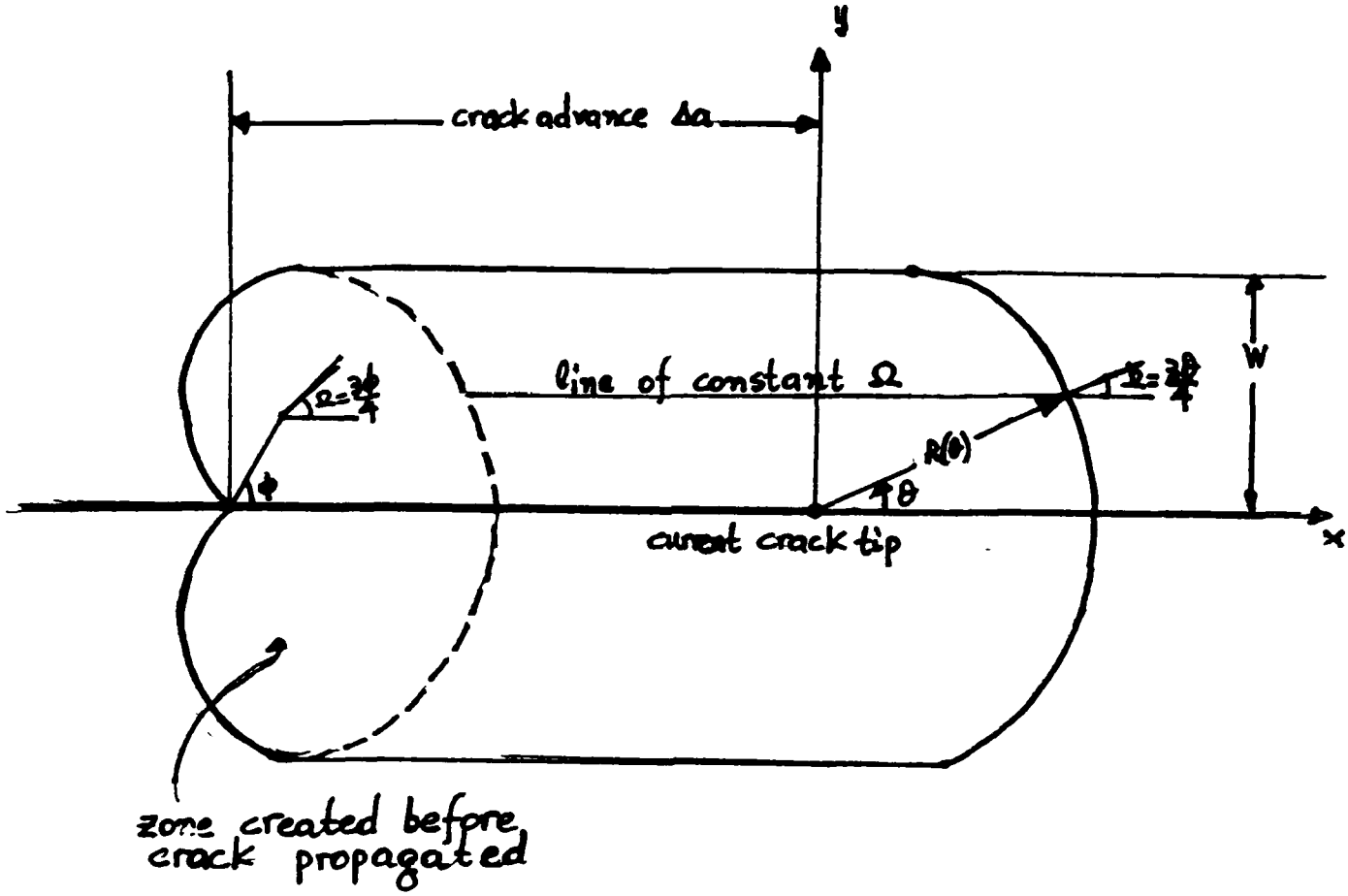
y
crack advance Δa
W
line of constant Ω
Ω = 3φ/4
Ω = 3θ/4
R(θ)
φ
θ
current crack tip
x
zone created before
crack propagated

fig 3

INTRODUCTION

The self consistent aproach to the stress-induced microcracking of brittle materials, as already mentioned, is based on two major notions. The notion of a microcracking criterion and that of effective elastic properties of the microcracked material. The microcracking criterion relates the induced microcrack density ε to the existing stress magnitude. The effective elastic properties of the microcracked material are then functions of the initial elastic properties and the microcrack density. Budansky and O'Connell [1], introduced the microcrack density parameter ε given by equation (1)

$$\varepsilon = \frac{2N}{\pi} \left\langle \frac{A^2}{P} \right\rangle \tag{1}$$

where N=number of microcracks per unit volume, A is the area of the microcrack surface and P is the perimeter of the microcrack. Using energy balance considerations and fracture mechanics analysis they were able to derive mathematical expressions relating the effective elastic properties of the actual state to those of the unmicrocracked elastic state, through the microcracking density ε. We will make use of the work of Fu and Evans [10] to construct a microcracking criterion which will relate increases in the microcracking density to increases in stress magnitudes. Together with the self consistent results of Budiansky and O'Connell [1], the microcracking criterion can be used to develop a constitutive law for the inelastic behavior of a microcracking continuum.

Our interest is in the development of microcracks near the tips of major cracks. To study this phenomenon in an approximate way, we use the constitutive law for the microcracking material in finite element calculations of either plane strain or plane stress deformation near the crack tip. These

results are relevant to the question of microcrack toughening in brittle materials. Before we proceed to describe these results we will discuss briefly some previous work on this problem.

Hoagland, et al. [2], proposed a simplified method for estimating the density of microcracks in the vicinity of a major crack tip. They assume a set of randomly oriented lines, which are the traces of the potential microcrack planes, and which become microcracks when the stress normal to the line exceed a critical value. They also assume that the dimension of the microcracks is very much less than the major crack size of the model. In determining the stress intensity, they used the singular elastic stress field near the crack tip. Later studies done by Evans [3], suggest that the uniform microcrack density analysis presented by Hoagland et al. is inaccurate because there is an increased density of microcracks at the higher stress levels, which more strongly biases the microcrack density towards the crack tip.

In 1980 Hoagland and Embury [4], suggested a numerical procedure for modeling the number and distribution of microcracks around a crack tip, as a function of the applied stress intensity. The procedure accounts approximately for microcrack-microcrack and microcrack-crack interactions. This work is actually an extension of their original concept of nucleating microcracks based on a uniform fracture stress by adding new stress fields, whenever a new microcrack is nucleated. Although Hoagland and Embury arrived at some useful conclusions concerning the stress induced microcracking in the vicinity of a major crack, their results are restricted to a two-dimensional problem with through thickness microcracks extended along the third dimension. In contrast to that the theory developed by Budiansky and O'Connell accounts for microcracks with finite third dimension (i.e.,

circular, elliptical, etc.) and allows this effect to be introduced in an approximate way.

A more thorough investigation of the mechanics of microcrack toughening was carried out by Fu and Evans [10]. In their work they established the basis of a continuum mechanics description of the microcrack toughening process. The constitutive behavior of the microcrack zone is based on the overall strain response of a microcracking medium, subject to a uniform stress field. A generalized microcracking criterion for microcracking at facets subject to general stress is proposed. Stress induced microcracking is initiated at a threshold load. Above the threshold load, the stress/strain behavior becomes nonlinear. During unloading, linearity resumes and hysteresis is present, corresponding to dissipation of strain energy.

THE MICROCRACKING CRITERION AND CONSTITUTIVE LAW

Fu and Evans [10] studied the phenomenon of stress induced microcracking of grain boundary facets. These facets are generally subject to residual stresses caused by thermal expansion anisotropy of the neighboring grains. When a high tensile stress is applied, favorably oriented facets crack. The crack is confined to that facet and it takes a much higher stress to cause it to propagate out of its initial grain boundary interface. As a consequence, the process of microcracking is at least initially stable, with a steadily increasing stress causing the nucleation of more cracks rather than the propagation of existing ones.

From experiments and fracture mechanics analysis, Fu and Evans concluded that a particular facet will crack if it is larger than a critical size which depends on the resolved applied stress and the residual stress on the interface. In this notion is implicit the idea that facets can microcrack due

to the residual stress alone if the facet exceeds a critical size. Fu and Evans were able to phrase their results in terms of a parameter ε introduced by Budiansky and O'Connell [1] to describe microcrack density. When there are N circular microcracks per unit volume and the microcracks are of uniform size with radius a then $\varepsilon = Na^3$. Fu and Evans studied microcracking due to macroscopically uniform biaxial stress fields (with principal stresses $\sigma_1 > \sigma_2$, $\sigma_1 > 0$, $k = \sigma_2/\sigma_1$). From their analysis and observations, they proposed

$$\varepsilon = \lambda(\underset{\sim}{\sigma})(\sigma_1 - \sigma_C) \quad \text{for} \quad \sigma_1 > \sigma_C \tag{2}$$

where λ is a parameter that depends on stress state and material properties but independent of stress magnitude. For example λ for k=1 is twice the value of λ for k=0. The parameter ε represents the density of microcracks introduced by the applied stress that is in excess of any initial density. Thus the microcrack density ε increases linearly with stress and does so up to a saturation level, after which it remains constant. ε is unchanged by a reduction of stress.

We require a criterion for microcracking which can be used in more general states of multiaxial stress. For this purpose we will modify equation (2) to become.

$$\varepsilon = \lambda(\sigma_R - \sigma_C) \quad \text{if} \quad \sigma_R > \sigma_C \tag{3}$$

where $\sigma_R = \sqrt{\sigma_{ij}\sigma_{ij}}$ is an effective stress, σ_C is the critical stress for microcracking initiation and λ is a material constant independent of stress state. Of course equation (3) only applies when the largest principal stress is tensile and increases monotonically. The criterion (3) is somewhat different from that proposed by Fu and Evans [10]. If we take the uniaxial

stress case with $\sigma_1 = \sigma$ as a datum then both criteria give $\varepsilon = \lambda_u(\sigma - \sigma_C)$ where λ_u is the value of λ from Fu and Evans theory for uniaxial tension. For equal biaxial tension ($\sigma_1 = \sigma_2 = \sigma$), Fu and Evans' criterion gives $\varepsilon = 2\lambda_u(\sigma - \sigma_C)$ whereas the one we have proposed leads to $\varepsilon = \lambda_u(\sqrt{2}\sigma - \sigma_C)$. Thus our criterion shows a reduced rate of microcracking in biaxial tension compared to the rate suggested by Fu and Evans but microcracking starts at a lower stress according to our criterion. It can be argued that the microcrack density in biaxial tension would not be double that for uniaxial stress, since a given facet cannot be cracked twice. That is, unless the families of facets cracked by each applied stress component are mutually exclusive. However we are interested mainly in a simple constitutive law with appropriate characteristics for microcracking to illustrate what will occur near major crack tips. We will develop more exact microcracking laws in future work.

We summarize our microcracking criterion as follows.

For monotonically increasing stress, if

$\sigma_R < \sigma_C$ then $\varepsilon = 0$	Material remains unmicrocracked	
$\sigma_C < \sigma_R < \sigma_M$ then $\varepsilon = \lambda(\sigma_R - \sigma_C)$	The microcrack density is increasing linearly with σ	(4)
$\sigma_R > \sigma_M$ then $\varepsilon = \lambda(\sigma_M - \sigma_c) = \varepsilon_M$	The microcrack density is saturated.	

Furthermore ε cannot decrease. The stress/strain relation given for a macroscopic element of material is linear for non-microcracked regions ($\varepsilon=0$), becomes nonlinear for regions with increasing microcrack density $0<\varepsilon<\varepsilon_M$ and again becomes linear for fully microcracked regions ($\varepsilon = \varepsilon_M$). During unloading linearity resumes and when material unloads to zero stress no permanent strains are present as shown in fig. (1).

It should be noted that the microcrack distribution produced by a deviatoric applied stress coupled with the residual stress will be anisotropic. However, Fu and Evans used the isotropic theory of Budiansky and O'Connell [1] to determine macroscopic moduli for the microcracked material. that is they used ε as if it represented a random distribution of microcracks rather than an oriented one. We will follow Fu and Evans in this regard to obtain an approximate continuum theory for microcracking.

We have found that we can approximate Budiansky and O'Connell's results as follows.

$$\frac{\bar{E}}{E} = \frac{\bar{\nu}}{\nu} = 1 - \frac{16}{9}\varepsilon = \frac{1}{f} \tag{5}$$

where E, ν and $\bar{E}$, $\bar{\nu}$ are Young's moduli and Poisson's ratio for the material before and after stress induced microcracking respectively. Note that $\bar{E}$ and $\bar{\nu}$ *are defined at constant* ε. *Thus the constitutive equation for the* microcracking solid becomes

$$e_{ij} = \frac{f+\nu}{E}\sigma_{ij} - \frac{\nu}{E}\sigma_{kk}\delta_{ij} \tag{6}$$

where $\underset{\sim}{e}$ is the macroscopic strain, $\underset{\sim}{\sigma}$ is the macroscopic stress, δ_{ij} is the kronecker delta and rules for f are given by equations (3), (4) and (5).

The constitutive equation (6) is only valid for values of the microcracking parameter f within the interval $1<f<\infty$, fig (3). This together with equation (5) defines the limiting values of the microcracking density ε, $0 < \varepsilon < \frac{9}{16}$ (See fig (3)). The upper bound of ε with the aid of equation (3) yield a relation between the critical stresses σ_C, σ_M and the parameter λ i.e., $\sigma_M - \sigma_C < \frac{9}{16} \cdot \frac{1}{\lambda}$ (See fig (4)).

FORMULATION OF CRACK TIP PROBLEM

The high stresses near the tip of a long crack will cause microcracking in the near tip region in the material of interest to us, as shown in fig (5). We will restrict our attention to the situation where the zone of microcrack damage is very small compared to the body containing the crack. We will refer to this situation as small scale microcracking. In this case, the microcrack zone will lie within a region of uncracked material. some distance outside the zone, the stresses will be almost the same as when the material does not microcrack. When small scale microcracking prevails, these stresses will be the singular linear elastic crack tip stresses.

It follows that the plane small scale microcracking problem can be solved by considering a plane region around the crack tip to which are applied boundary tractions given by the linear elastic stress field, i.e.

$$T_i = n_j \sigma_{ij} = \frac{K_I}{\sqrt{2\pi r}} n_j \Sigma_{ij}(\theta) \qquad (7)$$

where $\underset{\sim}{T}$ are the boundary tractions, $\underline{n}$ is the outward unit normal to the region boundary, K_I is the mode I (tensile opening mode) stress intensity factor and (r,θ) are polar coordinates originating at the crack tip as shown in fig (6). The function $\underset{\sim}{\Sigma}$ determines the angular distribution of stress and its form can be found in the article by Rice [23]. The crack surfaces are traction free. To ensure small scale microcracking, K_I must be limited to a level low enough that the zone size is small compared to the region for which the analysis is being carried out

The governing equations of equilibrium and compatibility are enforced through the principle of virtual work

$$\int_A \sigma_{ij}\, \delta e_{ij}\, dA = \int_{S_T} T_i\, \delta u_i\, ds \tag{8}$$

in the absence of body forces, where A is the plane area being analyzed, S_T is the perimeter where tractions are prescribed, $\underset{\sim}{u}$ are the *displacements and the* symbol δ indicates a virtual variation of the quantity following it and the variation disappears on $S - S_T$.

The constitutive law for the material has been described in the previous section. However, we will find it useful to state the following form.

$$\sigma_{ij} = c_{ijkl}\, e_{kl} = \frac{E}{f+\nu}\, e_{ij} + \frac{E \cdot \nu}{(f-2\nu)(f+\nu)}\, e_{kk}\, \delta_{ij} \tag{9}$$

where $f = \dfrac{1}{1 - \frac{16}{9}\,\varepsilon}$ and $\varepsilon = \varepsilon(\underset{\sim}{\sigma})$ as in equation (3)

For plane problems

$$e_{\alpha\beta} = \frac{f+\nu}{E}\,[\sigma_{\alpha\beta} - \nu^*\sigma_{\gamma\gamma}\,\delta_{\alpha\beta}] \qquad \alpha,\ \beta,\ \gamma = 1,\ 2 \tag{10α}$$

$$\sigma_{\alpha\beta} = \frac{E}{f+\nu}\,[e_{\alpha\beta} + \frac{\nu^*}{(1-2\nu^*)}\, e_{\gamma\gamma}\,\delta_{\alpha\beta}] \tag{10β}$$

where $\nu^* = \frac{\nu}{f}$ for plane strain and $\nu^* = \frac{\nu}{f+\nu}$ for plane stress. The governing equations, together with the appropriate boundary conditions corresponding to a specified geometry, define a boundary value problem whose solution we will obtain numerically.

THE FINITE ELEMENT EQUATIONS

The finite element equations can be derived from the principle of virtual work given by equation (8). Finite element interpolations together with

equation (8) and the constitutive law (9) and (10.β), give rise to the nonlinear finite element equations

$$[k(u_n)]\{u_n\} = \{F\} \qquad (11)$$

where [k] is the stiffness matrix, $\{u_n\}$ the nodal displacement vector and {F} the force vector. The notation $[k(u_n)]$ indicates the dependence of the stiffness on the nodal displacements due to the nonlinear constitutive law.

In the finite element analysis, a 4 noded quadrilateral isoparametric element with 4 stations for the integration of stiffness was used. The finite element equations (11) were solved using an interative method updating the stiffness matrix in every iteration. The microcracking parameter f was found to be the root of a sixth order polynomial in f which satisfies the conditions imposed on f earlier in this work i.e. $1<f<\infty$. The coefficients of the polynomial are strain dependent and had to be recomputed in every iteration [see Appendix II].

To ensure small scale microcracking, the outer radius of the mesh was chosen to be 15 to 20 times the outer radius of a damaged zone, estimated from the stresses in the absense of microcracking.

RESULTS

Stress-strain fields

Figs (7) to (8) display the stresses and strains ahead of the crack tip for various choices of λ and ε_M. λ is the rate of increase of the microcrack density with respect to the effective stress and $\varepsilon_M = \lambda(\sigma_M-\sigma_c)$ is the saturation value of the microcrack density.

In the unmicrocracked region, both stresses and strains agree quite closely with the solution obtained for an unmicrocracked material. The elastic strain and stress fields constrain the deformation due to

microcracking in the damaged zone. The above constraint together with the weakening of the material in the damaged zone due to microcracking, causes stress relaxation in the region of intermediate microcracking. Very close to the crack tip the microcracking density is saturated and the stress and strain fields become singular again. We observe that the amount of stress relaxation increases with λ and it reaches its maximum level for $\lambda = \infty$. At this point we notice the importance of the presence of the zone of intermediate microcracking, for its presence ensures a smooth transition for both the strain and stress fields from the outer to the inner asymptotic fields. The absence of the above region would lead to infinite strain and stress gradients along the boundary of the fully microcracked material and the unmicrocrack material [see Appendix I]. We also notice that in the stress relaxation region, the effective stress which in our case is the equivalent stress $\sigma_R = \sqrt{\sigma_{ij}\,\sigma_{ij}}$ is consistent with the microcracking law eq (3), fig (2) that we used. In the particular case of $\lambda = \infty$, $\sigma_R = \sigma_c = 1.0$ as we expected. In this situation, the partially microcracked zone is like a perfectly plastic zone. The zone with saturated microcrack density is dominated by microcracking deformation with larger strains and stresses at lower levels than would prevail in the absence of microcracking.

The shape and size of the transformed zone

A typical microcrack zone is shown in fig. (5). Three characteristic quantities describing the microcrack zones that we studied were consistently computed. x_m is the distance along the x axis at which the microcrack zone boundary crosses the x axis. h_m denotes the y coordinate of the farthest point along the y direction to experience microcracking and θ_m is the polar angle corresponding to the same point. The boundary of the inner zone, where

the microcrack density is saturated is also characterized by the corresponding quantities x_s, h_s and θ_s fig. (5).

Fig. (9) to fig (9γ) show how the above quantities depend on the second critical stress σ_M, for fixed values of σ_c and $\varepsilon_M = \lambda(\sigma_M - \sigma_c)$. The size of the fully microcracked zone is inversely proportional to the value of the second critical stress σ_M. Similarly high saturation values of the microcrack density yield small saturation zone. There is an increase in the size of the above zone in both directions as λ increases or σ_M decreases. In no case does the inner zone becomes identical with the whole damaged zone because as we said earlier the existences of a zone of intermediate microcracking is an essential feature of the microcracking law eq(3). The microcrack zone boundary depends on the first critical stress σ_C. For fixed values of both the first critical stress σ_C and the saturation microcrack density the microcrack boundary tends to stretch along the x axis while reduction of h_m is observed, as λ increases. The angles θ_m and θ_s corresponding to h_m and h_s drop from 78° for small values of λ, to 49° as λ becomes infinite. Fig (10) shows microcrack zones obtained through our finite element analysis. Fig (11) and (12) show the profile of the microcrack density ahead of the crack tip for various values of σ_M.

Plane stress results

Similar results to those of the plane strain case were obtained for the plane stress case. The transverse constraint of the plane strain case produces large transformation zones. the overall response of a microcracking material was found to be similar for both plane strain and plane stress cases.

DISCUSSION

Using the concept of the microcrack density ε first introduced by Budiansky and O'Connell [1] together with a further simplified microcracking law proposed by Fu and Evans [10], we establish the basis of a continuum mechanics description for the phenomenon of stress-induced microcracking in a brittle polycrystalline composite. With appropriate integration of the constitutive relations we were able to obtain information as to what happens in the process zone at the vicinity of the crack tip of a major crack under a mode I loading in a material susceptible to microcracking. For appropriate choices of parameters, the transformation zone, as in the case of small scale yielding in a ductile material, is well contained. The stress and strain fields exhibiting the characteristics shown in fig (7) and (8) are well behaved. When the first critical stress σ_C and the saturation value ε_M are specified, the second critical stress σ_M or the variable λ appearing in the microcracking law control the rate at which the material microcracks and affects the stress and strain fields as well as the shape and size of the transformation zone.

At this point, we have all the necessary tools for a full scale investigation of the phenomenon of microcracking. Such an investigation should address the question of the possible effects on material toughening due to microcracking. Further work is necessary to elucidate the nature of the crack propagation criterion. In addition studies done by McMeeking and Evans [6] and Budiansky et al. [7], suggest that the toughness of certain ceramics can be substantially enhanced through the controlled use of martensitic transformation. Faber [9] found that microcracking contributes to the toughness of Z_rO_2 - ceramics and Fu and Evans [10] found that stress induced microcracking enhances the toughness of brittle polycrystalline aggregates.

The finite element analysis will substantially contribute to a better understanding of the mechanics of stress induced microcrack toughening in brittle material. As we saw earlier in our analysis, a zone with saturated microcrack density always exists. We may be able to treat this zone as being composed of homogeneous elastic material and use a Griffith criterion for propagation of the major crack into this zone. McMeeking, in unpublished work, has shown that the material obeying the constitutive law of eq. (3-6) is nonlinear hyperelastic. It follows that the J-integral is path independent throughout the material in both unmicrocracked and microcracked regions. As a consequence, the energy release rate for the microcracking material will have the same value as in the nonmicrocracking material at the same applied loads. Thus if the critical value for propagation is unchanged, then no microcrack toughening can occur. However, the critical energy release rate for fully microcracked material may differ from that for the unmicrocracked case. A simple model of the crack growing from microcrack facet to microcrack facet suggests that the average critical energy release rate would be less and so microcrack embrittlement would occur. However, aspects of R-curve type behavior and more realistic microcracking laws may hold the clue to microcrack toughening. Some of these issues have been addressed by Faber [9] and we will consider such issues in the future.

ACKNOWLEDGEMENT

This research was supported by the Office of Naval Research through Contract NR 064-N00014-81-K-0650 with the University of Illinois.

APPENDIX I

We consider an element consisting of two dissimilar material

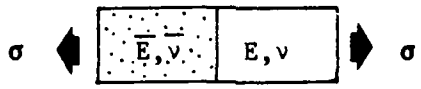

E, ν are the Young modulus and Poisson's ratio for an unmicrocracked material.

$\bar{E}$, $\bar{\nu}$ are the corresponding moduli for a microcracked material.

We require that the material remains continuous after deformation. Thus from equilibrium and compatibility we get the interface conditions

$$\left.\begin{aligned} \bar{\sigma}_{xx} &= \sigma_{xx} \\ \bar{e}_{yy} &= e_{yy} \\ \bar{\sigma}_{xy} &= \sigma_{xy} = 0 \end{aligned}\right\} \qquad \text{interface conditions.}$$

The constitutive relations for plane elasticity case are

unmicrocracked solid

$$e_{\alpha\beta} = \frac{H\nu}{E}\left(\sigma_{\alpha\beta} - \nu^* \sigma_{\gamma\gamma}\, \delta_{\alpha\beta}\right. \qquad \nu^* = \nu \quad \text{Plane strain}$$

$$\sigma_{\alpha\beta} = \frac{E}{1+\nu}\left(e_{\alpha\beta} + \frac{\nu^*}{(1-2\nu^*)}\, e_{\gamma\gamma}\, \delta_{\alpha\beta}\right) \qquad \nu^* = \frac{\nu}{1+\nu} \quad \text{Plane stress}$$

microcracked solid

$$\bar{e}_{\alpha\beta} = \frac{f+\nu}{E}\left(\bar{\sigma}_{\alpha\beta} - \bar{\nu}^*\bar{\sigma}_{\gamma\gamma}\, \delta_{\alpha\beta}\right) \qquad \bar{\nu}^* = \frac{\nu}{f} \quad \text{Plane strain}$$

$$\bar{\sigma}_{\alpha\beta} = \frac{E}{f+\nu}\left(\bar{e}_{\alpha\beta} + \frac{\bar{\nu}^*}{(1-2\bar{\nu}^*)}\, \bar{e}_{\gamma\gamma}\, \delta_{\alpha\beta}\right) \qquad \bar{\nu}^* = \frac{\nu}{f+\nu} \quad \text{Plane stress}$$

where $f = \dfrac{1}{1 - \frac{16}{9}\varepsilon}$, where ε is the microcrack density.

Fig. 8 exx strain ahead of the crack tip

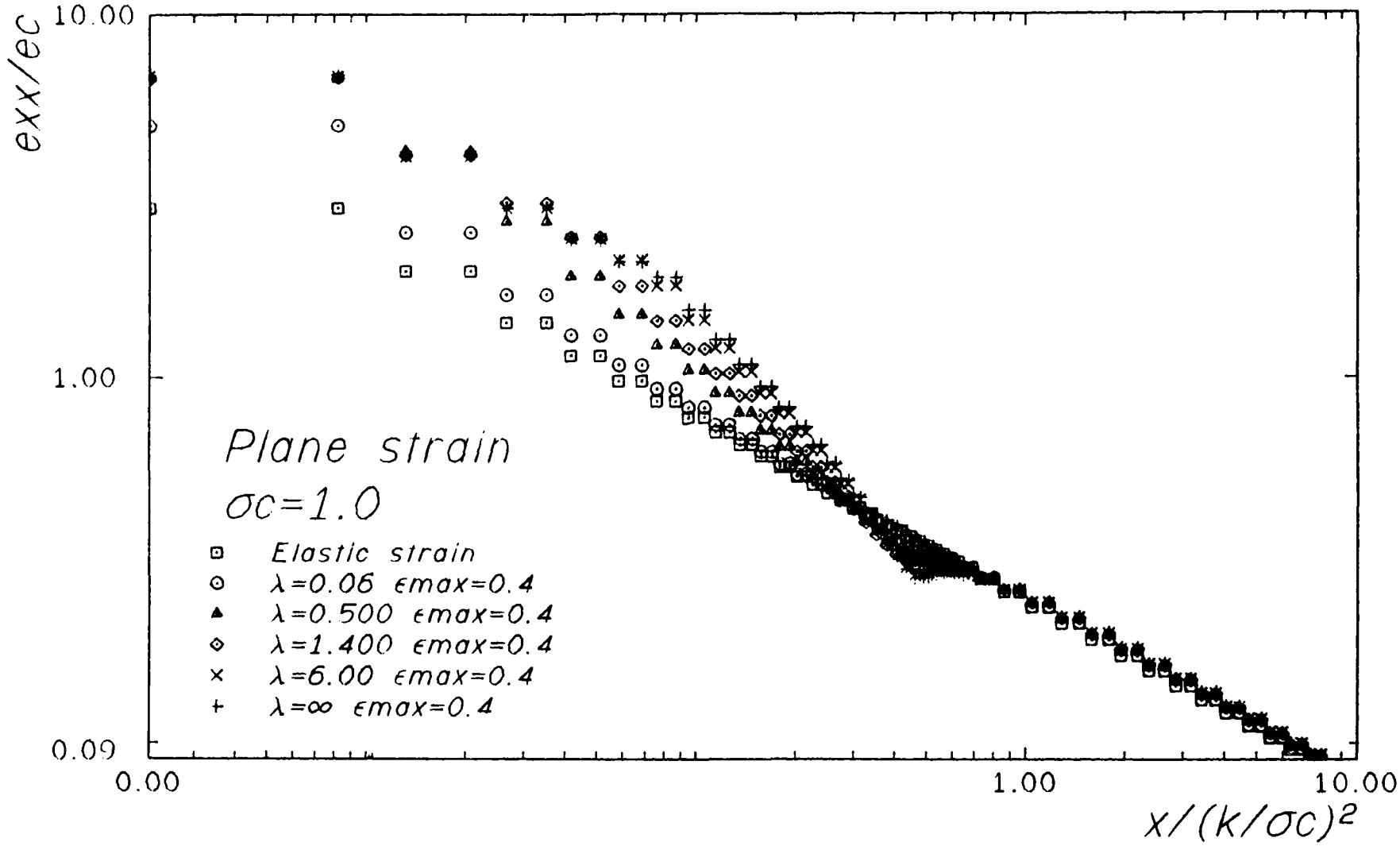

Fig. 7β Equivalent stress ahead of the crack tip

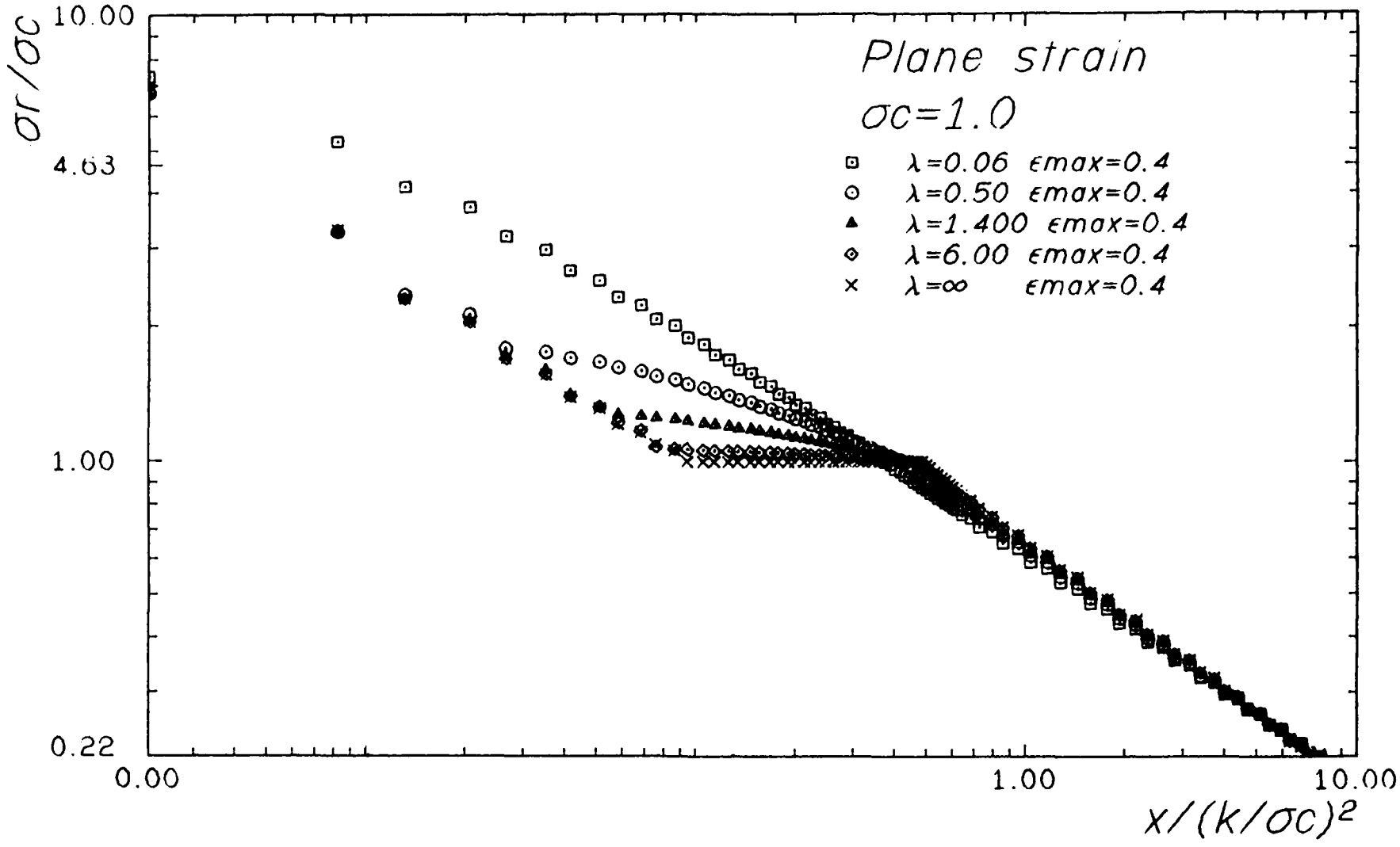

Fig. 7a σyy stress ahead of the crack tip

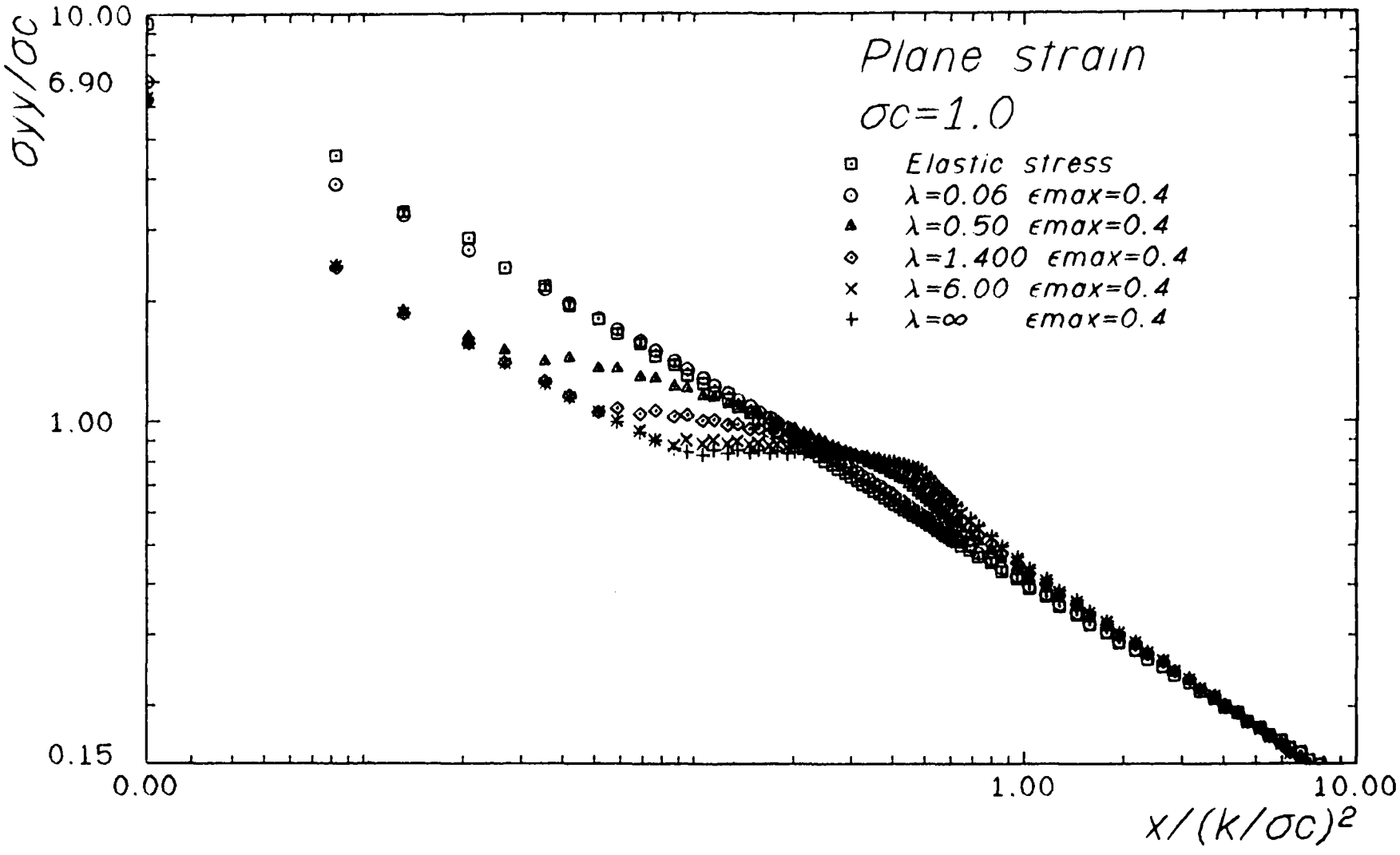

Fig. 7 σxx stress ahead of the crack tip

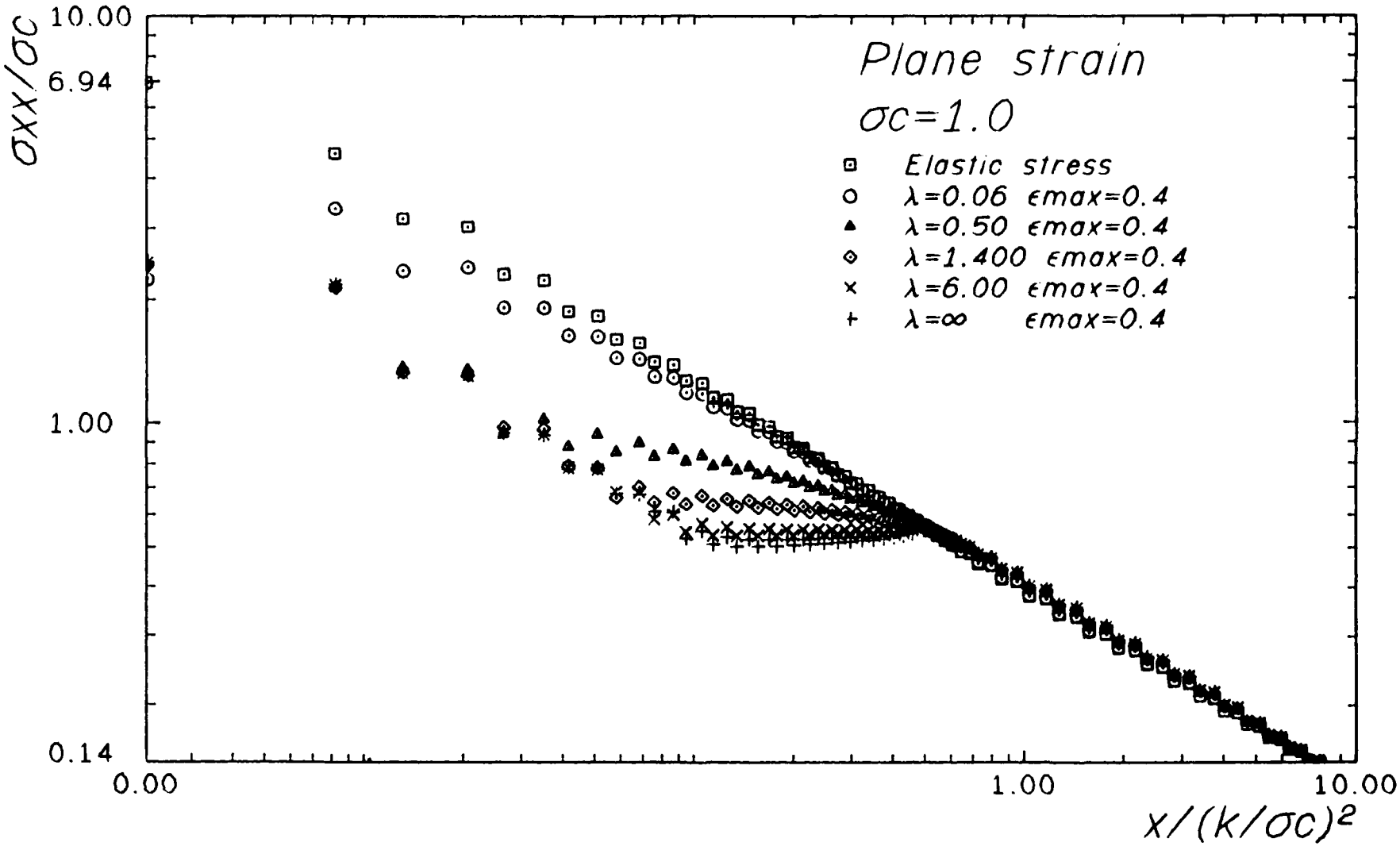

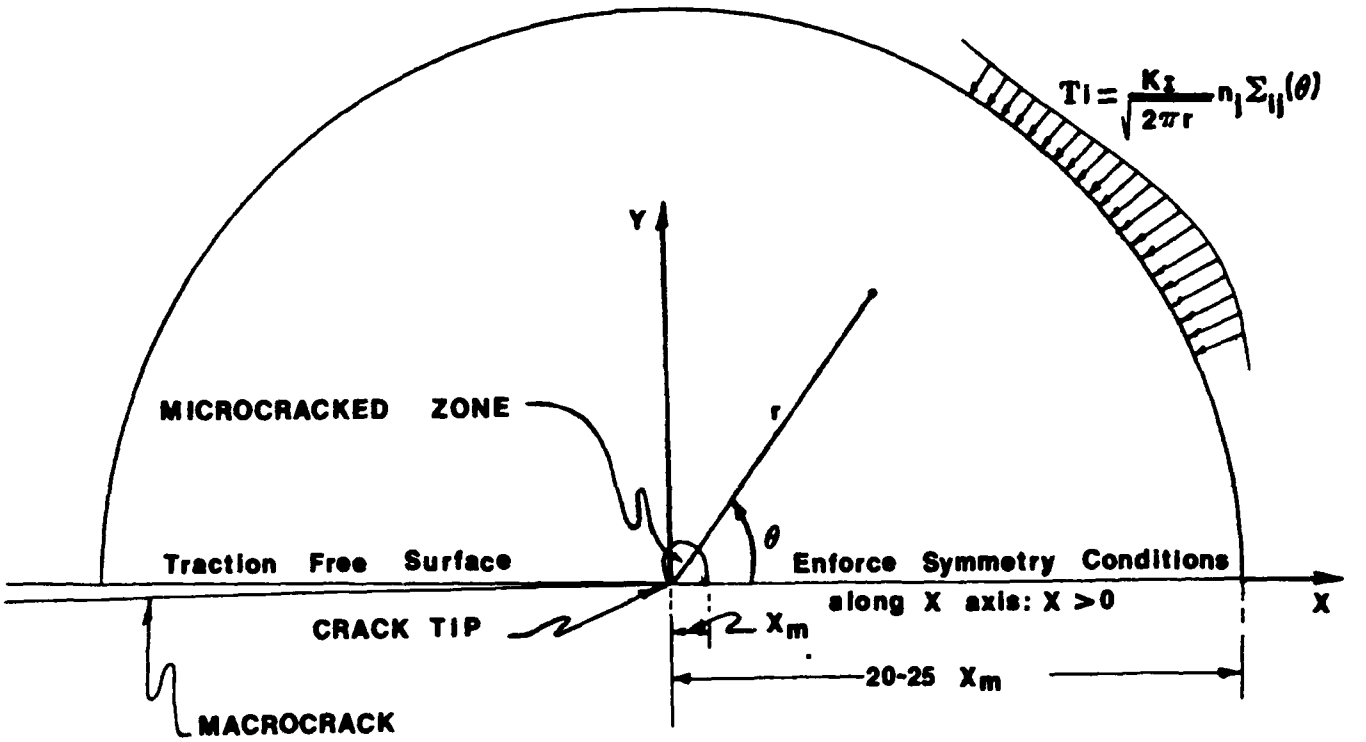

Fig. 6 The BOUNDARY CONDITIONS used in solving the FINITE ELEMENT equations

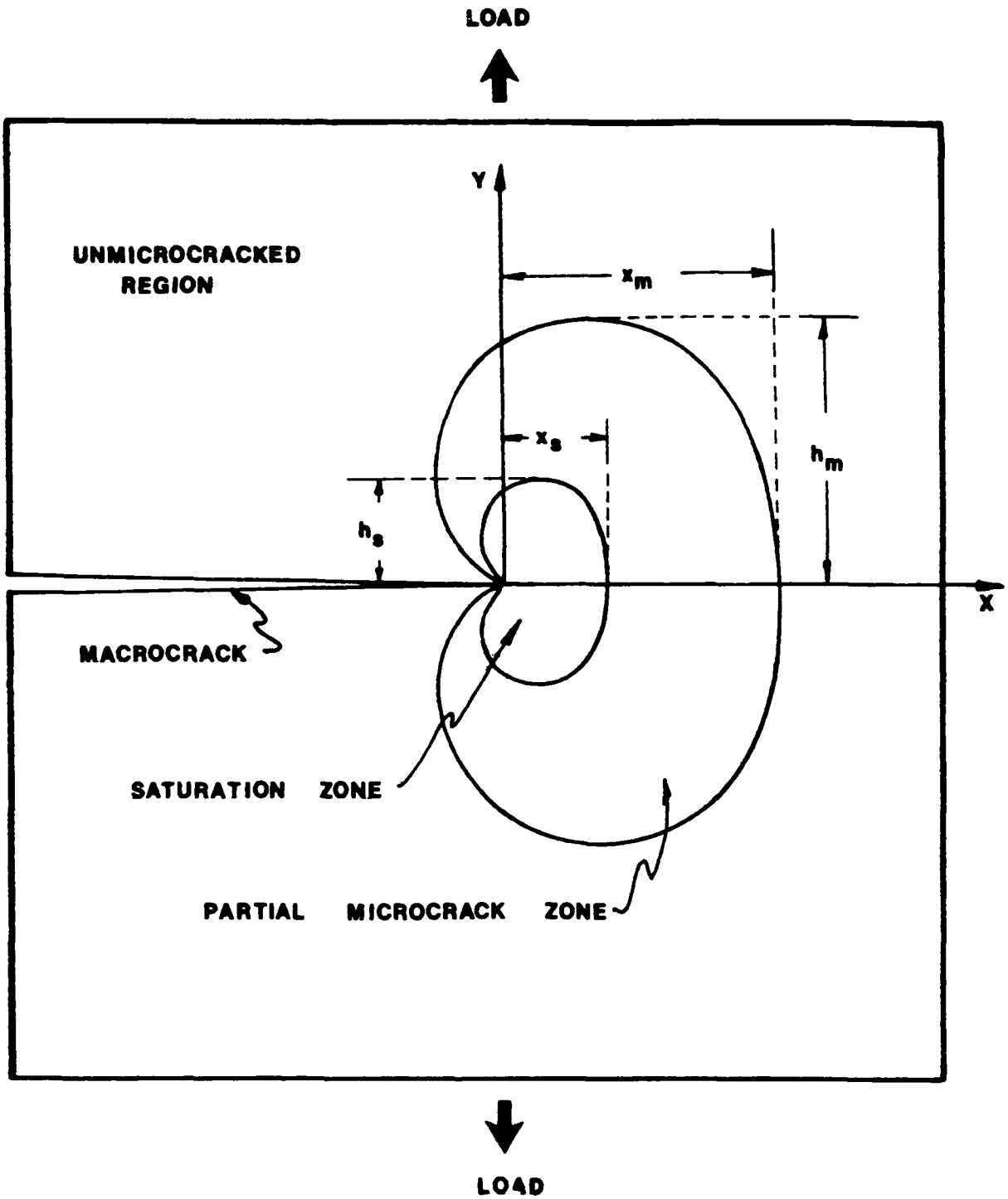

Fig. 5 Microcracking at the vicinity of the crack tip of a semi-infinite macrocrack under mode I Loading

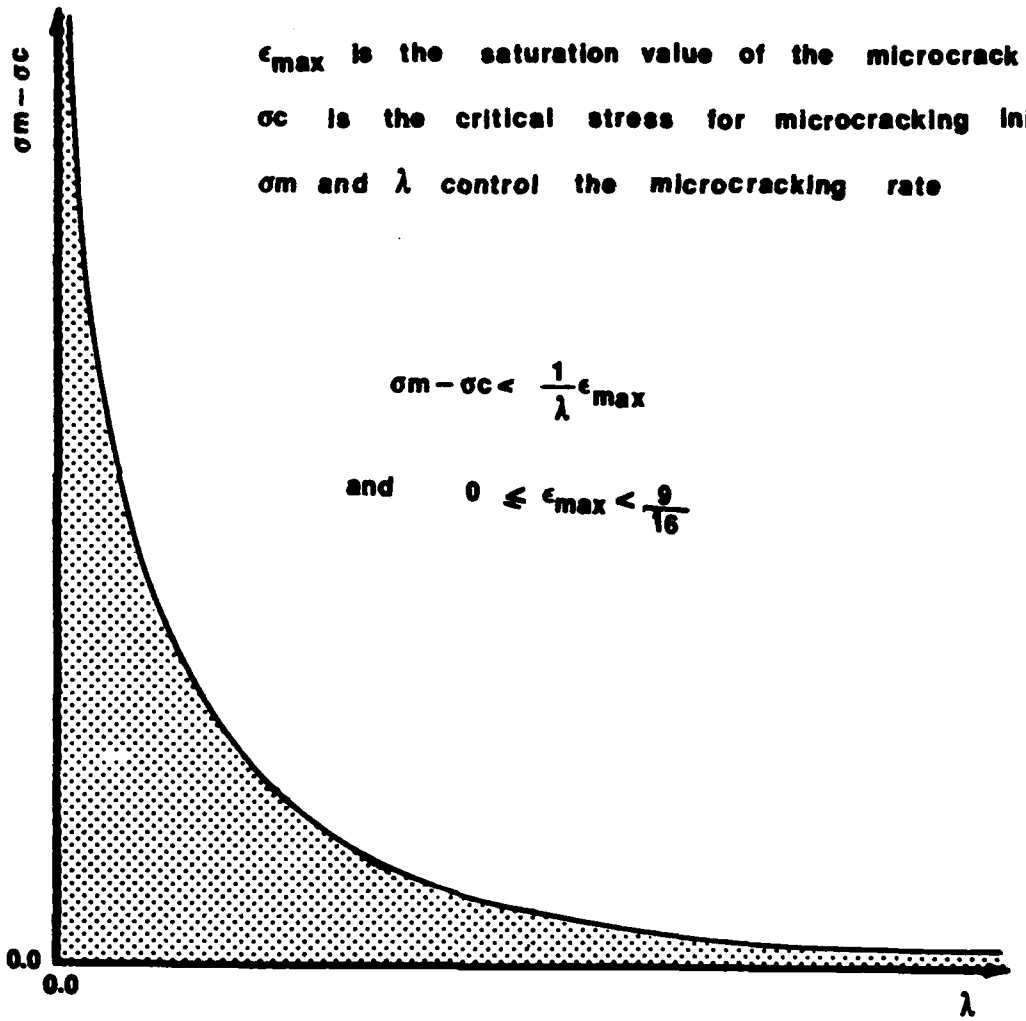

Fig. 4 Relations between the constants $\epsilon_{max}, \sigma c, \sigma m$ and λ

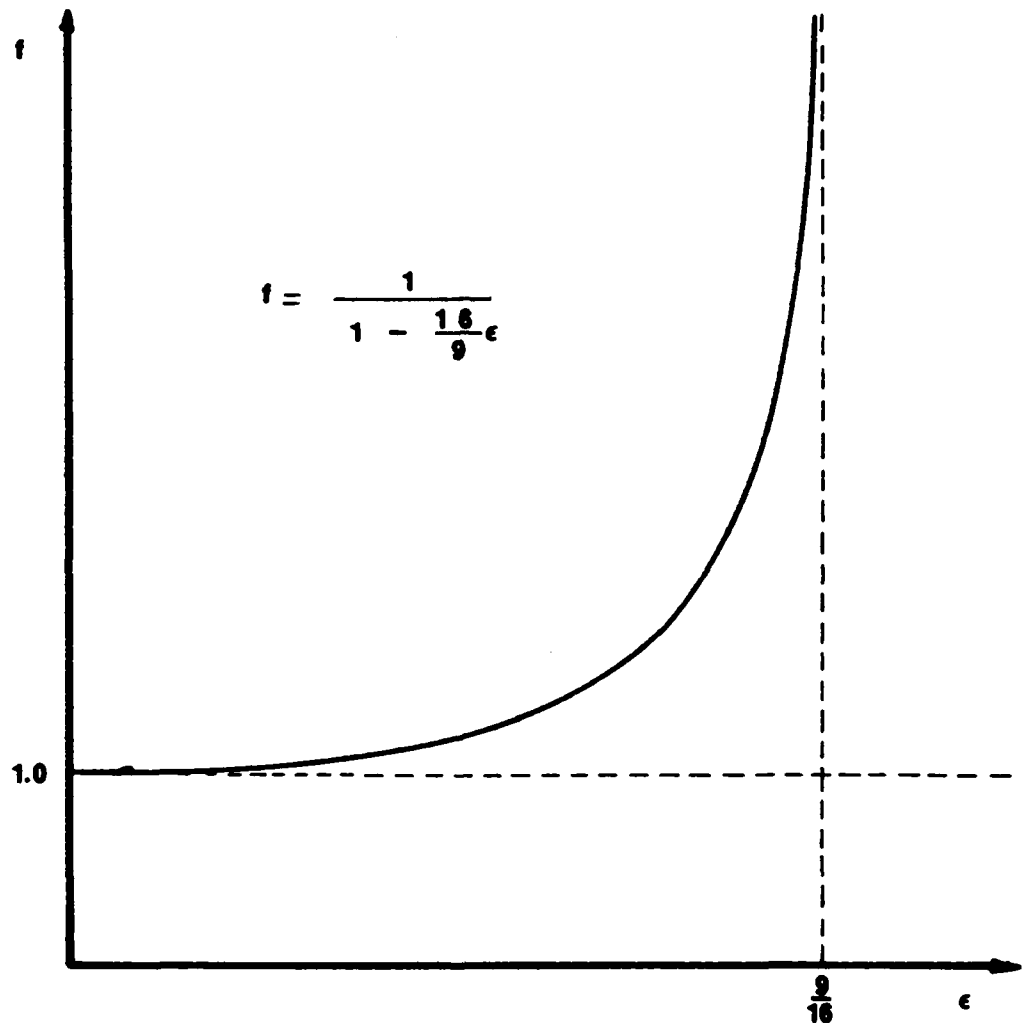

Fig. 3 Microcracking parameter f versus microcracking density ϵ

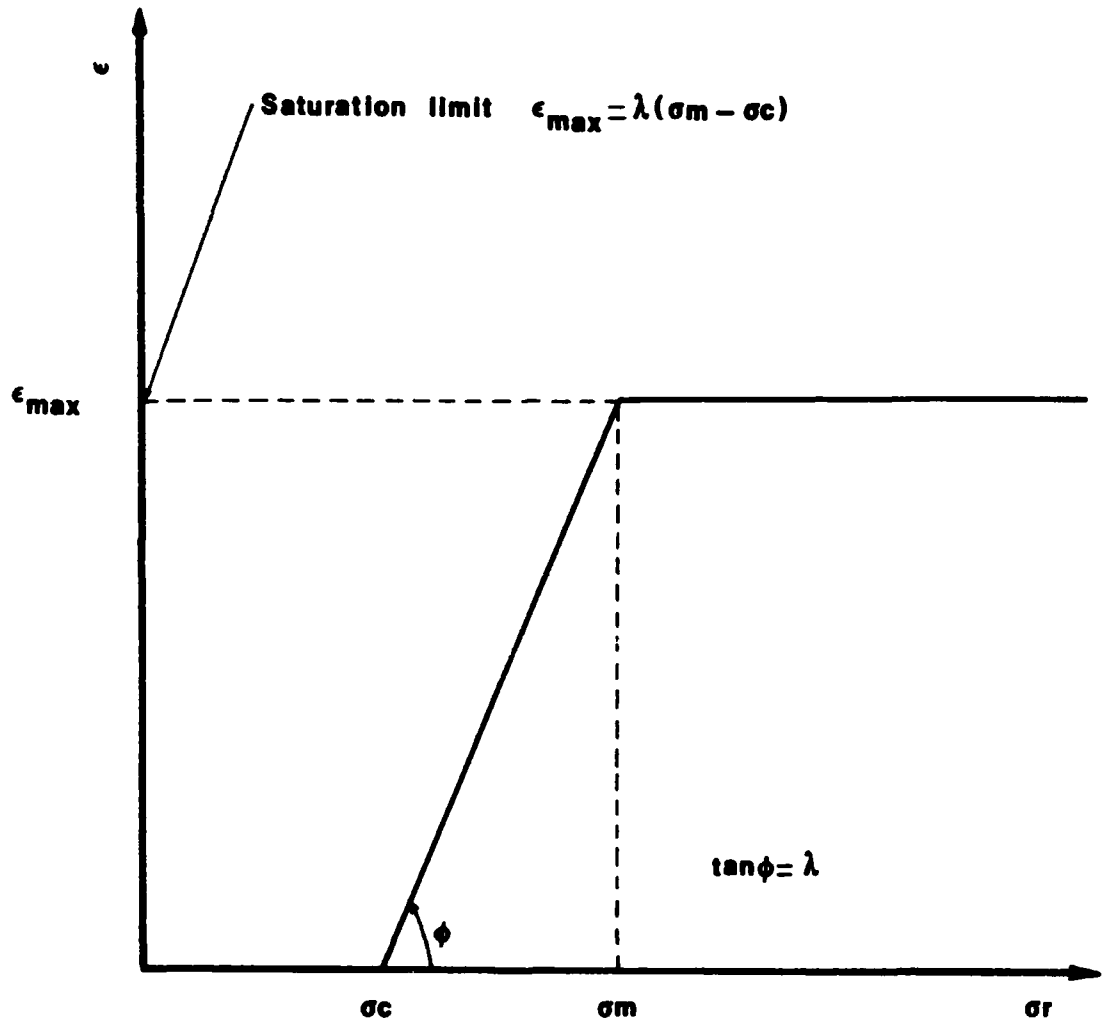

Fig. 2 Microcracking density ε versus equivalent stress σr

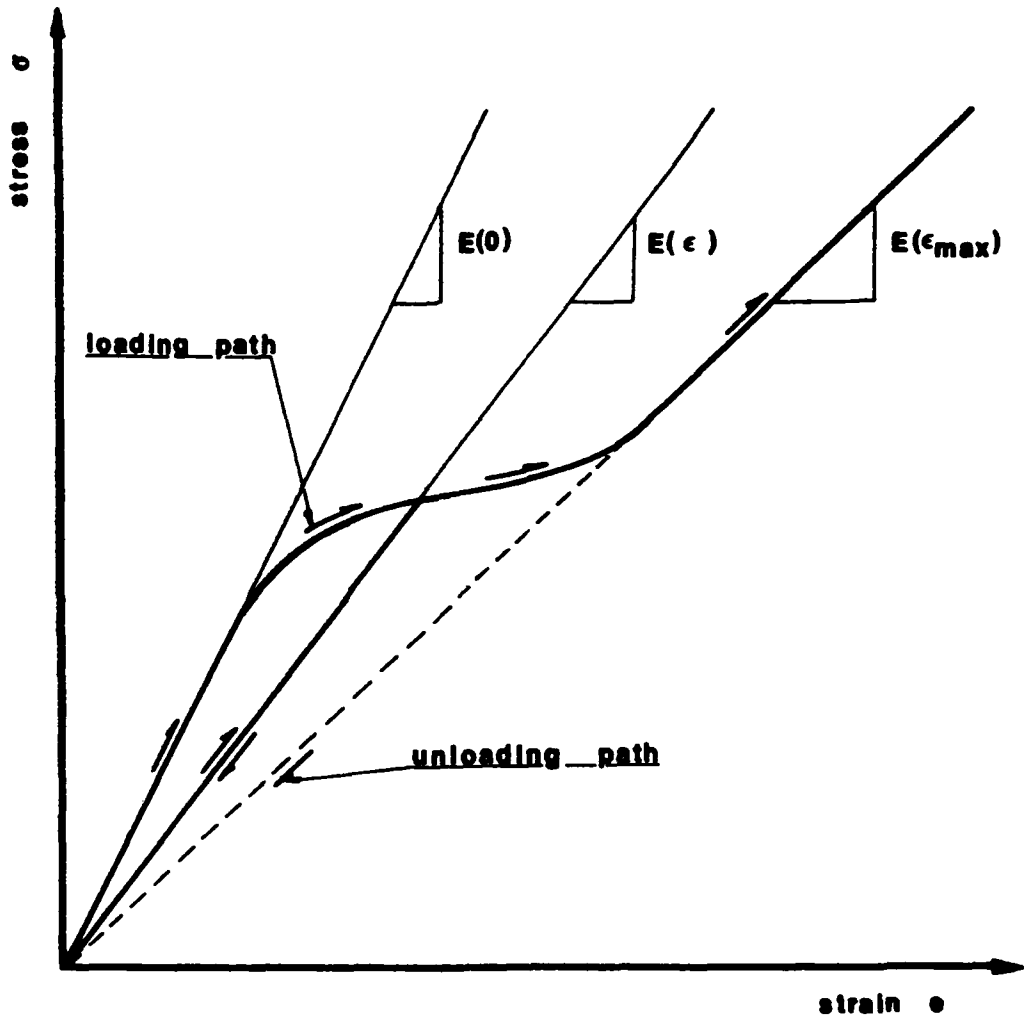

Fig.1 Stress–Strain curve for a microcracked material

References

1. B. Budiansky and R. J. O'Connell. "Elastic moduli of Cracked Solid" Int. J. Solids Structures Vol. 12, 81-97 (1975).

2. R. G. Hoagland, J. D. Embury and D. J. Green. "On the density of microcracks formed during the fracture of ceramics" Scr. Metall., 9, 9, 907 (1975).

3. A. G. Evans "On the formation of a crack tip microcrack zone." Scr. Metall. 10, 1, 93-97 (1976).

4. R. G. Hoagland and J. D. Embury. "A treatment of inelastic deformation around a crack tip due to microcracking" J. Am. Ceram. Soc, 63, 7, 404 (1980).

5. Y. Fu and A. G. Evans. "Microcrack zone formation in single phase polycrystals" Acta Metal. Vol 30, 1619-1625 (1982).

6. R. M. McMeeking and A. G. Evans. "Mechanics of Transformation Toughening in Brittle materials." J. Amer. Ceram. Soc. 65(5), 242-245 (1982).

7. B. Budiansky, J. W. Hutchinson and J. C. Lampropoulos, "Continuum theory of dilatant transformation toughening in Ceramics." Int. J. Solids Structures Vol 19, 337-355, (1983).

8. A. G. Evans and K. T. Faber. "Crack-growth resistance of Microcracking Brittle Materials." J. Amer. Ceram. Soc. 67, 4, 255-260 (1983).

9. K. T. Faber "Microcracking Contributions to the toughness of ZrO_2-Based Ceramics.. To appear in Advances in ceramics 11: Poceedings of the second International conference on the science and technology of Zirconia.

10. Yen Fu, "Mechanics of microcracking toughening in ceramics" Ph.D. Thesis U.C.B.C. (1983).

11. Rice, J. R. "Mathematical Analysis in the Mechanics of Fracture" in Fracture, An Advanced Treatise (Ed. H. Liebowitz) Academic Press, 192-308 (1968).

let $\alpha = \lambda\sigma_C + \frac{9}{16}$

$\beta = \lambda\sigma_C \cdot \nu + \frac{9}{16}(\nu-1)$

$\gamma = -\frac{9}{16} \cdot \nu$

then <u>for plane strain:</u>

$$a_6 = \alpha^2$$

$$a_5 = 2\alpha\beta - 4\nu\alpha^2$$

$$a_4 = \beta^2 + 2\alpha\gamma - 8\nu\alpha\beta + 4\nu^2\alpha^2 - \lambda^2E^2[e_x^2 + e_y^2 + \tfrac{1}{2}\gamma_{xy}^2]$$

$$a_3 = 2\beta\gamma - 4\nu(\beta^2 + 2\alpha\gamma) + 8\alpha\beta\nu^2 - 2\lambda^2E^2\nu[(e_x+e_y)^2 - 2\nu[e_x^2 + e_y^2 + \tfrac{1}{2}\gamma_{xy}^2] \quad (8)$$

$$a_2 = \gamma^2 - 8\nu\beta\gamma + (\beta^2 + 2\alpha\gamma)4\nu^2 - (\lambda E\nu)^2[4(e_x^2 + e_y^2 + \tfrac{1}{2}\gamma_{xy}^2 - (e_x + e_y)^2]$$

$$a_1 = 8\beta\gamma\nu^2 - 4\nu\gamma^2$$

$$a_0 = 4\nu^2\gamma^2$$

<u>for plane stress</u>

$$a_6 = \alpha^2$$

$$a_5 = 2a\beta - 2\nu\alpha^2$$

$$a_4 = \beta^2 + 2\alpha\gamma - 4\nu\alpha\beta + \nu^2\alpha^2 - \lambda^2E^2[e_x^2 + e_y^2 + \tfrac{1}{2}\gamma_{xy}^2]$$

$$a_3 = 2\beta\gamma - 2\nu(\beta^2 + 2\alpha\gamma) + 2\alpha\beta\nu^2 - \lambda^2E^2\nu[4e_xe_y - \gamma_{xy}^2] \quad (9)$$

$$a_2 = \gamma^2 - 4\beta\gamma\nu + \nu^2(\beta^2 + 2\alpha\gamma) - (\lambda E\nu)^2[e_x^2 + e_y^2 + \tfrac{1}{2}\gamma_{xy}^2]$$

$$a_1 = 2\beta\gamma\nu^2 - 2\nu\gamma^2$$

$$a_0 = \nu^2\gamma^2 .$$

APPENDIX II

The microcracking law given by equation (3) earlier in this paper allow us to determine the microcrack density ε for a given stress state. It is more convenient to determine ε or $f = 1/(1 - \frac{16}{9}\varepsilon)$ for a given strain state.

from the constitutive law $\sigma_{ij} = \frac{E}{f+\nu}[e_{ij} + \frac{\nu}{f-2\nu} e_{kk}\,\delta_{ij}]$ (1)

we get $\sigma_R = [\sigma_{ij}\,\sigma_{ij}]^{1/2} = \frac{E}{f+\nu}[e_{ij}\,e_{ij} + \nu\,\frac{2f-\nu}{(f-2\nu)^2}\,e_{kk}^2]^{1/2}$ (2)

then we have the following cases in computing f.

i) $\sigma_R(f) < \sigma_C \Rightarrow \quad \varepsilon = 0 \Rightarrow \quad f = \dfrac{1}{1 - \frac{16}{9}\varepsilon} = 1.$ (3)

ii) $\sigma_R(f) > \sigma_M \Rightarrow \varepsilon = \varepsilon_M = \lambda(\sigma_M - \sigma_C) \Rightarrow f = \dfrac{1}{1 - \frac{16}{9}\varepsilon_M}.$ (4)

iii) $\sigma_C < \sigma_R(f) < \sigma_M \Rightarrow \varepsilon = \lambda(\sigma_R - \sigma_C).$ (5)

substituting σ_R from equation (2) in eqn (5) we have

$$\frac{9}{16}(1 - \frac{1}{f}) = \lambda\,\frac{E}{f+\nu}[e_{ij}\,e_{ij} + \nu\,\frac{2f-\nu}{(f-2\nu)^2}\,e_{kk}^2]^{1/2} - \lambda\sigma_C. \qquad (6)$$

which is a sixth order polynomial in f of the form

$$a_6 f^6 + a_5 f^5 + a_4 f^4 + a_3 f^3 + a_2 f^2 + a_1 f + a_0 = 0 \qquad (7)$$

whose coefficients are given below.

stress discontinuity

we allow $\bar{\sigma}_{xx} = \sigma_{xx}$ and require $\bar{e}_{yy} = e_{yy}$

we get $(f+\nu)(1-\bar{\nu}^*)\bar{\sigma}_{yy} = (1-\nu^*)\sigma_{yy} + (\bar{\nu}^*(f+\nu) - \nu^*(1+\nu))\sigma_{xx}$

or $\bar{\sigma}_{yy} = \frac{1}{f}\sigma_{yy}$ for Plane stress

and $\bar{\sigma}_{yy} = f\frac{1-\nu^2}{f^2-\nu^2}\sigma_{yy} - (f-1)\frac{\nu^2}{f^2-\nu^2}\sigma_{xx}$ for Plane strain

strain discontinuity

we allow $\bar{e}_{yy} = e_{yy}$ and require $\bar{\sigma}_{xx} = \sigma_{xx}$

we get $\bar{e}_{xx} = [\frac{\nu^*}{1-\bar{\nu}^*}\frac{(f+\nu)(1-2\bar{\nu}^*)}{(1-\nu)(1-2\nu^*)} - \frac{\bar{\nu}^*}{1-\bar{\nu}^*}]\, e_{yy} - \frac{1-\nu^*}{1-\bar{\nu}^*}\frac{(f+\nu)(1-2\bar{\nu}^*)}{(1-\nu)(1-2\nu^*)}\, e_{xx}$

Plane strain: $\bar{e}_{xx} = (\frac{f-2\nu}{(1-2\nu)(1-\nu)} - \frac{1}{f-\nu})\nu e_{yy} + \frac{1-\nu}{f-\nu}\frac{(f-\nu)(f-2\nu)}{(1-\nu)(1-2\nu)}\, e_{xx}$

Plane stress: $\bar{e}_{xx} = \frac{\nu}{f}(\frac{f^2-1}{1-\nu^2}\, e_{yy} + \frac{1}{f}\frac{f+\nu}{1+\nu}\, e_{xx})$

Notice that for f=1 (unmicrocracked material) $\bar{\sigma}_y = \sigma_y$ and $\bar{e}_{xx} = e_{xx}$, both stress and strains are continuous. for microcracked materials f>1 and $\bar{\sigma}_y < \sigma_y$ whereas $\bar{e}_{xx} > e_{xx}$. The strains are larger in the microcracked region and the stresses fall to a lower value.

Fig. 8a eyy strain ahead of the crack tip

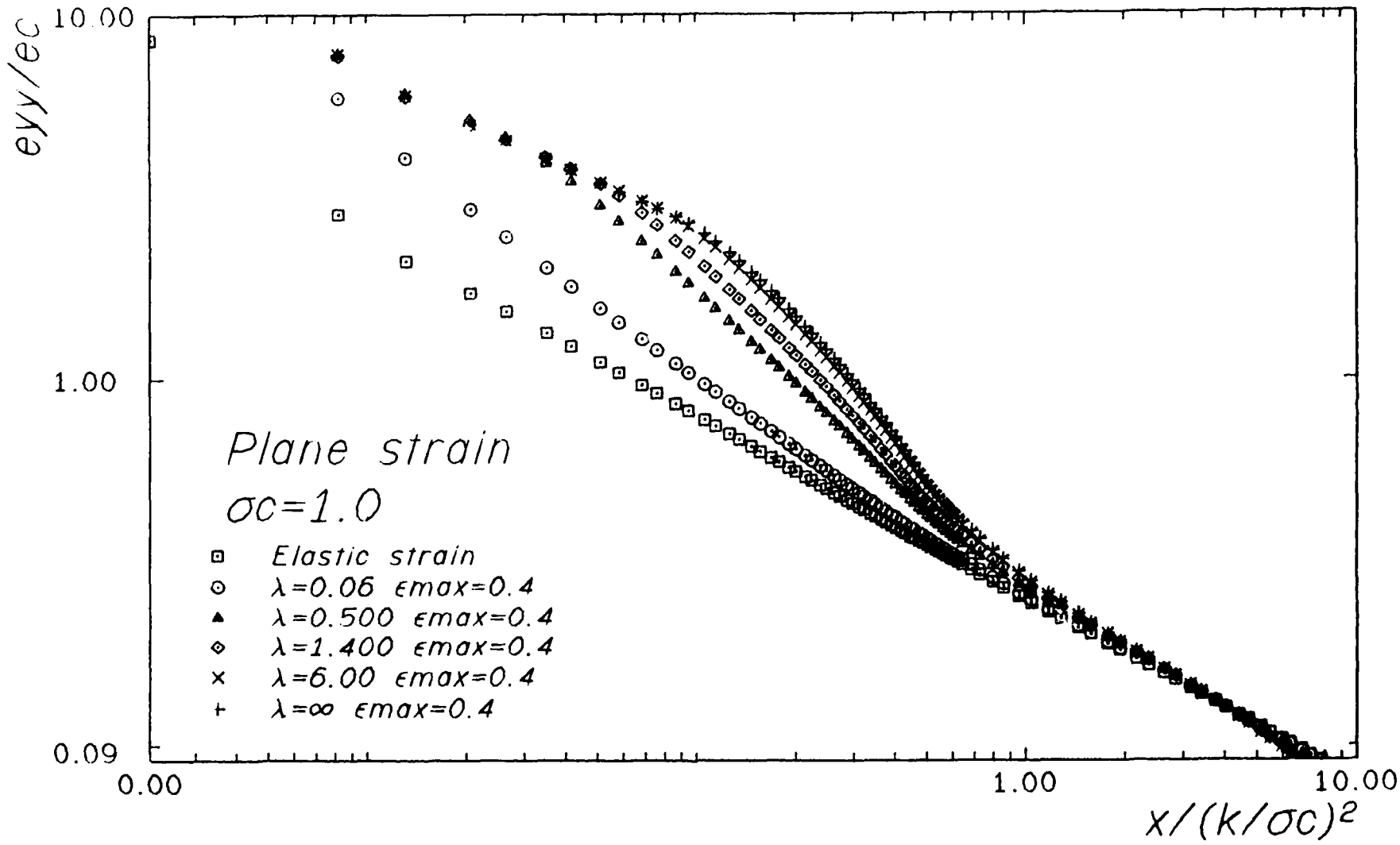

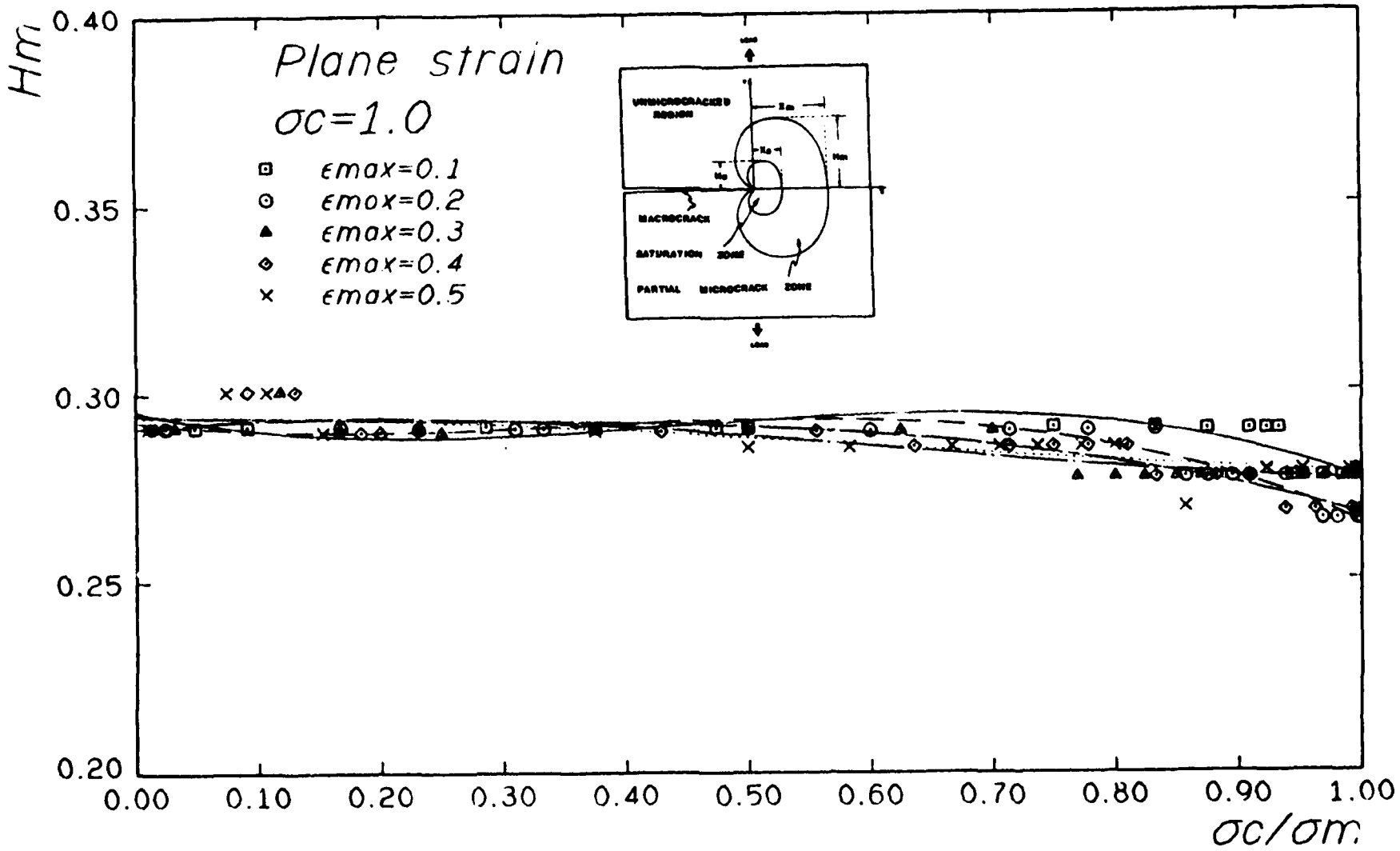

Fig. 9 Hm Maximum height of microcracked zone

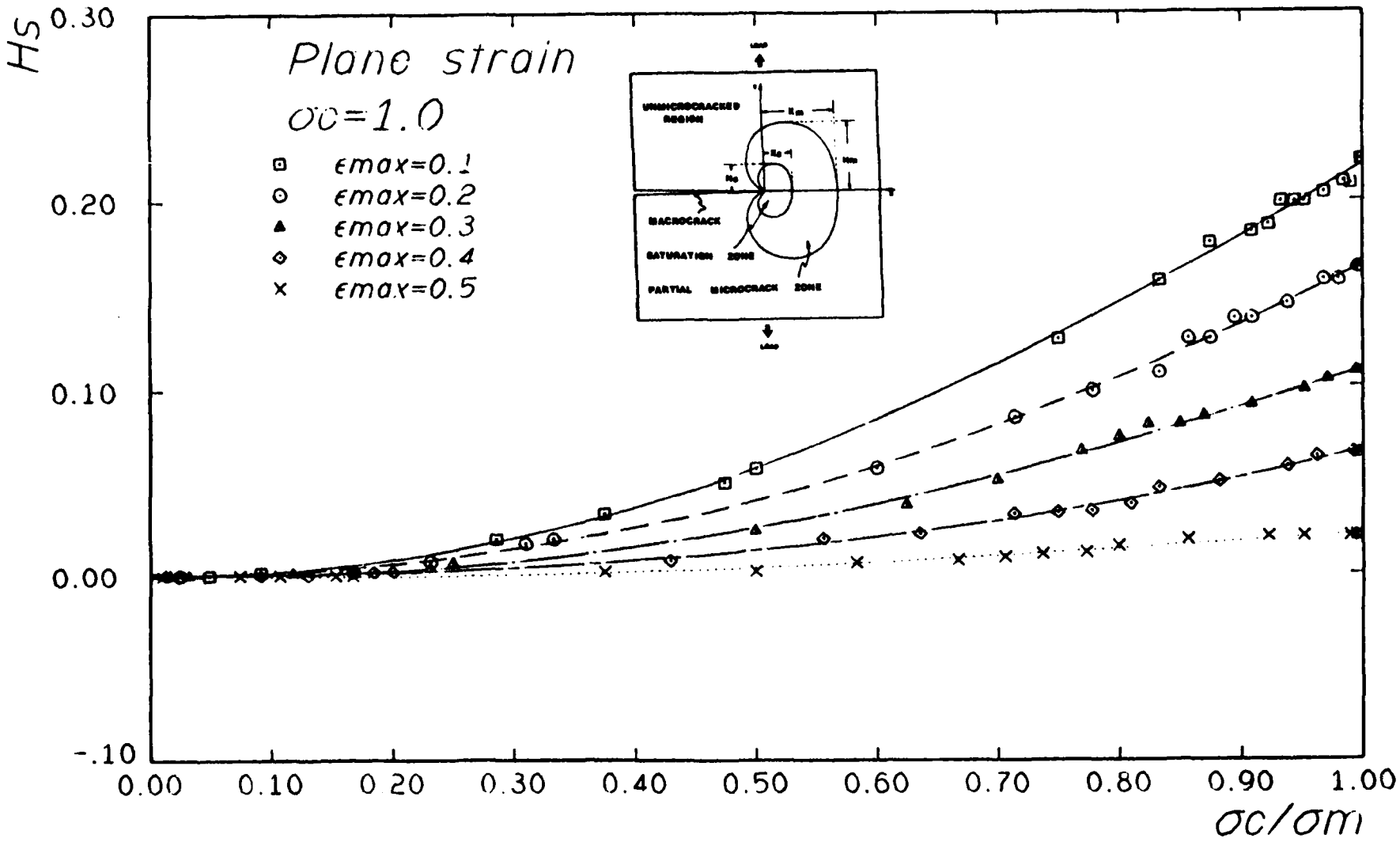

Fig. 9a Hs Maximum height of saturated zone

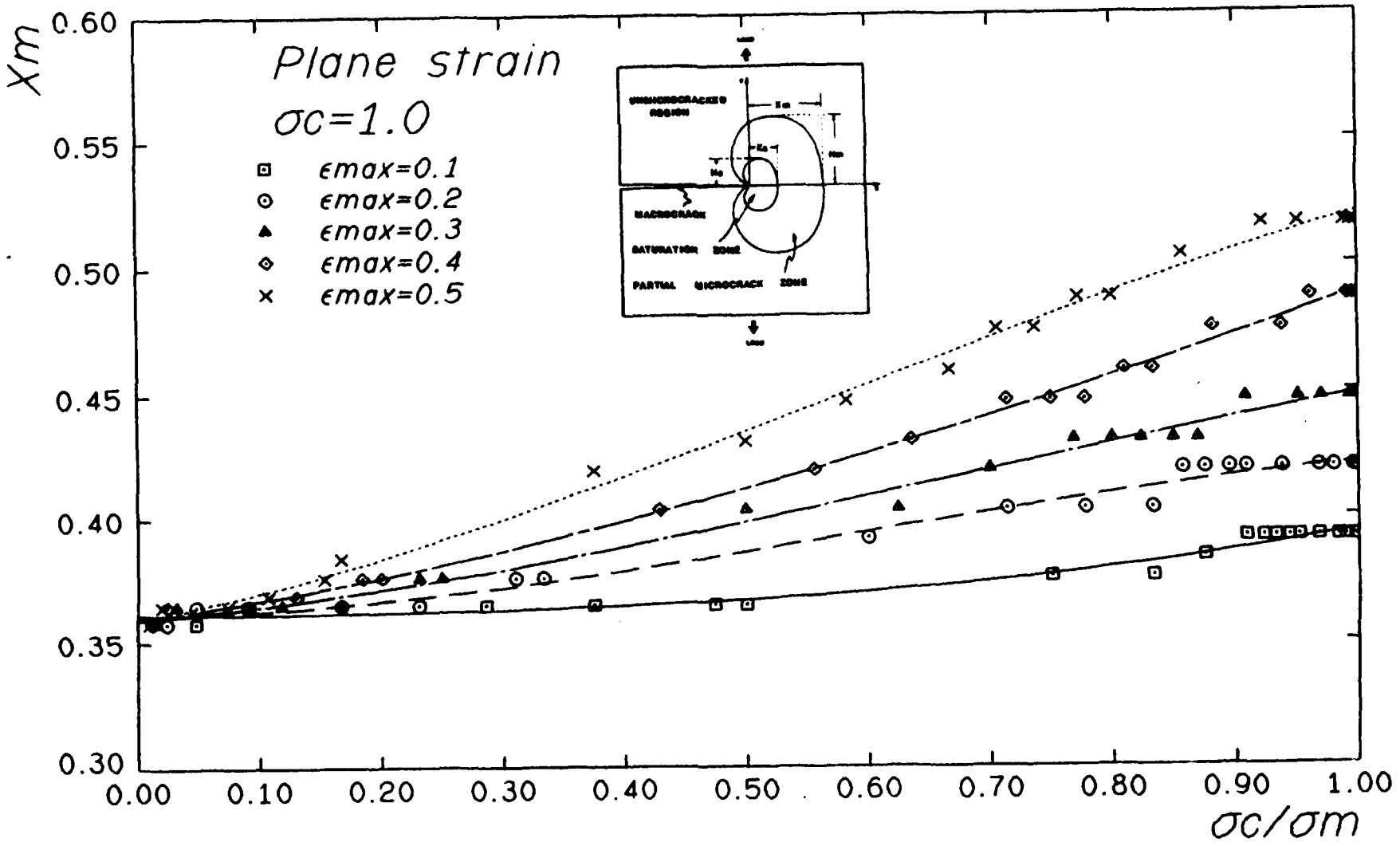

Fig. 9β Xm Maximum length of microcraced zone

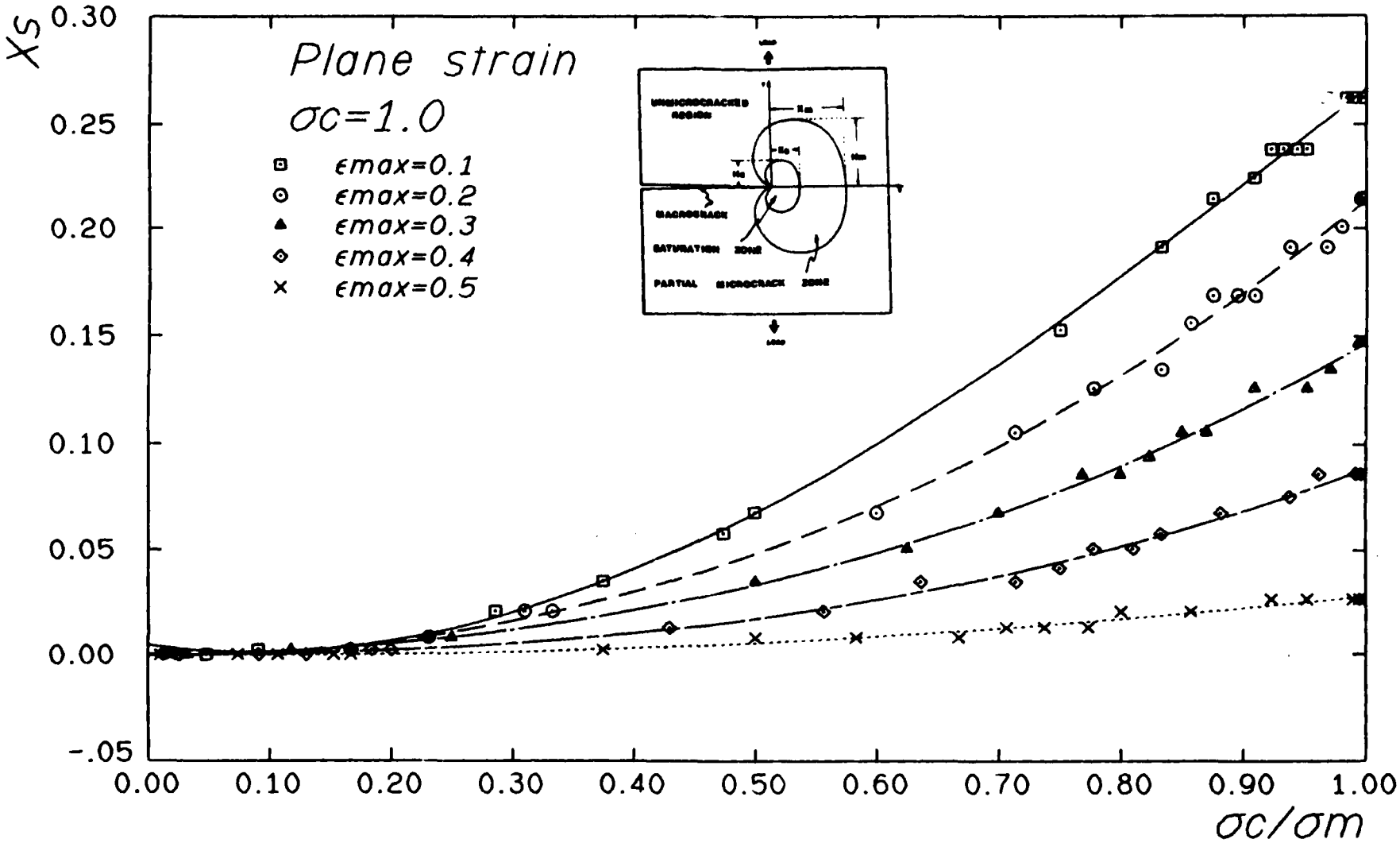

Fig. 9γ Xs Maximum length of saturated zone

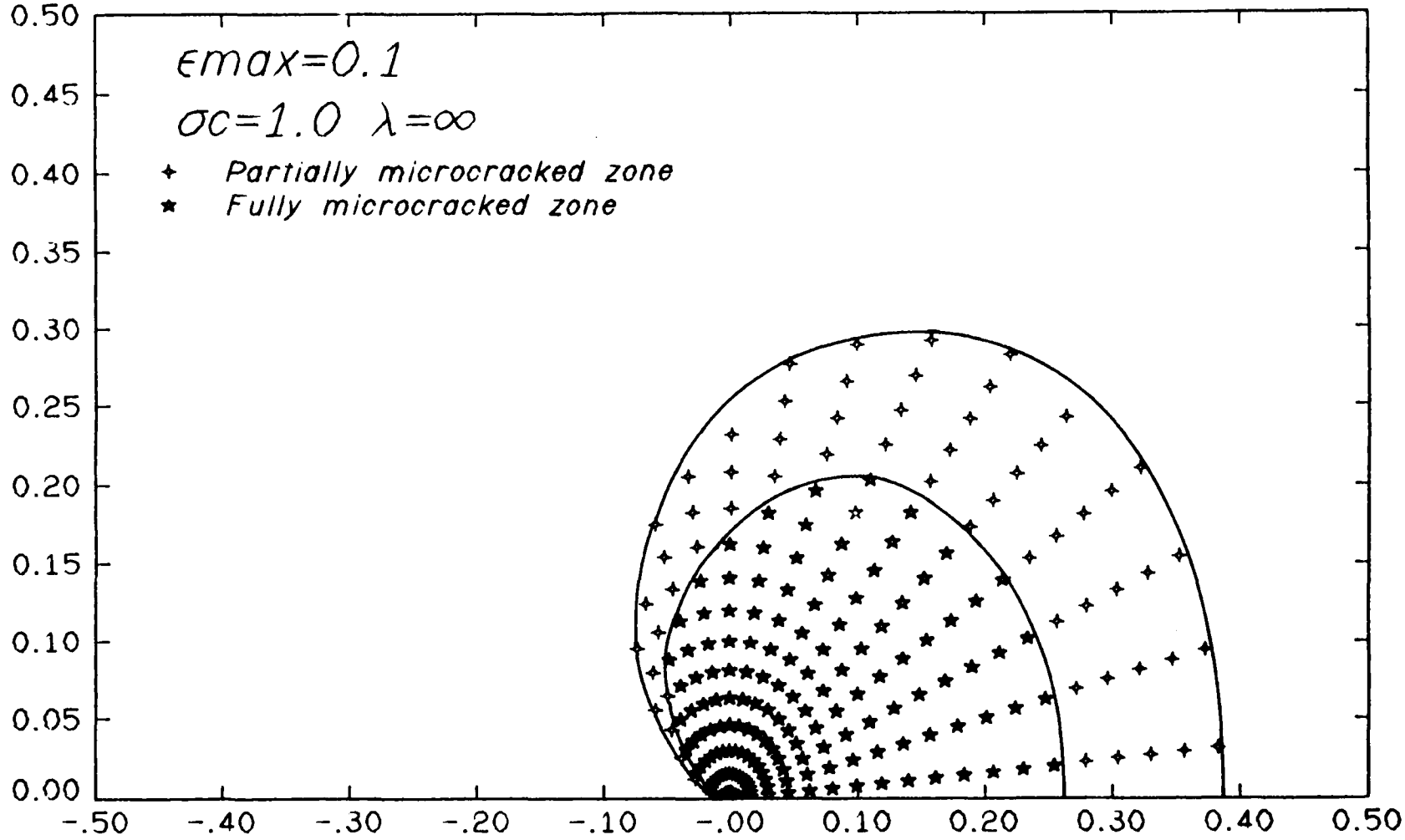

Fig. 10 The transformation zone around the crack tip

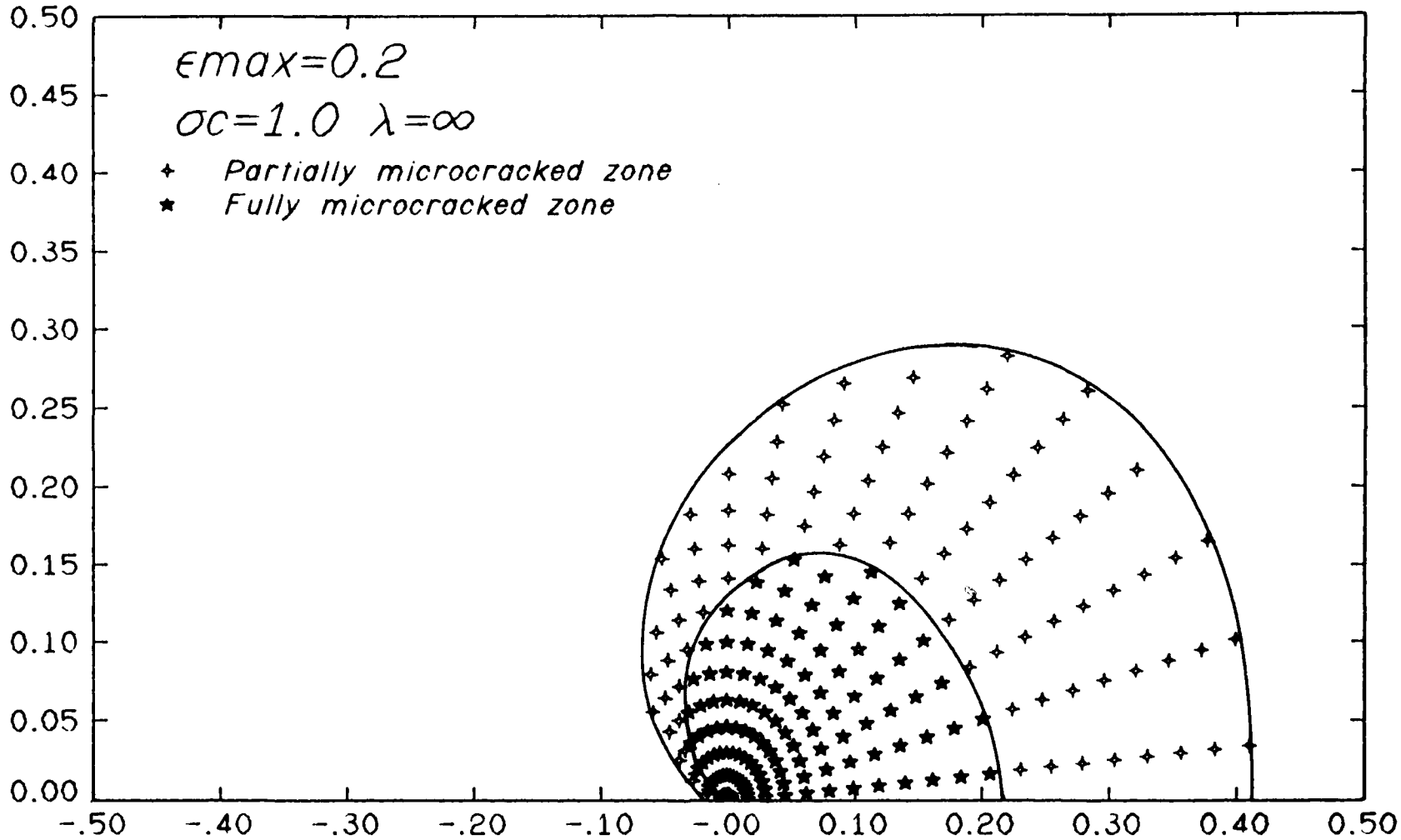

Fig. 10β The transformation zone around the crack tip

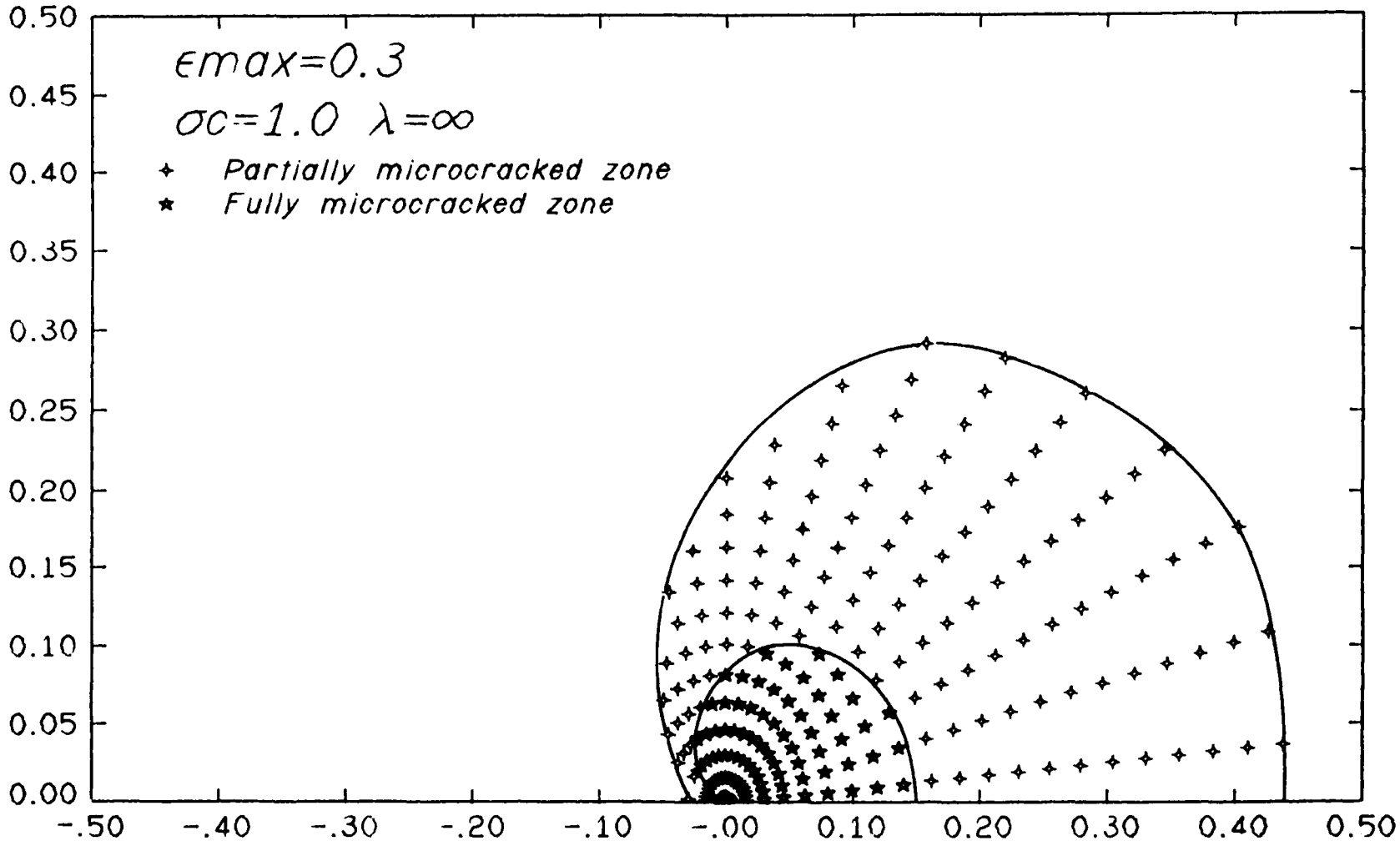

Fig. 10γ The transformation zone around the crack tip

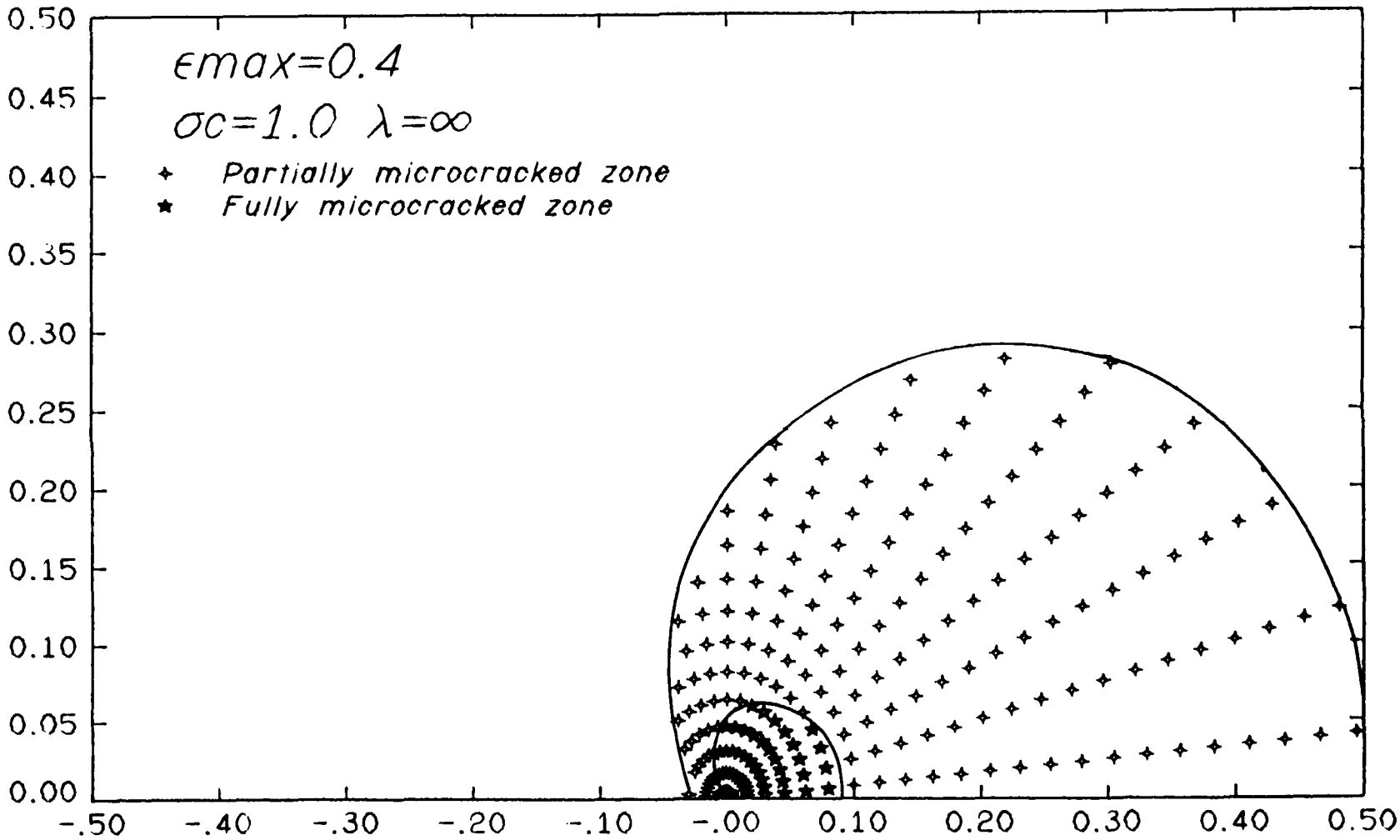

Fig. 10δ The transformation zone around the crack tip

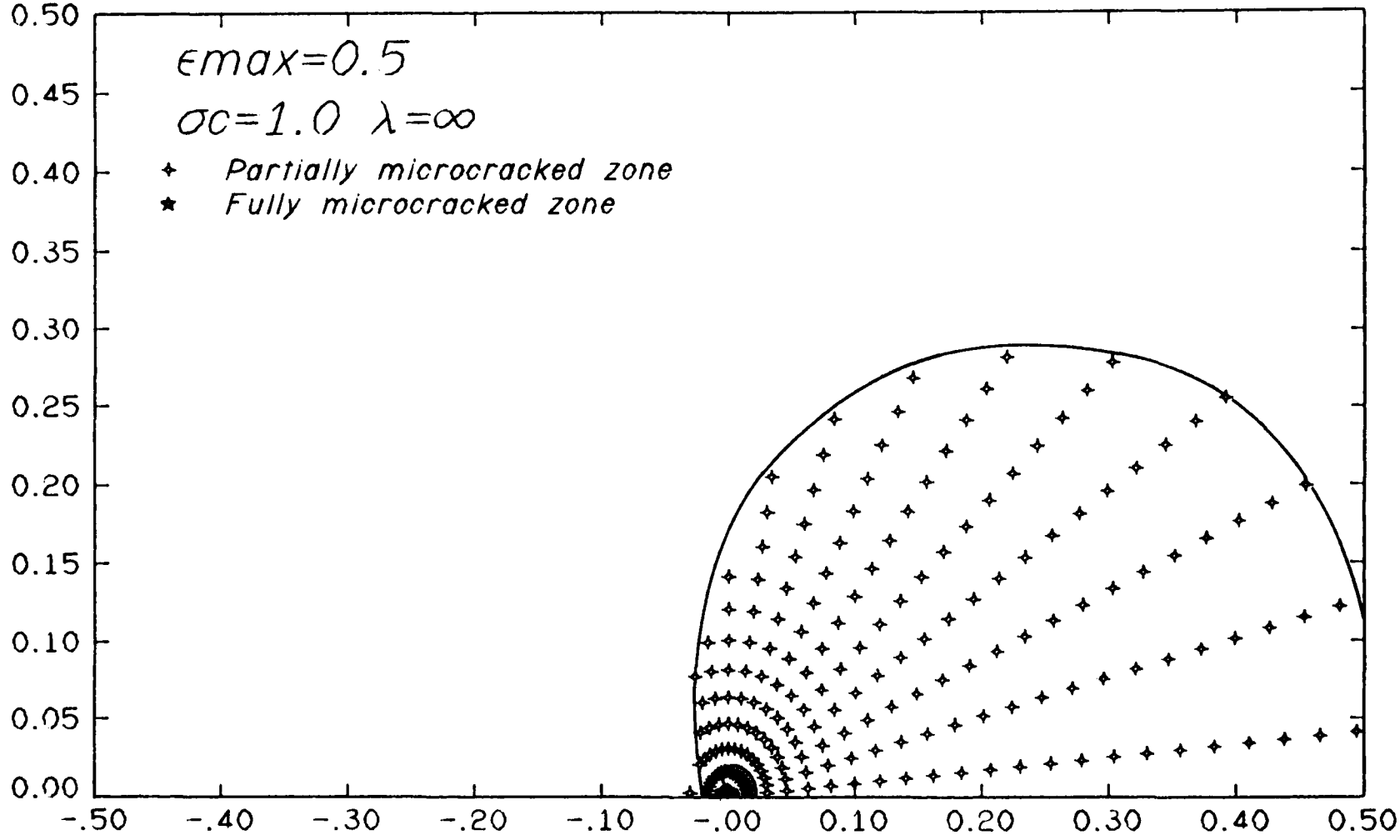

Fig. 10ε The transformation zone around the crack tip

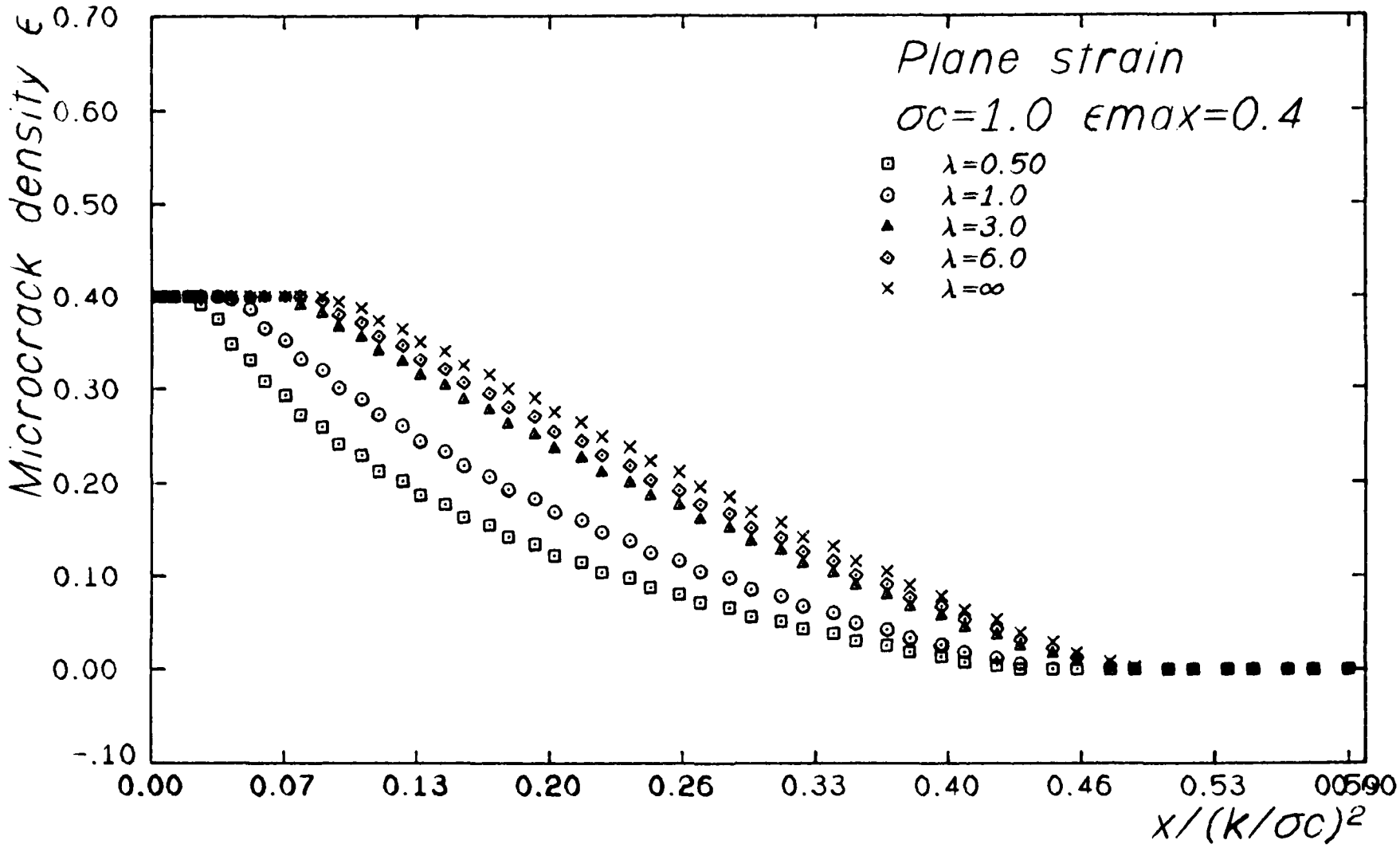

Fig. 11 Microcrack density ahead of the crack tip

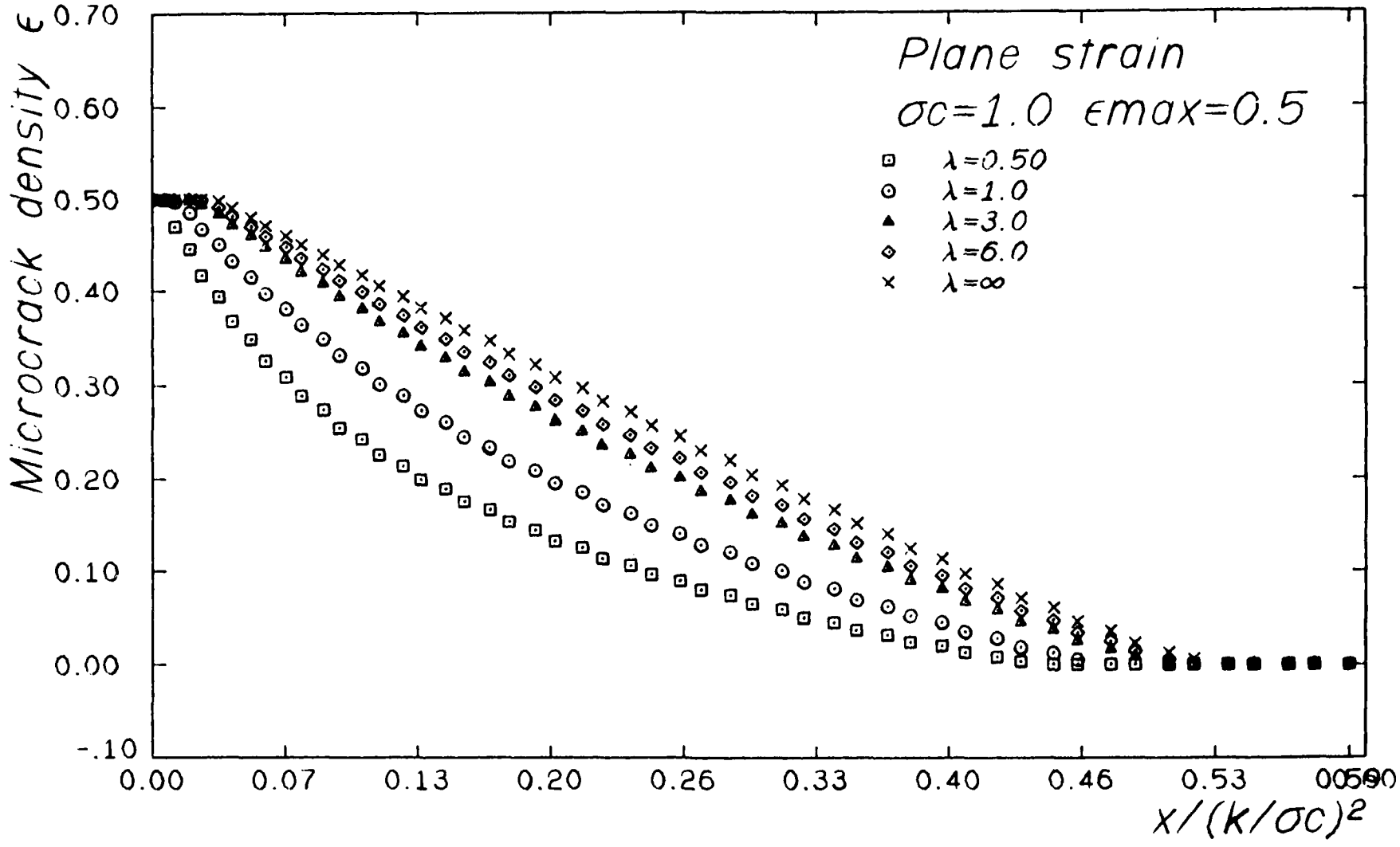

Fig. 12 Microcrack density ahead of the crack tip

Stress Intensity Factors for Slightly Kinked, Partially Closed Cracks in Compression

N. Aravas and R. M. McMeeking
Department of Theoretical and Applied Mechanics
University of Illinois at Urbana-Champaign
Urbana, IL 61801

April 1984

SUMMARY

A solution is presented for the elastic stress intensity factors at the tips of a slightly kinked, partially closed crack in compression. The solution is accurate to first order in the deviation of the crack surface from a straight line and is carried out using perturbation procedures analogous to those of Banichuk [5], Goldstein and Salganik [6] and Cotterell and Rice [7] for the problem of an open crack. Comparison with the exact solution indicates that the asymptotic solution is accurate for values of the angle between the straight crack and its out-of-plane kinks up to about 20°.

1. INTRODUCTION

Experiments on glass plates containing pre-existing planar through cracks oriented at an angle to the direction of the axial compression have revealed that the relative sliding of the faces of the pre-existing cracks does not result in co-planar crack growth, but rather produces at the tips of the pre-existing cracks small tension cracks which deviate at sharp angles from the sliding plane [1-4]. These experiments are designed to be models for the propagation of cracks in rocks in compression. In this paper, we are concerned with the calculation of stress intensity factors at the tips of the kinked open extensions of a closed sliding through crack. The same method can be extended to a curved crack with several closed sections. The solution obtained is accurate to first order in the deviation of the crack surface from a straight line drawn between the kink tips and is carried out using perturbation procedures similar to those used in Refs. [5-9] for the problem of the open crack. The results can be stated in terms of known solutions for a single straight crack or a co-linear array of straight cracks.

AD-A154 049 THE MECHANICS OF INTERNAL STRESS AND MICROCRACK TOUGHENING MECHANISMS IN CERAMICS(U) ILLINOIS UNIV AT URBANA DEPT OF THEORETICAL AND APPLIED MECHA.. 2/2

UNCLASSIFIED AM McMeeking APR 85 N00014-81-K-0650 F/G 11/2 NL

END

FILMED

DTIC

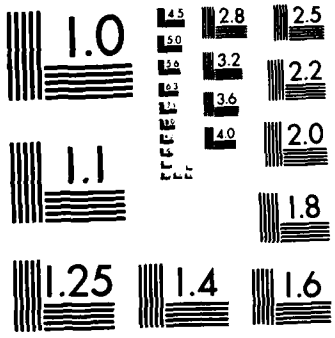

MICROCOPY RESOLUTION TEST CHART
NATIONAL BUREAU OF STANDARDS-1963-A

A complete solution to the problem of the sliding kinked crack has been given by Nemat-Nasser and Horii [3], who used a continuous distribution of dislocations to model the crack and its kinks. In order to find the stress intensity factors, they solved numerically a singular integral equation for the dislocation distribution. In contrast, we can avoid the solution of the singular integral equation by using the results of the asymptotic analysis for the stress intensity factors. However, the validity of the asymptotic solution is limited to small deviations of the crack surface from a straight line. Comparisons with the exact solution given in Ref. [3] indicate that the first order solution for the mode I stress intensity factor is accurate for values of the angle between the straight crack and its out-of-plane kinks up to about 20°.

2. GENERAL FORMULATION OF THE PROBLEM

2.1 Formulation of the boundary value problem

Consider an infinite plate of a homogeneous, isotropic, linearly elastic, brittle solid containing a curved crack on $y = \lambda(x)$, with its tips at the positions $x = \pm a$ (Fig. 1). A uniform state of stress σ_{xx}^{∞}, σ_{yy}^{∞} and σ_{xy}^{∞} is applied at infinity, with $\sigma_{yy}^{\infty} < 0$ and $\sigma_{xy}^{\infty} < 0$, where tension is regarded as positive. The corresponding two-dimensional boundary value problem is given by

$$\begin{aligned} &\sigma_{ji,j} = 0 \\ &2\varepsilon_{ij} = u_{i,j} + u_{j,i} \qquad \text{in } V , \\ &\sigma_{ij} = C_{ijk\ell}\varepsilon_{k\ell} \end{aligned} \tag{1}$$

$$\sigma_{ij} = \sigma_{ij}^{\infty} \qquad \text{at infinity,} \tag{2}$$

$$\sigma_{nn}(x, \lambda) = \sigma_{ns}(x, \lambda) = 0 \qquad \text{on the open portions of the crack,} \tag{3}$$

$$\sigma_{ns}(x, \lambda) = \mu\sigma_{nn}(x, \lambda) \qquad \text{on the sliding portions}$$

$$u_n^+(x, \lambda) = u_n^-(x, \lambda) \qquad \text{of the crack,} \tag{4}$$

where σ_{ij} , ε_{ij} and u_i are the stress, strain and displacement fields in the region V occupied by the body, $C_{ijk\ell}$ is the fourth order tensor of the elastic moduli, σ_{nn} and σ_{ns} are the normal and shear tractions at the crack surface, u_n is the displacement in the direction normal to the crack surface, μ is the coefficient of friction, $A_{,i}$ is $\partial A/\partial x_i$ and the superscripts plus and minus denote the value of the indicated quantity on the upper and lower surfaces of the crack. Note that the open and sliding portions of the crack are, in general, not known in advance and their determination becomes part of the solution.

2.2 Small-parameter expansion

The essence of the approximation we use is that the solution to the problem with the curved crack is close, in some sense, to the solution of a similar problem for a straight crack. In fact, we shall use the solution to the following problem, involving a flat crack, as the leading or zeroth order approximation in our expansion. Let $\underset{\sim}{\sigma}^{(0)}$, $\underset{\sim}{\varepsilon}^{(0)}$ and $\underset{\sim}{u}^{(0)}$ be such that

$$\begin{aligned} &\sigma_{ji,j}^{(0)} = 0 \\ &2\varepsilon_{ij}^{(0)} = u_{i,j}^{(0)} + u_{j,i}^{(0)} \qquad \text{in } V' \\ &\sigma_{ij}^{(0)} = C_{ijk\ell}\varepsilon_{k\ell}^{(0)} \end{aligned} \tag{5}$$

and $\sigma_{ij}^{(0)} = \sigma_{ij}^{\infty}$ at infinity (6)

$\sigma_{yy}^{(0)}(x, 0) = \sigma_{xy}^{(0)}(x, 0) = 0$ on the open portions of the crack, (7)

$\sigma_{xy}^{(0)}(x, 0) = \mu\sigma_{yy}^{(0)}(x, 0)$ on the sliding portions

$u_y^+(x, 0) = u_y^-(x, 0)$ of the crack, (8)

where V' is the plane with a straight slit lying on the x-axis from $-a$ to a. If the slope of the actual crack, $\lambda'(x)$, has order of magnitude $\varepsilon \ll 1$ at its largest, then we can seek a perturbation expansion in ε for the solution to the problem of the curved crack, such that

$$\underset{\sim}{\sigma} = \underset{\sim}{\sigma}^{(0)} + \underset{\sim}{\sigma}^{(1)} + 0(\varepsilon^2) , \tag{9}$$

$$\underset{\sim}{\varepsilon} = \underset{\sim}{\varepsilon}^{(0)} + \underset{\sim}{\varepsilon}^{(1)} + 0(\varepsilon^2) , \tag{10}$$

$$\underset{\sim}{u} = \underset{\sim}{u}^{(0)} + \underset{\sim}{u}^{(1)} + 0(\varepsilon^2) , \tag{11}$$

where $\underset{\sim}{\sigma}^{(1)}$, $\underset{\sim}{\varepsilon}^{(1)}$ and $\underset{\sim}{u}^{(1)}$ are all $0(\varepsilon)$ compared to the leading order terms. We mention that $\lambda'(x) = 0(\varepsilon)$ also means that $\lambda(x)/a = 0(\varepsilon)$, because $\lambda(\pm a) = 0$. What remains now is the finding of the equations and the boundary conditions governing $\underset{\sim}{\sigma}^{(1)}$, $\underset{\sim}{\varepsilon}^{(1)}$ and $\underset{\sim}{u}^{(1)}$. We note at this stage that our approach is identical to that of Cotterell and Rice [7], except that they addressed the problem of a crack open everywhere. Furthermore, they found their solutions and expressed their expansions in terms of Muskhelishvili's [10] complex potentials. We prefer to work in terms of fundamental quantities, although it is entirely possible that the partially

closed, slightly curved crack can also be solved by a variation of the complex variable treatment of Cotterell and Rice [5].

We return now to the question of finding $\underset{\sim}{\sigma}^{(1)}$, $\underset{\sim}{\varepsilon}^{(1)}$ and $\underset{\sim}{u}^{(1)}$. In order to find the equations and boundary conditions governing $\underset{\sim}{\sigma}^{(1)}$, $\underset{\sim}{\varepsilon}^{(1)}$ and $\underset{\sim}{u}^{(1)}$, we substitute the expansions (9)-(11) into equations (1)-(4). We also use the fact that both $\lambda(x)$ and $\lambda'(x)$ are $O(\varepsilon)$ to write expansions in ε for the tractions and displacements on the crack surface $y = \lambda(x)$. Using a tensorial transformation, we find that the normal and shear tractions on the actual crack can be written as

$$\sigma_{nn}(x, \lambda) = \frac{1}{2}[\sigma_{xx}(x, \lambda) + \sigma_{yy}(x, \lambda)] + \frac{1}{2}[\sigma_{yy}(x, \lambda) - \sigma_{xx}(x, \lambda)]\cos 2\theta - \sigma_{xy}(x, \lambda)\sin 2\theta ,$$

$$\sigma_{ns}(x, \lambda) = \sigma_{xy}(x, \lambda)\cos 2\theta + \frac{1}{2}[\sigma_{yy}(x, \lambda) - \sigma_{xx}(x, \lambda)]\sin 2\theta ,$$

where $\theta = \lambda'(x) + O(\varepsilon^3)$. Then, using a Maclaurin series expansion in θ for $\sin 2\theta$ and $\cos 2\theta$, we find

$$\sigma_{nn}(x, \lambda) = \sigma_{yy}(x, \lambda) - 2\lambda'(x)\,\sigma_{xy}(x, \lambda) + O(\varepsilon^2) ,$$

$$\sigma_{ns}(x, \lambda) = \sigma_{xy}(x, \lambda) + \lambda'(x)[\sigma_{yy}(x, \lambda) - \sigma_{xx}(x, \lambda)] + O(\varepsilon^2) .$$

If we now write Maclaurin series expansions in y for σ_{xx} , σ_{yy} and σ_{xy} , the last two equations become

$$\sigma_{nn}(x, \lambda) = \sigma_{yy}(x, 0) - \lambda(x)\frac{\partial\sigma_{xy}(x, 0)}{\partial x} - 2\lambda'(x)\,\sigma_{xy}(x, 0) + O(\varepsilon^2) , \qquad (12)$$

$$\sigma_{ns}(x, \lambda) = \sigma_{xy}(x, 0) - \lambda(x) \frac{\partial \sigma_{xx}(x, 0)}{\partial x} + \lambda'(x)[\sigma_{yy}(x, 0) - \sigma_{xx}(x, 0)] + 0(\varepsilon^2) , \tag{13}$$

where we have also used the equilibrium equations $\partial\sigma_{xy}/\partial y = -\partial\sigma_{xx}/\partial x$ and $\partial\sigma_{yy}/\partial y = -\partial\sigma_{xy}/\partial x$.

In a similar way we can show that

$$u_n(x, \lambda) = u_y(x, 0) + \lambda(x)\varepsilon_{yy}(x, 0) - \lambda'(x)u_x(x, 0) + 0(\varepsilon^2) . \tag{14}$$

Using the expansions (9)-(11), equations (12)-(14) can be written as

$$\sigma_{nn}(x, \lambda) = \sigma_{yy}^{(0)}(x, 0) + \sigma_{yy}^{(1)}(x, 0) - \lambda(x) \frac{\partial \sigma_{xy}^{(0)}(x, 0)}{\partial x} - 2\lambda'(x)\sigma_{xy}^{(0)}(x, 0) + 0(\varepsilon^2) , \tag{15}$$

$$\sigma_{ns}(x, \lambda) = \sigma_{xy}^{(0)}(x, 0) + \sigma_{xy}^{(1)}(x, 0) - \lambda(x) \frac{\partial \sigma_{xx}^{(0)}(x, 0)}{\partial x} + \lambda'(x)[\sigma_{yy}^{(0)}(x, 0) - \sigma_{xx}^{(0)}(x, 0)] + 0(\varepsilon^2) , \tag{16}$$

$$u_n(x, \lambda) = u_y^{(0)}(x, 0) + u_y^{(1)}(x, 0) + \lambda(x)\varepsilon_{yy}^{(0)}(x, 0) - \lambda'(x)u_x^{(0)}(x, 0) + 0(\varepsilon^2) . \tag{17}$$

Finally, substituting eqns. (9)-(11) and (15)-(16) into the boundary value problem formulated in Section 3.1 (eqns. (1)-(4)), taking into account (5)-(8) and separating zero and first order terms, we find that $\underset{\sim}{\sigma}^{(1)}$, $\underset{\sim}{\varepsilon}^{(1)}$ and $\underset{\sim}{u}^{(1)}$ should be the solution to the following boundary value problem

$$\sigma^{(1)}_{ji,j} = 0$$

$$2\varepsilon^{(1)}_{ij} = u^{(1)}_{i,j} + u^{(1)}_{j,i} \qquad \text{in } V' \tag{18}$$

$$\sigma^{(1)}_{ij} = C_{ijk\ell}\varepsilon^{(1)}_{k\ell}$$

with

$$\sigma^{(1)}_{ij} = 0 \qquad \text{at infinity,} \tag{19}$$

$$\sigma^{(1)}_{yy}(x,\ 0) = 0 \qquad \text{on the open portions of the crack,} \tag{20}$$

$$\sigma^{(1)}_{xy}(x,0) = \mu\sigma^{(1)}_{yy}(x,0)+\lambda(x)\,\frac{d}{dx}\,[\sigma^{(0)}_{xx}(x,0)-\mu\sigma^{(0)}_{xy}(x,0)] -$$

$$- \lambda'(x)[(1+2\mu^2)\sigma^{(0)}_{yy}(x,0)-\sigma^{(0)}_{xx}(x,0)] \qquad \text{for } |x| < a\ , \tag{21}$$

$$u^{(1)}_y(x,\ 0^+) - u^{(1)}_y(x,\ 0^-) =$$

$$= -\lambda(x)[\varepsilon^{(0)}_{yy}(x,0^+)-\varepsilon^{(0)}_{yy}(x,0^-)]+\lambda'(x)[u^{(0)}_x(x,0^+)-u^{(0)}_x(x,0^-)] \tag{22}$$

on the closed sliding portion of the crack.

3. FORMULAE FOR THE STRESS INTENSITY FACTORS

Following Cotterell and Rice [7], let ω be the angle of the crack tip at $x = a$, given by $\omega = \lambda'(a)$ to first order. The normal $(\sigma_{\omega\omega})$ and shear $(\sigma_{r\omega})$ stresses acting along the prolongation of the crack at a small distance r from the tip at $x = a$ are obtained by setting $\lambda = \omega r + O(\varepsilon^3) = \omega(x - a) + O(\varepsilon^3)$ into equations (15) and (16). So,

$$\sigma_{\omega\omega} = \sigma_{yy}^{(0)}(x,0)-\omega(x-a)\frac{\partial\sigma_{xy}^{(0)}(x,\ 0)}{\partial x} -2\omega\sigma_{xy}^{(0)}(x,0)+\sigma_{yy}^{(1)}(x,0)+0(\varepsilon^2) \ ,$$

$$\sigma_{r\omega} = \sigma_{xy}^{(0)}(x,0)-\omega(x-a)\frac{\partial\sigma_{xx}^{(0)}(x,\ 0)}{\partial x} +\omega[\sigma_{yy}^{(0)}(x,0)-\sigma_{xx}^{(0)}(x,0)]+\sigma_{xy}^{(1)}(x,0)+0(\varepsilon^2) \ .$$

Then, the stress intensity factors can be calculated as

$$K_I = \lim_{r\to 0^+} (\sqrt{2\pi r}\ \sigma_{\omega\omega}) = K_I^{(0)} + K_{I\omega}^{(1)} + K_I^{(1)} + 0(\varepsilon^2) \ , \tag{23}$$

$$K_{II} = \lim_{r\to 0^+} (\sqrt{2\pi r}\ \sigma_{r\omega}) = K_{II}^{(0)} + K_{II\omega}^{(1)} + K_{II}^{(1)} + 0(\varepsilon^2) \ , \tag{24}$$

where $K_I^{(0)}$, $K_{II}^{(0)}$, $K_I^{(1)}$ and $K_{II}^{(1)}$ are the stress intensity factors for the zeroth (eqns. (5)-(8)) and first order (eqns. (18)-(22)) problems, and

$$K_{I\omega}^{(1)} = -\omega\sqrt{2\pi}\lim_{x\to a^+}\left[(x-a)^{3/2}\frac{\partial\sigma_{xy}^{(0)}(x,\ 0)}{\partial x} + 2(x-a)^{1/2}\sigma_{xy}^{(0)}(x,\ 0)\right]$$

$$K_{II\omega}^{(1)} = -\omega\sqrt{2\pi}\lim_{x\to a^+}\left\{(x-a)^{3/2}\frac{\partial\sigma_{xx}^{(0)}(x,0)}{\partial x} + (x-a)^{1/2}\left[\sigma_{yy}^{(0)}(x,0) - \sigma_{xx}^{(0)}(x,0)\right]\right\} \ .$$

Using the last two equations and a Williams [11] expansion for the near crack tip stress field, we can show that

$$K_{I\omega}^{(1)} = -\frac{3}{2}\,\omega\,K_{II}^{(0)} \ , \tag{25}$$

and $$K_{II\omega}^{(1)} = \frac{1}{2}\,\omega\,K_I^{(0)} \ . \tag{26}$$

From the formulation of the first order problem (eqns. (18)-(22)), it is clear that this can be considered as the superposition of the following two problems; problem (i) with a prescribed normal displacment and zero shear traction on the sliding portions of the crack and with the rest of the crack traction free, and problem (ii) with a prescribed shear traction and zero normal traction everywhere on the crack face. Thus, knowing the solution of the zeroth order problem (eqns. (5)-(8)) and having determined the sliding and open portions of the crack, we can determine $K_I^{(1)}$ from the solution of problem (i) mentioned above.

As far as $K_{II}^{(1)}$ is concerned, it is obvious that only the prescribed shear tractions at the crack surface of problem (ii) mentioned above that have opposite directions on the upper and lower surfaces of the crack have a non-zero contribution to $K_{II}^{(1)}$. With the definition

$$\bar{A}(x) = \frac{1}{2}\,[A(x,\,0^+) + A(x,\,0^-)]\ ,$$

$K_{II}^{(1)}$ is known (e.g., [12]) to be

$$K_{II}^{(1)} = -\frac{1}{\sqrt{\pi a}} \int_{-a}^{a} \bar{\sigma}_{xy}^{(1)}(x)\,\sqrt{\frac{a+x}{a-x}}\,dx\ , \tag{27}$$

where, according to (21),

$$\bar{\sigma}_{xy}^{(1)}(x) = \mu\bar{\sigma}_{yy}^{(1)}(x) + \lambda(x)\,\frac{d}{dx}\,[\bar{\sigma}_{xx}^{(0)}(x) - \mu\bar{\sigma}_{xy}^{(0)}(x)] -$$
$$- \lambda'(x)[(1 + 2\mu^2)\bar{\sigma}_{yy}^{(0)}(x) - \bar{\sigma}_{xx}^{(0)}(x)]\ . \tag{28}$$

On the other hand, it is possible that the stress field of the zeroth order problem, $\underset{\sim}{\sigma}^{(0)}$, has the characteristic $\frac{1}{\sqrt{r}}$ elastic singularity at several

points in the interval $|x| < a$; since derivatives of $\underset{\sim}{\sigma}^{(0)}$ with respect to x are involved in the formula for $\bar{\sigma}_{xy}^{(1)}$ (eqn. (28)), non-integrable singularities will appear in eqn. (27). To overcome this difficulty, we assume, for the moment, that the stress components $\sigma_{ij}^{(0)}(x, 0)$ are all bounded and differentiable with respect to x in the interval $|x| < a$; this makes $\sigma_{xy}^{(1)}(x, 0)$ also bounded on the crack face. In the case where $\sigma_{ij}^{(0)}(x, 0)$ are singular at some point in the interval $|x| < a$, the singularities are removed by replacing $\sigma_{ij}^{(0)}(x, 0)$ by bounded functions that reduce continuously to zero (or any other value that makes $\sigma_{ij}^{(0)}(x, 0)$ continuous) over distances closer than a small distance δ to the point where the singularities appear. Later it is shown that it is possible to let δ tend to zero, i.e., effectively to remove the restriction of bounded and differentiable $\sigma_{ij}^{(0)}(x, 0)$.

We return now to the calculation of $K_{II}^{(1)}$. With the above continuity assumptions on $\sigma_{ij}^{(0)}$ we can integrate by parts eqn. (28) to find

$$K_{II}^{(1)} = -\frac{1}{\sqrt{\pi a}} \int_{-a}^{a} \{\mu\bar{\sigma}_{yy}^{(1)} - \lambda'[(1 + 2\mu^2)\bar{\sigma}_{yy}^{(0)} - \bar{\sigma}_{xx}^{(0)}] +$$

$$+ [-\lambda' + \tfrac{1}{2}\lambda'(a)](\bar{\sigma}_{xx}^{(0)} - \mu\bar{\sigma}_{xy}^{(0)})\} \sqrt{\frac{a + x}{a - x}}\, dx - \tag{29}$$

$$- \frac{1}{\sqrt{\pi a}} \int_{-a}^{a} (\bar{\sigma}_{xx}^{(0)} - \mu\bar{\sigma}_{xy}^{(0)})[\tfrac{1}{2}\lambda'(a) - \frac{a\lambda + (a - x)\lambda'(a)}{(a - x)^2} \sqrt{\frac{a - x}{a + x}}\, dx .$$

It should be noted that $a\lambda(x) + (a-x)\lambda'(a) = \frac{d}{dx}[a\lambda(x) + (a-x)\lambda'(a)] = 0$ at $x = a$, so there is no divergence at the upper limit of the second integral in (29). It can also be seen that an integrable singularity can exist in $\bar{\sigma}_{ij}^{(0)}(x)$, provided it is not at $x = \pm a$, as was also noted in [7]. Specifically, in terms of our earlier discussion, δ can be shrunk to zero and in

that limit, the result of equation (29) for $K_{II}^{(1)}$ approaches the result obtained by inserting directly into (29) the singular, actual $\bar{\sigma}_{ij}^{(0)}(x)$. Such considerations, based essentially on the fact that the final result of equation (29) for $K_{II}^{(1)}$ contains $\bar{\sigma}_{ij}^{(0)}(x)$ only (and not derivatives with respect to x), allow us to conclude that (29) is valid for all integrable $\bar{\sigma}_{ij}^{(0)}(x)$ (i.e., not necessarily bounded or continuous).

We mention again that part of the solution to our problem is the finding of the sliding portions of the crack. Having found the sliding portions of the crack and the solution of the zeroth order problem, we can proceed to solve the first order problem and use the formulae given in this section to find the first order correction to the stress intensity factors.

4. THE PROBLEM OF THE KINKED CRACK

A particular case of the curved crack is the kinked crack shown in Fig. 2. The shape of the kinked crack is given by

$$\lambda(x) = \begin{cases} \dfrac{mb}{b-a}(x+a) & \text{for } -a < x < -b , \\ mx & \text{for } |x| < b , \\ \dfrac{mb}{b-a}(x-a) & \text{for } b < x < a . \end{cases}$$

In this case, $\omega = \lambda'(a) + O(\varepsilon^3) = \dfrac{mb}{b-a} + O(\varepsilon^3)$.

Following our previous discussion, we assume that both m and $\dfrac{mb}{b-a}$ are $O(\varepsilon)$, which is equivalent to assuming that $\lambda'(x)$ is $O(\varepsilon)$. We mention again that we are concerned with the case where both σ_{yy}^{∞} and σ_{xy}^{∞} are negative and so, it can be assumed that the portion of the crack in the interval $|x| < b$ remains closed during the application of the load. Thus,

the sliding portion of the crack is the interval $|x| < b$ and the open portions are the intervals $b < |x| < a$. Of course, there is a possibility that the applied stresses σ_{ij}^{∞} and the orientation of the kinked crack are such that the whole crack remains closed and does not slide. To check whether this happens, we can solve the problem assuming that the crack opens in the interval $b < |x| < a$; if the calculated K_I at the tips of the kinks is negative, the tip of the kinks remain closed and the assumption that the crack opens in the whole intervals $b < |x| < a$ is in error.

4.1 Solution of the zeroth order problem

The zeroth order problem can be considered as the superposition of the four problems shown in Fig. 3, where $F(x)$ is the distribution of the $\sigma_{yy}^{(0)}(x, 0)$ stress component of problem no. 1. We note that for problem no. 4 the shear stress on the crack face, $\sigma_{xy}^{(0)}(x, 0) = \mu F(x)$, opposes the relative sliding of the crack faces. The quantities of interest for each of the four problems mentioned above are given in the following. In the solutions presented in the rest of this section, conditions of plane strain are assumed; in order to get the plane stress solutions we simply replace ν by $\frac{\nu}{1+\nu}$.

4.1.1 Problem no. 1

The solution to this problem has been given by Erdogan [5] and is as follows

$$\sigma_{yy}^{(0)}(x, 0) = \frac{\sigma_{yy}^{\infty}}{\sqrt{(b^2 - x^2)(a^2 - x^2)}} \left[a^2 \frac{E(k)}{K(k)} - x^2\right] = F(x) , \tag{30}$$

$$\sigma_{xx}^{(0)}(x, 0) = F(x) - \sigma_{yy}^{\infty} ,$$

$$\sigma_{xy}^{(0)}(x, 0) = 0 ,$$

$$u_x^{(0)}(x,\ 0^+) = u_x^{(0)}(x,\ 0^-)\ ,$$

$$\varepsilon_{yy}^{(0)}(x,\ 0^+) = \varepsilon_{yy}^{(0)}(x,\ 0^-) \qquad \text{for} \quad |x| < b\ ;$$

and

$$\sigma_{xx}^{(0)}(x,\ 0) = -\sigma_{yy}^{\infty} \qquad \text{for} \quad b < |x| < a\ ,$$

where $K(k)$ and $E(k)$ are the complete elliptic integrals of the first and second kind respectively and $k = \sqrt{1 - b^2/a^2}$.

Also, the stress intensity factors for this problem are

$$K_I^{(0)} = \frac{\sigma_{yy}^{\infty}\sqrt{\pi a}}{k}\left[1 - \frac{E(k)}{K(k)}\right]\ ,$$

and $K_{II}^{(0)} = 0$.

Problem no. 2 consists of a plane strain tension. The solution to this problem is quite obvious; therefore we proceed to problem no. 3.

4.1.2 <u>Problem no. 3</u>

The solution to this problem is known (e.g., [12]) to be

$$\sigma_{xx}^{(0)}(x,\ 0^{\pm}) = \mp\ \sigma_{xy}^{\infty}\ \frac{2x}{\sqrt{a^2 - x^2}}\ ,$$

$$\sigma_{yy}^{(0)}(x,\ 0^{\pm}) = \sigma_{xy}^{(0)}(x,\ 0^{\pm}) = 0\ ,$$

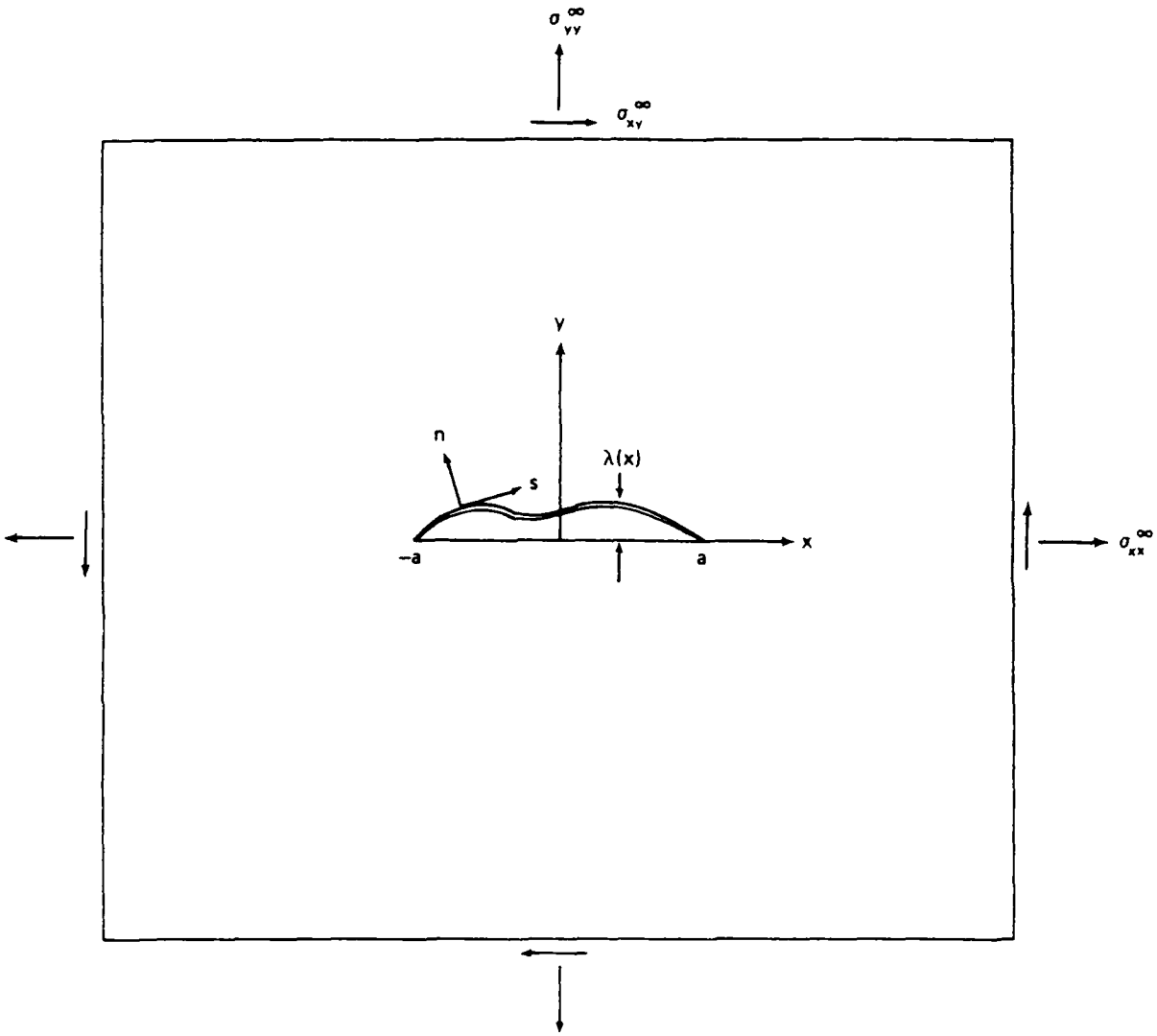

Figure 1

Fig. 1. Infinite plate containing a curved crack.

Fig. 2. Infinite plate containing a kinked crack.

Fig. 3. Superposition used in the solution of the zeroth order problem.

Fig. 4. Superposition used in the solution of the first order problem.

Fig. 5. Infinite plate containing a kinked crack oriented at 36° to the overall compression.

Fig. 6. Stress intensity factor at the tips of the kinked crack shown in Fig. 5 ($\mu = 0.3$).

Finally, using eqns. (46), (47) and (51) we find the stress intensity factor to be

$$K_I = -(\sigma_{xy}^{\infty} - \mu\sigma_{yy}^{\infty})\sqrt{\pi a}\,\frac{m}{1-\nu}\,\frac{k^3 - (2-\nu)k^2 + (1 - 2\nu + 2C)k + \nu}{2k^2}\,.$$

$$\phi'(z) = \overline{\Omega}'(z) = \frac{2G}{\pi(\kappa + 1)} \frac{1}{X(z)} \int_{-b}^{b} \frac{dh}{dx} X(x) \frac{dx}{x - z} + \frac{C_o}{X(z)} , \tag{52}$$

where $h(x)$ is the function determining the shape of the wedge of length 2b (see Fig. 4), $X(z) = \sqrt{(a^2 - z^2)(b^2 - z^2)}$ and the constant C_o is determined from the equation

$$\frac{1}{\pi} \int_{b}^{a} \frac{1}{\sqrt{(a^2 - x^2)(x^2 - b^2)}} \left[\int_{-b}^{b} \frac{dh}{dt} \sqrt{(a^2 - t^2)(b^2 - t^2)} \frac{dt}{t - x} \right] dx -$$

$$- \frac{\kappa + 1}{2G} \frac{K(k)}{a} C_o = -h(b) .$$

As discussed in Section 4.2, the shape of the wedge for our problem is given by

$$h(x) = m \frac{\sigma_{xy}^{\infty} - \mu\sigma_{yy}^{\infty}}{G} \frac{(1 - \nu)a^2 - x^2}{\sqrt{a^2 - x^2}} , \quad |x| < b . \tag{53}$$

Substituting (53) into (52) and carrying out the integrations, we find

$$\phi'(z) = \overline{\Omega}'(z) = - \frac{ma^2}{2(1 - \nu)} \frac{\sigma_{xy}^{\infty} - \mu\sigma_{yy}^{\infty}}{\sqrt{(z^2 - a^2)(z^2 - b^2)}}$$

$$\left[\nu \frac{z\sqrt{z^2 - b^2} - a\sqrt{a^2 - b^2}}{z^2 - a^2} + \frac{z^2 - z\sqrt{z^2 - b^2}}{a^2} - \frac{2\nu a^2 + b^2}{2a^2} + C\right]$$

where

$$C = \frac{1}{K(k)} \left\{ \frac{-K(k)k^3 + [(1 + 2\nu)K(k) - 2E(k)]k + 2\nu}{2k} + \right.$$

$$\left. + \nu \int_{b}^{a} \frac{x\sqrt{x^2 - b^2} - a\sqrt{a^2 - b^2}}{a^2 - x^2} \frac{dx}{\sqrt{(a^2 - x^2)(x^2 - b^2)}} \right\} .$$

For a prescribed shear traction $\sigma_{xy}(x, 0)$ along the crack face, it is known (e.g., [12]) that

$$\phi'(z) = \overline{\Omega}'(z) = -\frac{i}{2\pi\sqrt{z^2 - a^2}} \int_{-a}^{a} \sigma_{xy}(x, 0)\sqrt{a^2 - x^2}\,\frac{dx}{x - z}\,. \tag{49}$$

In our problem

$$\sigma_{xy}(x, 0) = \begin{cases} \mu F(x) & \text{for } |x| < b\,, \\ 0 & \text{for } b < |x| < a\,, \end{cases} \tag{50}$$

where $F(x)$ is defined in eqn. (30). Substituting (49) into (50) and carrying out the integration we find

$$\phi'(z) = \overline{\Omega}'(z) = -\frac{i}{2}\mu\sigma_{yy}^{\infty}\left\{\left[z^2 - a^2\frac{E(k)}{K(k)}\right]\frac{1}{\sqrt{(z^2 - a^2)(z^2 - b^2)}} - \frac{z}{\sqrt{z^2 - a^2}}\right\}.$$

Finally, using eqns. (46)-(48) and the definition

$$K_I + iK_{II} = \lim_{x\to a^+}\sqrt{2\pi(x - a)}\,[\sigma_{yy}(x, 0) + i\sigma_{xy}(x, 0)] \tag{51}$$

we find the results shown in Section 4.1.3.

APPENDIX 2

The solution to the problem of the opening of a finite crack by a rigid wedge has been given by Markuzon [14]. In terms of Muskhelishuili's [10] complex potentials, the solution is shown to be

APPENDIX 1

The problem no. 4 in Fig. 3 is formulated in terms of the complex potentials ϕ and ψ of Muskhelishvili [10]. The stresses and displacements can be expressed as

$$\sigma_{xx} + \sigma_{yy} = 2[\phi'(z) + \overline{\phi'(z)}] \ , \tag{43}$$

$$\sigma_{yy} - \sigma_{xx} + 2i\sigma_{xy} = 2[\bar{z}\phi''(z) + \psi'(z)] \ , \tag{44}$$

$$2G(u_x + iu_y) = \kappa\phi(z) - z\overline{\phi'(z)} - \overline{\psi(z)} \ , \tag{45}$$

where $\kappa = 3 - 4\nu$ for plane strain and $\kappa = (3 - \nu)/(1 + \nu)$ for plane stress, the overbar denotes the complex conjugate and prime stands for differentiation with respect to $z = x + iy$

Introducing the analytic function

$$\Omega(z) = z\phi'(z) + \psi(z)$$

eqns. (43)-(45) can be written as

$$\sigma_{xx} + \sigma_{yy} = 2[\phi'(z) + \overline{\phi'(z)}] \ , \tag{46}$$

$$\sigma_{yy} - \sigma_{xx} + 2i\sigma_{xy} = 2[(\bar{z} - z)\phi''(z) - \overline{\Omega(z)} - \phi'(z)] \ , \tag{47}$$

$$2G(u_x + iu_y) = \kappa\phi(z) - (z - \bar{z})\,\overline{\phi'(z)} - \overline{\Omega(z)} \ . \tag{48}$$

in a finite body. Int. J. Fracture 21, 67 (1983).

10. N. I. Muskhelishvili, Some basic problems on the mathematical theory of elasticity. Noordhoff (1952).

11. M. L. Williams, On the stress distribution at the base of a stationary crack. J. Appl. Mech. 24, 109 (1957).

12. J. R. Rice, Mathematical analysis in the mechanics of fracture. Fracture-An advanced treatise (Ed. H. Liebowitz) Vol. 2, Chap. III. Academic Press, New York (1968).

13. F. Erdogan, On the stress distribution in plates with collinear cuts under arbitrary loads. Proc. 4th U.S. Nat. Congress Appl. Mech., 547 (1962).

14. I. A. Markuzon, On splitting of a brittle body by a wedge of finite length. Prik. Mat. Mekh. 25, 356 (1961).

ACKNOWLEDGEMENT

This work was carried out with support from the Office of Naval Research under Contract N00014-81-K-0650 and while RMM was a Science and Engineering Research Council Fellow at the University of Cambridge, England.

REFERENCES

1. W. F. Brace and E. G. Bombolakis, A note on brittle crack growth in compression. J. Geophys. Res. 68, 3709 (1963).
2. E. Hoek and Z. T. Bieniawski, Brittle fracture propagation in rock under compression. Int. J. Fract. Mech. 1, 137 (1965).
3. S. Nemat-Nasser and H. Horii, Compression-induced nonplanar crack extension with application to splitting exfoliation and rockburst. J. Geophy. Res. 87, 6805 (1982).
4. M. F. Ashby, private communication.
5. N. V. Banichuk, Using a small-parameter method to determine the form of a curved crack. Izv. Akad. Nauk SSSR Mekh. Tverd. Tela 7, 130 (1970) (English translation in Mechanics of Solids 5, 114 (1970)).
6. R. V. Goldstein and R. L. Salganik, Brittle fracture of solids with arbitrary cracks. Int. J. Fracture 10, 507 (1974).
7. B. Cotterell and J. R. Rice, Slightly curved or kinked cracks. Int. J. Fracture 16, 155 (1980).
8. B. L. Karihaloo, L. M. Keer, S. Nemat-Nasser and A. Oranratnachai, Approximate description of crack kinking and curving. J. Appl. Mech. 48, 515 (1981).
9. Y. Sumi, S. Nemat-Nasser and L. M. Keer, On crack branching and curving

be valid, depend on both ℓ/c and θ. But, roughly speaking, the asymptotic solution is seen to be accurate for values of θ up to about 20°. Unfortunately, the values of K_{II} for small values of θ are not given in Ref. [3]; so, comparisons of the asymptotic result for K_{II} with the exact solution were not possible.

6. CLOSURE

A first order solution has been obtained for the stress intensity factors at the tips of the kinked extension of a sliding crack. The validity of the asymptotic solution is limited to kinked cracks with small deviations from straightness. There are several situations where this deviation is indeed small. As an example, consider the case of a glass plate or a rock block containing several small cracks at different orientations. Under the application of a compressive load, the cracks with an angle to the direction of compression, γ, greater than $\gamma_c = \tan^{-1}\frac{1}{\mu}$ will remain closed and only those with $\gamma < \gamma_c$ can, possibly, slide and propagate. It is also known ([1]-[4]) that these cracks tend to propagate towards the direction of compression. So, if the coefficient of friction, μ, is very high (which makes γ_c small) the crack propagation will create kinked cracks with small deviations from straightness. For situations like these, the asymptotic results can be used to determine the stress intensity factors and to make predictions for the direction of further propagation. In addition, fatigue due to non-proportional loads can cause the development of cracks that are not straight and are partially closed, although open at the tip. For cases where the deviation from the straight line is small, the methods devised here can be used, although a criterion for determining where the closed portions lie would have to be developed.

$$K_{II} = K_{II}^{(0)} + \frac{1}{2}\,\omega\, K_{I}^{(0)} + K_{II}^{(1)} + O(\varepsilon^2) ,$$

where $K_I^{(0)}$, $K_{II}^{(0)}$, $K_I^{(1)}$ and $K_{II}^{(1)}$ are given in equations (38), (39), (41) and (42) respectively. Equations (41) and (42) show that $K_I^{(1)}$ and $K_{II}^{(1)}$ depend on Poisson's ratio ν . This means that they have different values under plane strain or plane stress conditions. On the other hand, it is known that, in the absence of body forces, the stress intensity factors for traction boundary value problems are the same under plane strain or plane stress conditions and independent of the elastic constants. The reason that ν enters the expressions of the asymptotic solution for the stress intensity factors is that the displacement field of the zeroth order problem, which depends on ν , was used to formulate the first order problem. As a result, the in-plane components of the first order correction to the stress field and the corresponding corrections to the stress intensity factors depend on ν . However, numerical calculations of $K_I^{(1)}$ and $K_{II}^{(1)}$ show that their dependence on ν is very weak and that their values for plane strain and plane stress conditions are practically indistinguishable, which validates the first order correction.

Next, we apply our results to the problem of a infinite plate containing a kinked crack oriented at 36° to the overall compression (Fig. 5). The exact solution, given in Ref. [3], and the asymptotic results for K_I are plotted in Fig. 6 versus the angle between the straight crack and its out-of-plane kinks, θ , for several values of the ratio of the length of the kink, ℓ , to the length of the straight crack, c . In general, the region of accuracy of the asymptotic solution depends on both ℓ/c and θ , because the values of m and ω in our analysis, which must be small for the asymptotic solution to

where

$$C = \frac{1}{K(k)} \left\{ \frac{-K(k)k^3 + [(1 + 2\nu)K(k) - 2E(k)]k + 2\nu}{2k} + \right.$$

$$\left. + \nu a \int_b^a \frac{x\sqrt{x^2 - b^2} - a\sqrt{a^2 - b^2}}{a^2 - x^2} \frac{dx}{\sqrt{(a^2 - x^2)(x^2 - b^2)}} \right. .$$

We proceed now to the calculation of the mode II stress intensity factor for the first order problem, $K_{II}^{(1)}$, which can be determined either by solving problem no. 2 in Fig. 4 or, equivalently, using eqn. (29). We note that $\bar{\sigma}_{xx}^{(0)}(x)$, $\bar{\sigma}_{yy}^{(0)}(x)$ and $\bar{\sigma}_{xy}^{(0)}(x)$ all have the characteristic $\frac{1}{\sqrt{r}}$ singularity at $x = \pm b$; but as discussed in Section 3, eqn. (29) for $K_{II}^{(1)}$ can still be used, provided that the singularities are integrable, which is indeed the case. So, using the solution of the zeroth order problem derived in the previous section and applying eqn. (29), after some lengthy, but straightforward, integrations we find

$$K_{II}^{(1)} = \mu K_I^{(1)} + (\sigma_{yy}^{\infty} - \sigma_{xx}^{\infty}) \sqrt{\pi a} \frac{mb}{b - a} \left(1 - \frac{2a}{\pi b} \sin^{-1} \frac{b}{a}\right) + 2\mu^2 m \sigma_{yy}^{\infty} \sqrt{\pi a} +$$

$$+ \sigma_{yy}^{\infty} \sqrt{\pi a} \frac{m}{2k} \left\{1 - 5\mu^2 + (1 + 3\mu^2) \frac{E(k)}{K(k)} - \frac{1 - \mu^2}{k^2} \left[1 - \frac{E(k)}{K(k)}\right]\right\} , \qquad (42)$$

where $K_I^{(1)}$ is given in eqn. (40).

5. DISCUSSION AND COMPARISON WITH THE EXACT SOLUTION

The obtained asymptotic solution for the stress intensity factors at the tips of a kinked crack is of the form

$$K_I = K_I^{(0)} - \frac{3}{2} \omega K_{II}^{(0)} + K_I^{(1)} + O(\varepsilon^2) ,$$

$$\bar{\sigma}_{yy}^{(0)}(x) = \bar{\sigma}_{xy}^{(0)}(x) = 0 \tag{37}$$

for $b < |x| < a$.

Also, the stress intensity factors for the zeroth order problem are given by

$$K_I^{(0)} = \frac{\sigma_{yy}^{\infty}\sqrt{\pi a}}{k}\left[1 - \frac{E(k)}{K(k)}\right] , \tag{38}$$

$$K_{II}^{(0)} = (\sigma_{xy}^{\infty} - \mu\sigma_{yy}^{\infty})\sqrt{\pi a} + \mu K_I^{(0)} . \tag{39}$$

4.2 Stress intensity factors for the first order problem

As discussed in Section 3, the first order problem can be considered to be the superposition of the two problems shown in Fig. 4.

The mode I stress intensity factor $K_I^{(1)}$ is determined by solving problem no. 1 in Fig. 4, which is actually the problem of the opening of a finite crack by a rigid wedge. The general solution to this problem has been given by Markuzon [14]. Taking into account eqn. (22) and the solution of the zeroth order problem derived in the previous section, we find that, for our particular case, the shape of the wedge, $h(x)$, is given by

$$2h(x) = u_y^{(1)}(x,0^+) - u_y^{(1)}(x,0^-) = 2m\,\frac{\sigma_{xy}^{\infty} - \mu\sigma_{yy}^{\infty}}{G}\,\frac{(1-\nu)a^2 - x^2}{\sqrt{a^2 - x^2}} , \quad |x| < b . \tag{40}$$

Using the above formula for the shape of the wedge and Markuzon's [14] solution, we find the mode I stress intensity factor to be (see Appendix 2)

$$K_I^{(1)} = -(\sigma_{xy}^{\infty} - \mu\sigma_{yy}^{\infty})\sqrt{\pi a}\,\frac{m}{1-\nu}\,\frac{k^3 - (2-\nu)k^2 + (1 - 2\nu + 2C)k + \nu}{2k^2} , \tag{41}$$

$$\sigma_{xx}^{(0)}(x,\ 0^{\pm}) = \mp 2\mu\sigma_{yy}^{\infty}\left\{ \frac{1}{\sqrt{(x^2 - b^2)(a^2 - x^2)}}\left[x^2 - a^2\frac{E(k)}{K(k)}\right] - \frac{x}{\sqrt{a^2 - x^2}}\right\}$$

$$\text{for} \quad b < |x| < a \ .$$

Also,

$$K_I^{(0)} = 0 \ ,$$

$$K_{II}^{(0)} = \frac{\mu\sigma_{yy}^{\infty}\sqrt{\pi a}}{k}\left[1 - k - \frac{E(k)}{K(k)}\right] .$$

4.1.4 Superposition

Superimposing the solutions of the four problems shown in Fig. 3, we find the quantities of interest of the solution to the zeroth order problem to be

$$\bar{\sigma}_{xx}^{(0)}(x) = F(x) - \sigma_{yy}^{\infty} + \sigma_{xx}^{\infty} \ , \tag{31}$$

$$\bar{\sigma}_{yy}^{(0)} = F(x) \ , \tag{32}$$

$$\bar{\sigma}_{xy}^{(0)}(x) = \mu F(x) \ , \tag{33}$$

$$\varepsilon_{yy}^{(0)}(x,\ 0^{+}) - \varepsilon_{yy}^{(0)}(x,\ 0^{-}) = 2\nu\,\frac{\sigma_{xy}^{\infty} - \mu\sigma_{yy}^{\infty}}{G}\,\frac{x}{\sqrt{a^2 - x^2}} \ , \tag{34}$$

$$u_x^{(0)}(x,\ 0^{+}) - u_x^{(0)}(x,\ 0^{-}) = 2(1 - \nu)\,\frac{\sigma_{xy}^{\infty} - \mu\sigma_{yy}^{\infty}}{G}\sqrt{a^2 - x^2} \tag{35}$$

for $|x| < b$; and

$$\bar{\sigma}_{xx}^{(0)}(x) = -\sigma_{yy}^{\infty} + \sigma_{xx}^{\infty} \ , \tag{36}$$

$$\varepsilon_{yy}^{(0)}(x,\ 0^{\pm}) = \pm\nu\ \frac{\sigma_{xy}^{\infty}}{G}\ \frac{x}{\sqrt{a^2 - x^2}}\ ,$$

and $$u_x^{(0)}(x,\ 0^{\pm}) = \pm(1 - \nu)\ \frac{\sigma_{xy}^{\infty}}{G}\ \sqrt{a^2 - x^2} \quad \text{for} \quad |x| < a\ ,$$

where G is the shear modulus of the material.

In addition,

$$K_I^{(0)} = 0\ ,$$

and $$K_{II}^{(0)} = \sigma_{xy}^{\infty}\ \sqrt{\pi a}\ .$$

4.1.3 <u>Problem no. 4</u>

The solution to this problem is derived in Appendix 1 and is as follows

$$\sigma_{xx}^{(0)}(x,\ 0^{\pm}) = \pm\mu\sigma_{yy}^{\infty}\ \frac{2x}{\sqrt{a^2 - x^2}}\ ,$$

$$\sigma_{yy}^{(0)}(x,\ 0) = 0\ ,$$

$$\sigma_{xy}^{(0)}(x,\ 0) = \mu F(x)\ ,$$

$$\varepsilon_{yy}^{(0)}(x,\ 0^{\pm}) = \mp\nu\ \frac{\mu\sigma_{yy}^{\infty}}{G}\ \frac{x}{\sqrt{a^2 - x^2}}\ ,$$

$$u_x^{(0)}(x,\ 0^{\pm}) = \mp(1 - \nu)\ \frac{\mu\sigma_{yy}^{\infty}}{G}\ \sqrt{a^2 - x^2} \quad \text{for} \quad |x| < b\ ;$$

and

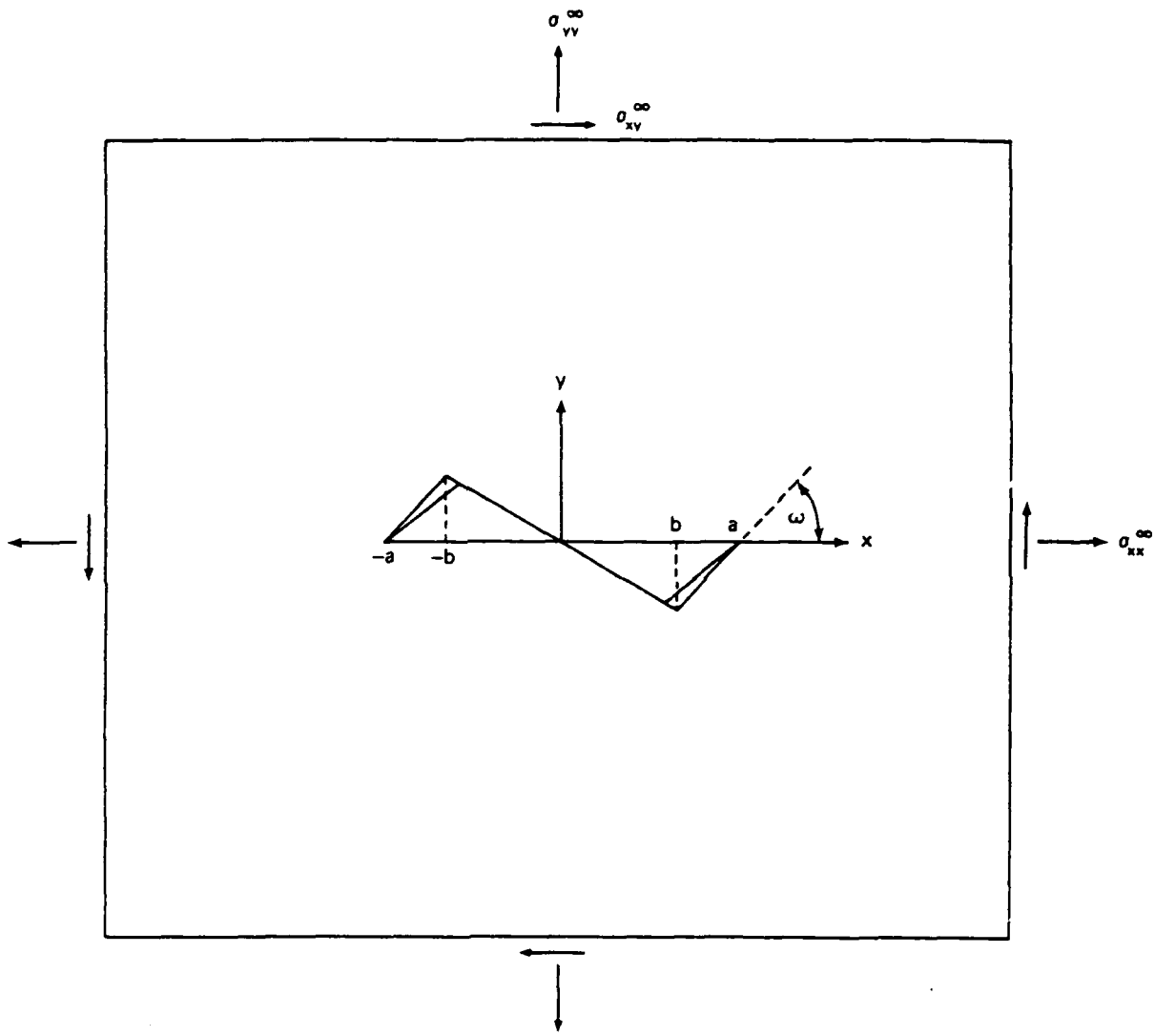

Figure 2

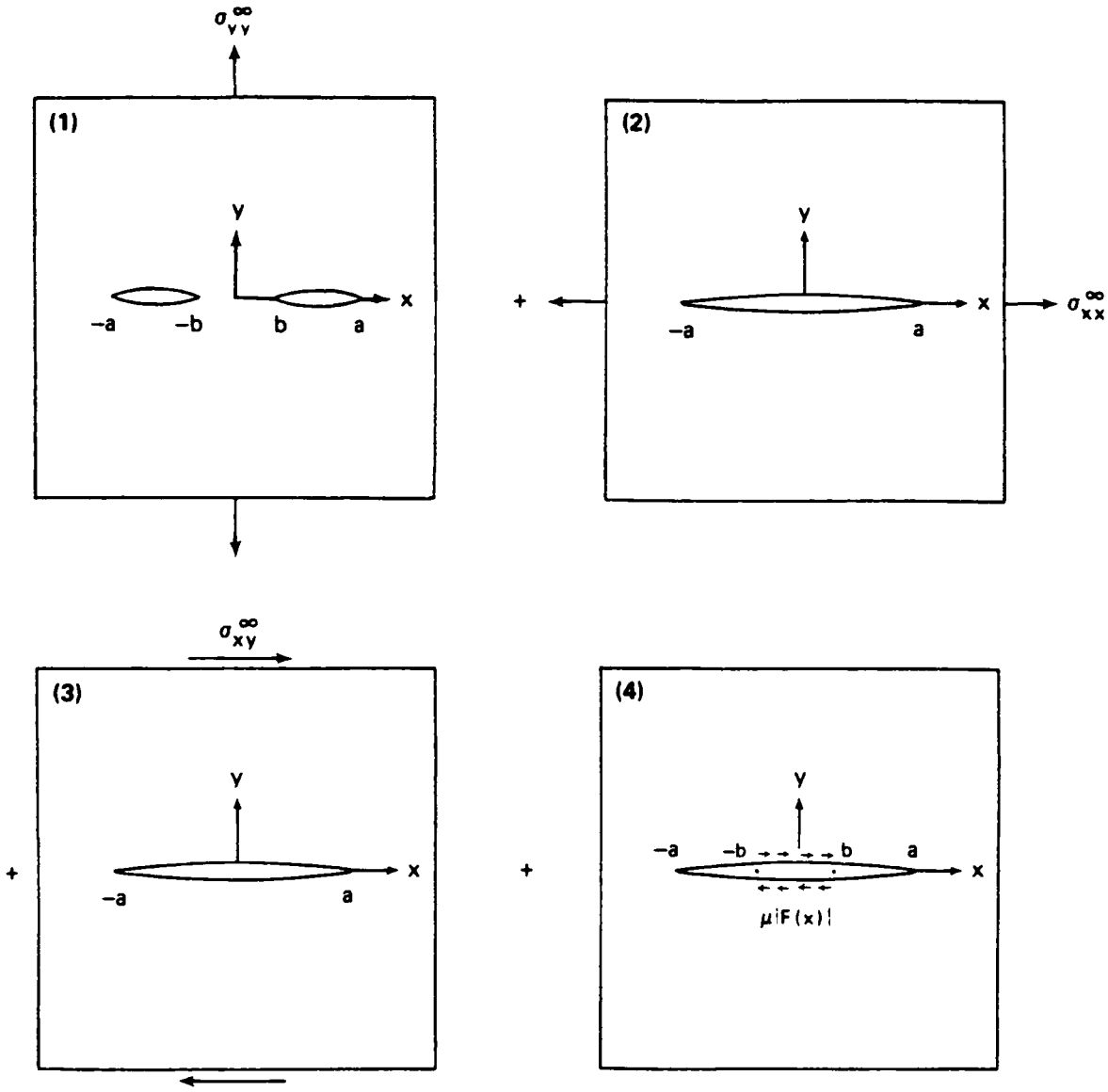
σ_{yy}^{∞}
(1)
y
x
−a
−b
b
a
+
(2)
y
x
−a
a
σ_{xx}^{∞}
σ_{xy}^{∞}
(3)
y
x
−a
a
+
+
(4)
y
x
−a
−b
b
a
$\mu|F(x)|$

Figure 3

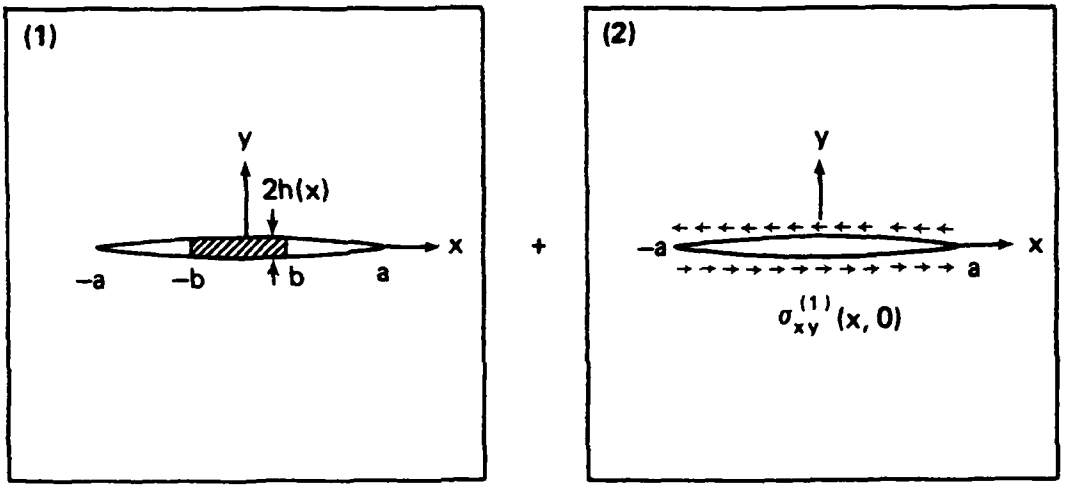

Figure 4

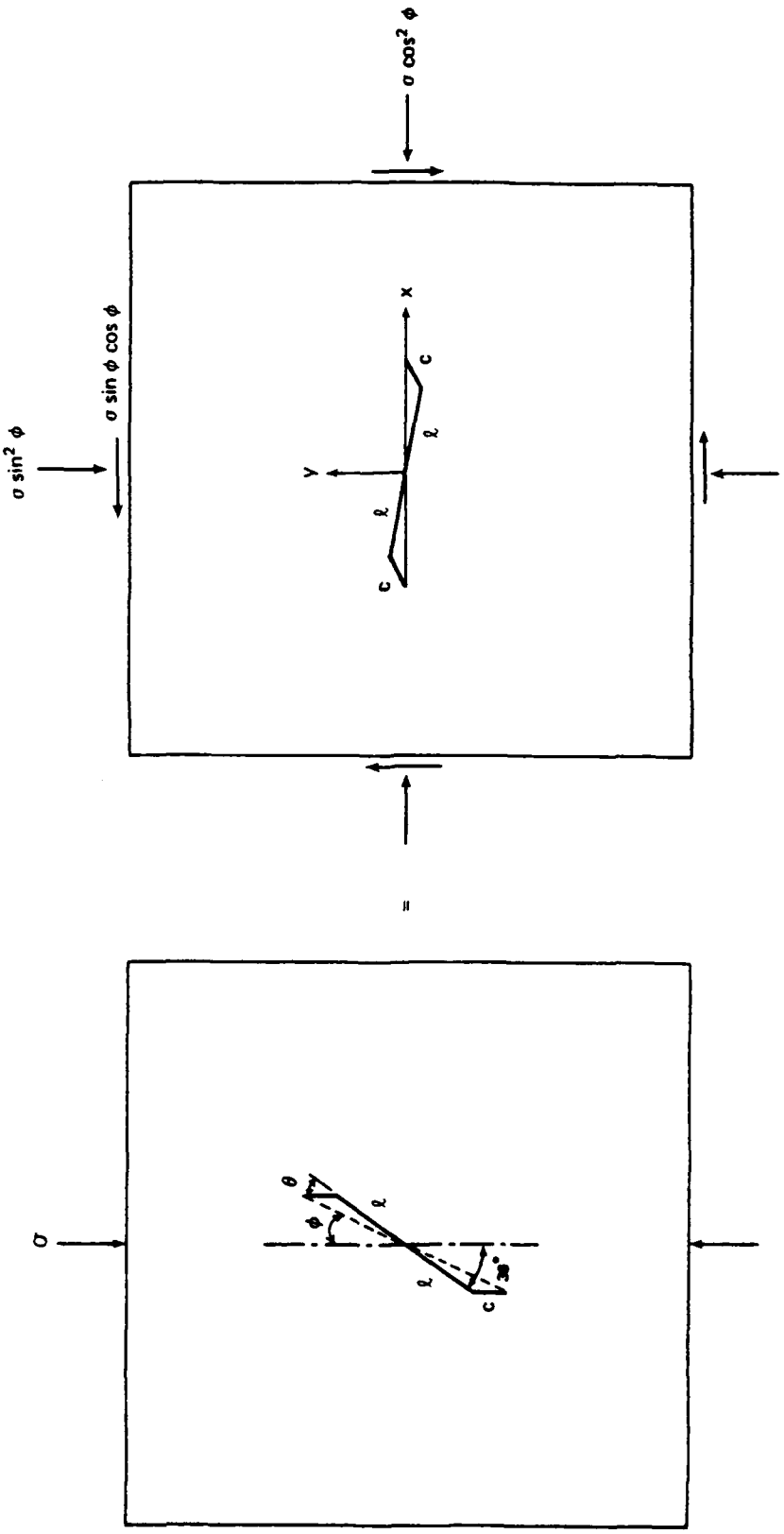

Figure 5

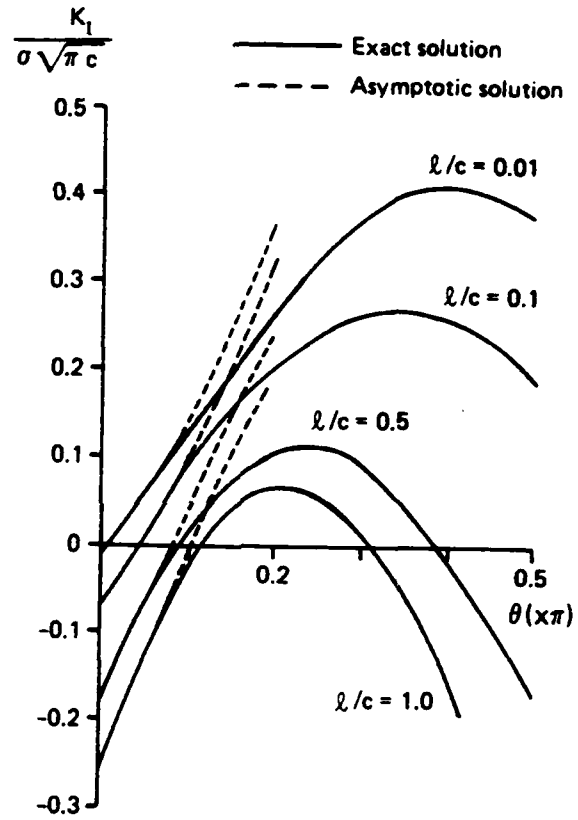
$\frac{K_I}{\sigma\sqrt{\pi c}}$
Exact solution
Asymptotic solution
0.5
0.4
0.3
0.2
0.1
0
-0.1
-0.2
-0.3
0.2
0.5
$\theta(x\pi)$
$\ell/c = 0.01$
$\ell/c = 0.1$
$\ell/c = 0.5$
$\ell/c = 1.0$

Figure 6

END

FILMED

6-85

DTIC